Structural and Biochemical Investigation of the *Escherichia coli* Oxygen Independent Coproporphyrinogen III Oxidase (HemN) and its Substrate

Von der Fakultät für Lebenswissenschaften

der Technischen Universität Carolo-Wilhelmina

zu Braunschweig

zur Erlangung des Grades einer

Doktorin der Naturwissenschaften

(Dr. rer. nat.)

genehmigte

D i s s e r t a t i o n

von Katrin Rand
aus Oldenburg (Oldb)

1. Referent: Honorarprofessor Dr. Dirk Heinz
2. Referentin: Dr. Gunhild Layer
eingereicht am: 06.07.2009
mündliche Prüfung (Disputation) am: 07.10.2009

Druckjahr 2009

Contents

Abbreviations

Å	Ångstrøm (1 Å = 0.1 nm)
aa	Amino acid(s)
AE	Activating enzyme
AIR	5-Aminoimidazole
ALA	5-Aminolevulinic acid
ALAS	ALA synthase
A_λ	Absorption at the wavelength λ in nm (equivalent to OD_λ)
Amp	Ampicillin
Amp^R	Ampicillin resistance
anSME	Anaerobic Sulfatase Maturating Enzymes
ARNR-AE	Anaerobic ribonucleotide reductase activating enzyme
BESSY	Berliner Elektronenspeicherring-Gesellschaft für Synchrotron Strahlung, Berlin, Germany
BSA	Bovine serum albumin
C_8E_4	Tetraethylene glycol monooctyl ether
C-	Carboxy terminus
CIA-machinery	Cytosolic iron-sulfur cluster assembly machinery
Cm	Chloramphenicol
Cm^R	Chloramphenicol resistance
copro'	Coproporphyrin III
copro'gen	Coproporphyrinogen III
CPO	Coproporphyrinogen III oxidase
CV	Column volume
CxxxCxxC	Amino acid motif; C, cysteine; x, any amino acid
Da	Dalton (equals the mass of 1/12 of the carbon ^{12}C isotope)
DESY	Deutsches Elektronensynchrotron, Hamburg, Germany
DNA	Deoxyribonucleic acid
DTT	Dithiothreitol
E. coli	*Escherichia coli*
EDTA	Ethylenediaminetetraacetic acid
EMBL	European molecular biology laboratory
ESI	Electrospray ionisation
ESRF	European synchrotron radiation facility
EtOH	Ethanol
FeS-cluster	Iron sulfur cluster
[4Fe-4S]-cluster	four iron four sulfur cluster
FNR	Fumarate and nitrate reduction
FPLC	Fast protein liquid chromatography
GD	Glycerol dehydratase
GluTR	Glutamyl-tRNA reductase, gene product of *hemA*
GSAM	Glutamate-1-semialdehyde-2,1-aminomutase, gene product of *hemL*
GSH sepharose	Glutathione sepharose
GST	Glutathione *S*-transferase, used as affinity tag

hardero'	Harderoporphyrin
hardero'gen	Harderoporphyrinogen
HemB	Porphobilinogen synthetase, gene product of *hemB*
HemC	Porphobilinogen deaminase, gene product of *hemC*
HemD	Uroporphyrinogen synthase, gene product of *hemD*
HemE	Uroporphyrinogen decarboxylase, gene product of *hemE*
HemF	Oxygen dependent coproporphyrinogen III oxidase, gene product of *hemF*
HemN	Oxygen independent coproporphyrinogen III oxidase, gene product of *hemN*
His_6	Six successive histidine residues, used as affinity tag
HMP-P	4-amino-5-hydroxymethyl-2-methylpyrimidine phosphate
HPLC	High performance liquid chromatography
HydA	[Fe]-hydrogenase
HydE	HydA maturating enzyme
HydG	HydA maturating enzyme
IEC	Ion exchange chromatography
IPTG	Isopropyl *β*-D-thiogalactopyranoside
isohardero'	isoharderoporphyrin
isohardero'gen	isoharderoporphyrinogen
Kan	Kanamycin
Kan^R	Kanamycin resistance
kDa	Kilodalton
LAM	Lysine-2,3-aminomutase
LB	Lysogeny broth
LipA	Lipoyl synthase, in *E. coli* gene product of *lipA*
MALDI-TOF MS	Matrix-Assisted Laser Desorption/ Ionization-Time of Flight Mass Spectrometry
MeOH	Methanol
MiaB	tRNA-methylthiotransferase
M_r	Molecular mass
MR	Molecular replacement
MS	Mass spectrometry
MTAN	5'-methylthioadenosine/*S*-adenosylhomocysteine nucleosidase
MW	Molecular weight
MWCO	Molecular weight cut-off
N-	Amino terminus
n.d.	Not determined
Nif	Nitrogen-fixation-specific
Ni-NTA	Nickel nitrilotriacetic acid
o.n.	Overnight
OD_λ	Optical density at the wavelength λ in nm (equivalent to A_λ)
PAC	Prespotted anchor chip
PAGE	Polyacrylamide gelelectrophoresis
PBGD	Porphobilinogen deaminase, see HemC
PBGS	Porphobilinogen synthase, see HemB
PBS	Phosphate buffered saline

PCA	$HClO_4$; perchloric acid
PCR	Polymerase chain reaction
PDB	Protein Data Bank
PEG	Polyethylene glycol
PFL-AE	Pyruvate formate lyase activating enzyme
PMS	Phenazine methosulfate
PPO	Protoporphyrinogen IX oxidase
proto'	Protoporphyrin IX
proto'gen	Protoporphyrinogen IX
p.s.i.	Pounds per square inch
RimO	Ribosomal modification enzyme O, gene product of *yliG*/*rimO*
r.m.s.	Root mean square
r.m.s.d.	Root mean square displacement
RNA	Ribonucleic acid
rpm	Rotations per minute
rt	Retention time
RT	Room temperature
SAM	*S*-(5-Adenosyl)-L-methionine
SDS	Sodium dodecyl sulfate
SMM	Spizizen minimal medium
ThiC	HMP-P synthase, gene product of *thiC*
ThiH	Gene product of *thiH* (involved in thiamine biosynthesis)
TIM	Triose phosphate isomerase
TIM barrel	Protein fold first described in triose phosphate isomerase
Tris	Tris-(hydroxymethyl) aminomethane
TU	Technical University
TYW1	Wybutosine generating enzyme (tRNA modification)
U3S	Uroporphyrinogen III synthase (see HemD)
uro'	Uroporphyrin III
uro'gen	Uroporphyrinogen III
V_M	Matthews coefficient
wt	Wildtype

Zusammenfassung

Die Hämbiosynthese ist einer der elementarsten Biosynthesewege der Natur. Unter anaeroben Bedingungen müssen dabei wichtige oxidative Syntheseschritte ohne molekularen Sauerstoff stattfinden. Eine dieser Reaktionen wird von HemN, der sauerstoffunabhängigen Coproporphyrinogen III Oxidase katalysiert. Obwohl der entsprechende katalytische Mechanismus noch nicht bekannt ist, konnte HemN anhand von spektroskopischen und bioinformatischen Daten sowie der Kristallstruktur der Enzymfamilie der Radical SAM Enzyme zugeordnet werden. In der Kristallstruktur von HemN wurde zusätzlich zu den charakteristischen Radical SAM Merkmalen ein weiteres SAM-Molekül gefunden, das möglicherweise an der Katalyse beteiligt ist. Entscheidende Fortschritte im Verständnis der HemN-Wirkungsweise werden durch detaillierte Kenntnisse über die Substratbindung erwartet. Entsprechend lag der Schwerpunkt dieser Arbeit auf biochemischen und kristallographischen Untersuchungen an HemN im Komplex mit dem Substrat Coproporphyrinogen III oder mit einem Reaktionsprodukt. Da sowohl HemN als auch Coproporphyrinogen III sehr empfindlich gegenüber molekularem Sauerstoff sind, ist die Gewährleistung einer sauerstofffreien Umgebung eine wichtige Voraussetzung für Experimente mit diesem Enzym.

Im Rahmen dieser Arbeit wurde eine anaerobe Arbeitsstation in unseren Laboren erfolgreich eingerichtet. Entsprechende Protokolle zur Reinigung und Kristallisation von HemN sowie zur Synthese des Substrates wurden dabei etabliert. Coproporphyrinogen III wurde über drei verschiedene Wegen erhalten: I) über enzymatische Synthese, II) über Na-Amalgam-Reduktion und III) über H_2/Pd-Hydrierung. Im Laufe der Arbeit gelang es, das sauerstoffempfindliche [4Fe-4S]-Cluster von HemN zu rekonstituieren und so im Gegensatz zu vorherigen Versuchen große Mengen an katalytisch aktivem Protein zu erhalten. Auf der Basis dieser etablierten Protokolle wurden zahlreiche Co-Kristallisations und Tränkungsexperimente sowohl mit HemN Wildtyp als auch mit einer an der SAM2-Bindung beteiligten HemN-Variante durchgeführt. Während der HemN Kristallisation wurden verschiedene Substrate kombiniert mit einem künstlichen Elektronendonor oder –Akzeptor eingesetzt.

Obwohl zahlreiche Datensätze aufgenommen, prozessiert und evaluiert wurden, konnte weder für HemN Wildtyp noch für die HemN-Varianten eine Kristallstruktur ermittelt werden, in der ein Substratmolekül oder ein Reaktionsprodukt eindeutig definiert war. Es wurde herausgefunden, dass HemN vorwiegend in einer Kristallform kristallisiert, die offensichtlich das Umklappen der C-terminalen Domäne, das für HemN postuliert wurde, verhindert und dadurch eine Komplexstruktur verhindert. Daher wurde HemN durch den gezielten Austausch einer einzelnen Aminosäure, die an Wildtyp Kristallkontakten beteiligt ist, in eine neue Kristallform gezwungen. Obwohl HemN hierdurch in einer neuen Kristallform kristallisierte, ist auch in dieser neuen Packung das Umklappen der C-terminalen Domäne unwahrscheinlich und Co-Kristallisations- und Tränkungs-experimente sind wenig Erfolg versprechend.

Die Ergebnisse dieser Arbeit deuten darauf hin, dass Harderoporphyrinogen das Zwischenprodukt der HemN Reaktion ist und liefern damit weitere Erkenntnisse über den HemN Reaktionsmechanismus.

Die Untersuchungen in dieser Arbeit ergänzen das Wissen über HemN und legen den Grundstein für die weitere Arbeit an diesem Enzym.

Summary

Heme biosynthesis is one of the most essential biosynthetic pathways in nature. Under anaerobic conditions crucial oxidative steps within this pathway have to proceed in the absence of molecular oxygen. One of these steps is accomplished by the oxygen independent coproporphyrinogen III oxidase HemN, which catalyzes the oxidative decarboxylation of coproporphyrinogen III to yield in protoporphyrinogen IX. Although the corresponding catalytic mechanism is not clear as yet, HemN could be assigned a Radical SAM enzyme based on spectroscopic and bioinformatic data as well as the crystal structure. In addition to the characteristic Radical SAM features, a second SAM molecule was identified in the structure which could potentially participate in HemN catalysis. Substantial progress in understanding the HemN reaction mechanism is expected by detailed knowledge of the substrate binding mode. The present study was therefore focused on biochemical and structural studies of purified HemN in complex with its substrate coproporphyrinogen III or its reaction products. Due to the oxygen sensitivity of HemN and coproporphyrinogen III the establishment of an anaerobic environment was the precondition for experimental studies on this enzyme.

Within the present study an anaerobic working station was successfully set up in our laboratory and protocols for HemN purification and crystallization as well as for the synthesis of its substrate coproporphyrinogen III were established. Three different methods have been applied to obtain coproporphyrinogen III: I) enzymatic synthesis, II) Na-amalgam reduction, and III) H_2/Pd-hydration. Later in this study a major drawback of the anaerobic purification of HemN could be overcome through successful reconstitution of the oxygen sensitive HemN [4Fe-4S]-cluster yielding large amounts of catalytically active protein. The established protocols were the basis for numerous co-crystallization and soaking experiments that have been set up. Intensive crystallographic studies were performed with wildtype protein and with HemN variants supposed to be involved in SAM2 binding. Different substrates in combination with an artificial electron donor or acceptor were utilized for crystallization.

Despite numerous data sets that have been collected, processed, and evaluated, neither for the wildtype nor for any mutant protein a crystal structure could be obtained with an unambiguously defined substrate, reaction intermediate, or product bound. One major obstacle for a successful complex structure solution was found to be the dominant HemN crystal packing, which may impair the domain movement postulated to occur upon substrate binding. HemN was therefore forced to crystallize in a new space group by rational mutation of a single residue involved in crystal contacts. Although a different crystal packing could be obtained this way, the postulated domain movement is unlikely to occur in the new crystal packing arrangement in co-crystallization or soaking experiments.

The results obtained in this work identified harderoporphyrinogen as a likely HemN reaction intermediate giving further insight into the HemN reaction mechanism.

The current study has complemented the knowledge about HemN and forms a basis for future work on HemN.

1 Introduction

1.1 Tetrapyrroles are Fundamental Chemical Compounds

Tetrapyrroles are cofactors or prosthetic groups consisting of four pyrrole rings that are essential for many fundamental processes in living organisms. The most common tetrapyrroles are Mg^{2+}-chelating, green chlorophylls used in photosynthesis and $Fe^{2+/3+}$-chelating red heme, the cofactor of hemoglobin and the dye of vertebrate blood. Heme is similarly vital for oxygen transport in muscles (myoglobin) (Wittenberg *et al.*, 1975), for respiration as the cofactor of cytochromes (Panek and O'Brian, 2002), and for many other enzymes such as peroxidases and catalases. In 2007 around 5 % of protein structures deposited in the Protein Data Bank (PDB) were heme proteins (Reedy *et al.*, 2008) emphasizing the overriding importance of heme.

All tetrapyrroles (except corrinoids) share a common core, the porphin ring (**Figure 1-1**), consisting of four pyrrole rings connected by methine bridges. Depending on the side chains, the complexed metal ion, and the oxidation state, tetrapyrroles exhibit characteristic colors and fluorescence. Porphyrins such as heme are fully substituted in all β-positions of the pyrrole rings and contain a system of fully conjugated double bonds. Hexahydroporphyrins or intermediates of the tetrapyrrole biosynthesis pathway, by contrast, lack this conjugated system. They are referred to as porphyrinogens and are both colorless and exhibit no fluorescence. Modifications of bridging carbons (mesoposition) include the removal of one methine bridge (C20, between pyrrole rings A and D) in Co^{2+}-chelating vitamin B_{12} (a corrinoid), or its incorporation in a fifth ring in

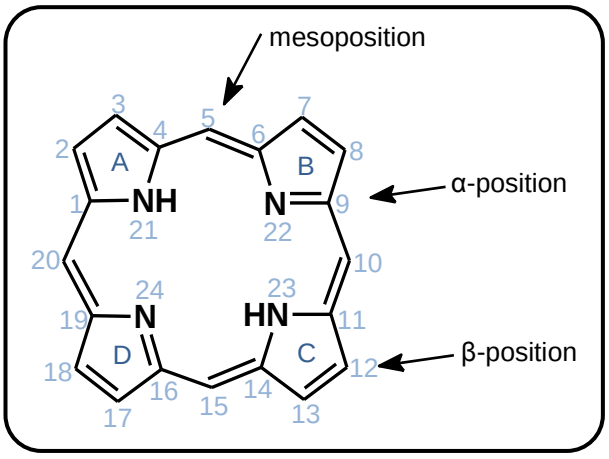

Figure 1-1: Porphin ring as the core structure of tetrapyrroles. Pyrrole rings are labeled A to D in a clockwise orientation, carbon atoms 1-20 and nitrogen atoms 21-24.

the chlorophylls (porphinoids) (Falk, 1964) (**Figure 1-2**). Further tetrapyrroles include siroheme, coenzyme F_{430}, and heme *d*1 (Frankenberg *et al.*, 2003). Tetrapyrroles mostly occur as a macrocycle as originally suggested in 1912 (Küster, 1912). Later, however, linear tetrapyrroles or bilins were also identified. They derive from cyclic tetrapyrroles by single cleavage. Bilirubin and biliverdin (bile pigments) as well as the phycobilins such as phycoerythrin and phycocyanin as part of the light harvesting phycobilisome complexes are prominent representatives.

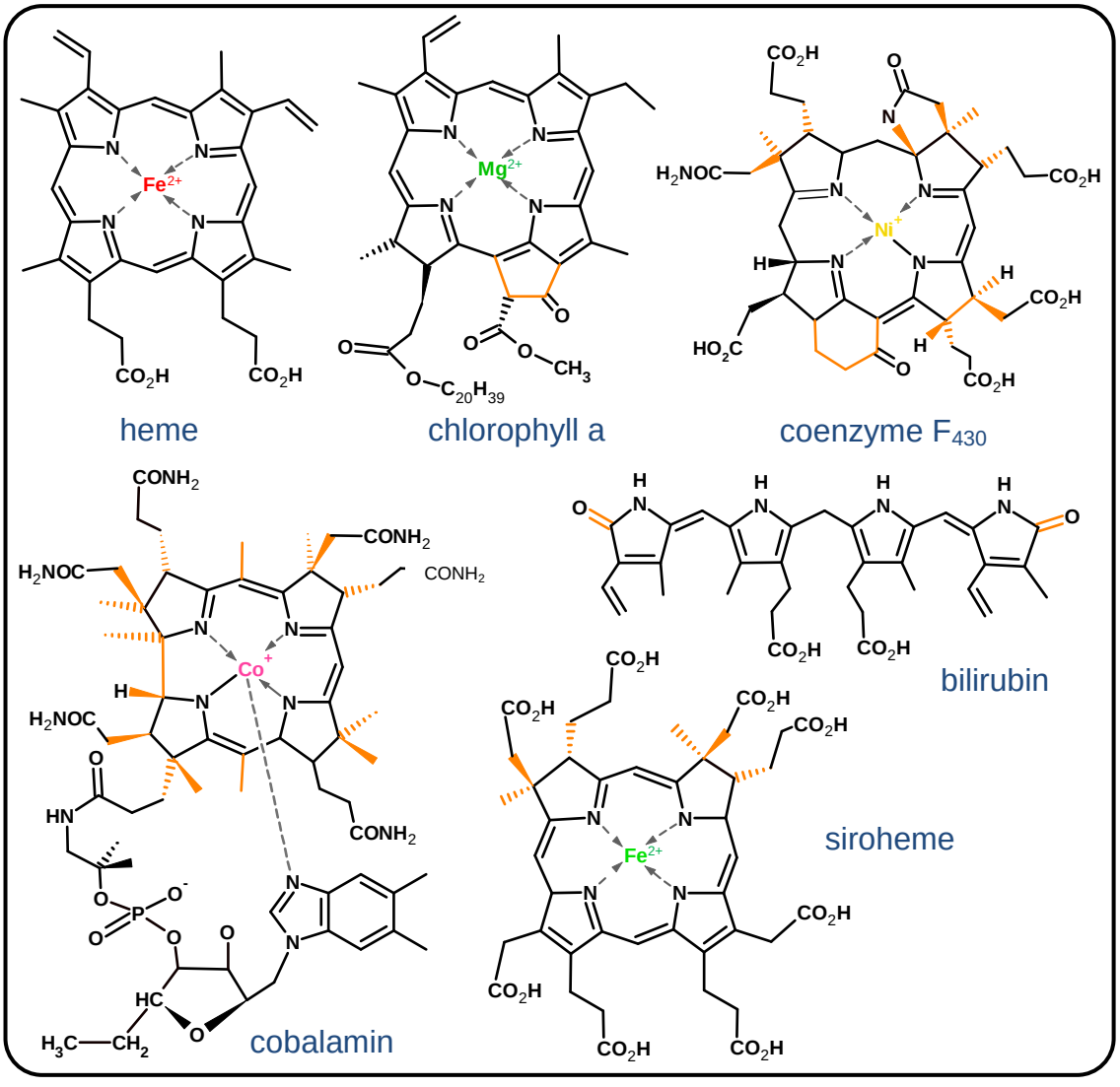

Figure 1-2: Structures of heme and other important representatives of naturally occurring tetrapyrroles. The colors of the tetrapyrroles are indicated by the colors of the chelated metal ions. Side chain substitutions changing the basic porphyrin structure are highlighted in orange.

Distinct features of tetrapyrroles allow their use in a range of technological and experimental applications. Their fluorescence makes them useful in activity assays of tetrapyrrole converting enzymes and phycobiliproteins are frequently employed as fluorescent markers in cell biology (Frankenberg *et al.*, 2003). Alternatively, the ability of porphyrins such as deuteroporphyrin and haematoporphyrin to absorb visible light and to generate reactive oxygen species allows their use in photodynamic therapies for the treatment of cancer (Dolmans *et al.*, 2003; Bertoloni *et al.*, 1984; Nitzan *et al.*, 1994). Protochlorophyllide, an intermediate in chlorophyll biosynthesis, has recently been proposed as a useful photosensitizer for photodynamic inactivation of antibiotic resistant bacteria requiring lower light intensities for bacteria inactivation than usually required for photodynamic inactivation procedures (Walther *et al.*, 2009). Protochlorophyllide may prove useful in applications like the sterilization of surfaces or food or in the treatment of burn wounds or skin infections. On the other hand this photoreactive characteristic of the tetrapyrroles can lead to severe clinical symptoms when tetrapyrroles accumulate unregulated as in the case of a group of inherited or acquired defects of enzymes involved in the heme biosynthetic pathway, the so-called porphyrias.

1.2 The First Steps in Heme Biosynthesis are Highly Conserved for All Tetrapyrroles

Essentially nothing was known about the biosynthesis of porphyrins prior to 1945, when Shemin and Rittenberg demonstrated by self-administration of [^{15}N]-labeled glycine that this amino acid is the source for heme nitrogen (Shemin and Rittenberg, 1945). Resulting intense studies of tetrapyrrole biosynthesis led to the identification of many of the enzymes involved. In the case of heme, the biosynthetic pathway has been fully described and a representative crystal structure of each enzyme has been solved and deposited in the PDB.

All tetrapyrroles including heme derive from the common precursor molecule 5-aminolevulinic acid (ALA) (**Figure 1-3**).

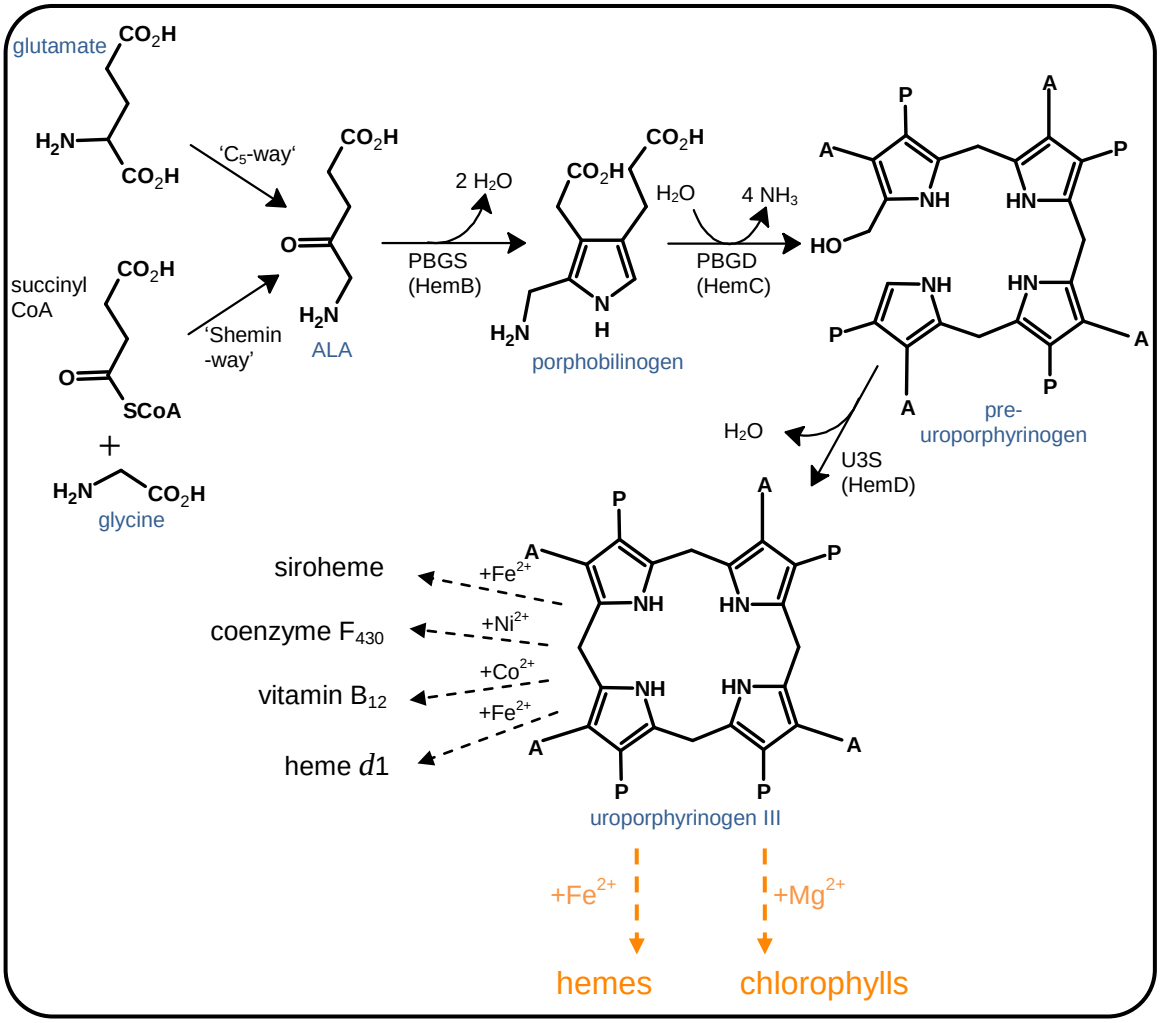

Figure 1-3: First steps of the tetrapyrrole synthesis. ALA is synthesized either by the 'Shemin-way' or the 'C_5-way'. Two molecules of ALA yield one molecule of porphobilinogen, four of which produce pre-uroporphyrinogen, which in turn is cyclized to uro'gen. Note the inversion of pyrrole ring D during this reaction. Names of enzymes catalyzing individual reactions are provided below the arrows. Uroporphyrinogen III is the last common intermediate in tetrapyrrole biosynthesis. A: acetate side chain; P: propionate side chain; ALA: 5-aminolevulinic acid; PBGS: porphobilinogen synthase; PBGD: porphobilinogen deaminase; U3S: uro'gen synthase.

ALA, however, is synthesized by two distinct routes. In the 'Shemin pathway', glycine and succinyl-CoA constitute the substrates for the synthesis of ALA (Shemin and Russell, 1953) catalyzed by the enzyme ALA synthase (ALAS) (Astner *et al.*, 2005; PDB entry: 2bwn). This path is common to animals, fungi, and α-proteobacteria (Kikuchi *et al.*, 1958). The second route or 'C_5-pathway' is found in most bacteria and plants and utilizes the carbon skeleton of glutamate. Overall, three enzymes are involved. First, glutamyl-tRNA synthetase activates glutamate by coupling it to $tRNA^{Glu}$ (Lapointe and Söll, 1972;

Schulze *et al.*, 2006; PDB entry: 2cfo). The NADPH-dependent glutamyl-tRNA reductase (GluTR) then generates glutamate-1-semialdehyde (GSA) (Ilag *et al.*, 1991; Jahn *et al.*, 1992; Moser *et al.*, 1999; Moser *et al.*, 2001; Schubert *et al.*, 2002; Moser *et al.*, 2002; PDB entry: 1gpj). GSA is, in turn, converted to ALA by glutamate-1-semialdehyde-2,1-aminomutase (GSAM) (Schulze *et al.*, 2006; PDB entry: 2cfb). The latter two enzymes presumably form a complex to protect the highly reactive intermediate GSA (Luer *et al.*, 2005).

Eight molecules of ALA are then used to construct uroporphyrinogen III (uro'gen), both the first cyclic and the last common intermediate of tetrapyrroles. These steps are conserved in all living organisms. First, two molecules of ALA are asymmetrically condensed by the porphobilinogen synthase (PBGS) to the pyrrole porphobilinogen (PBG) (Granick, 1954; Frankenberg *et al.*, 1999; Frère *et al.*, 2002; PDB entry: 1b4k). Four molecules of PBG are then linked by porphobilinogen deaminase (PBGD) to the unstable linear tetrapyrrole pre-uroporphyrinogen (Burton *et al.*, 1979). Finally, the orientation of ring D of pre-uroporphyrinogen is inverted and the molecule is cyclized by uro'gen synthase (HemD) resulting in uro'gen. Crystal structures of human apo-HemD and of HemD in complex with the product (Mathews *et al.*, 2001; Schubert *et al.*, 2008; PDB entries: 1jr2 and 3d8n) reveal a highly flexible protein requiring the movement of an entire domain from the open to the closed, substrate/product-bound conformation. The inversion of ring D means that heme and all intermediates are asymmetric molecules. In the absence of HemD pre-uroporphyrinogen cyclizes spontaneously without inversion of ring D resulting in the symmetric and toxic uroporphyrinogen I (Jordan *et al.*, 1979).

1.3 Biosynthesis of Heme and Chlorophyll from Uroporphyrinogen III

Uro'gen is the last common intermediate in tetrapyrrole biosynthesis. Its conversion to precorrin 2 leads to the synthesis of siroheme, heme *d*1, coenzyme F_{430}, and the corrinoids. The second branch, the focus of this section, leads to protoporphyrin IX (proto') (compare **Figure 1-3**). Its synthesis requires the consecutive decarboxylation of all four acetate side chains of uro'gen to methyl groups by uro'gen decarboxylase (HemE),

resulting in the product coproporphyrinogen III (copro'gen). The conversion of copro'gen to protoporphyrinogen IX (proto'gen) then involves the oxidative decarboxylation of the propionate side chains on pyrrole rings A and B to vinyl groups by copro'gen oxidase (CPO) (Sano and Granick, 1961), described in more detail in **section 1.4**.

Proto'gen is converted to proto' by the proto'gen oxidase (PPO) (Poulson, 1976; Koch *et al.*, 2004; PDB entry: 1sez). Proto' is the first oxidized tetrapyrrole with a largely planar, conjugated backbone resulting in absorption of visible light and hence a characteristic color. All preceding intermediates by contrast retain the reduced, non-planar, colorless skeleton of hexahydroporphyrins. Proto' marks the second major branching point in tetrapyrrole biosynthesis, as the last intermediate in heme and (bacterio)chlorophyll biosynthetic pathways. En route to heme, ferrochelatase inserts Fe^{2+} into proto' producing protoheme IX (heme b) (Dailey, 2002; Lecerof *et al.*, 2000; PDB entry: 1doz). Because the intermediate proto' is highly reactive, PPO and ferrochelatase form a complex to facilitate the direct transfer of this intermediate (Masoumi *et al.*, 2008).

1.4 Oxidative Decarboxylation of Coproporphyrinogen III by Two Distinct Enzymes in *E. coli*

The reaction preceding the production of proto' in heme biosynthesis involves the oxidative decarboxylation of copro'gen to the product proto'gen by copro'gen oxidase (CPO). The reaction and the molecules involved are outlined in **Figure 1-4**.

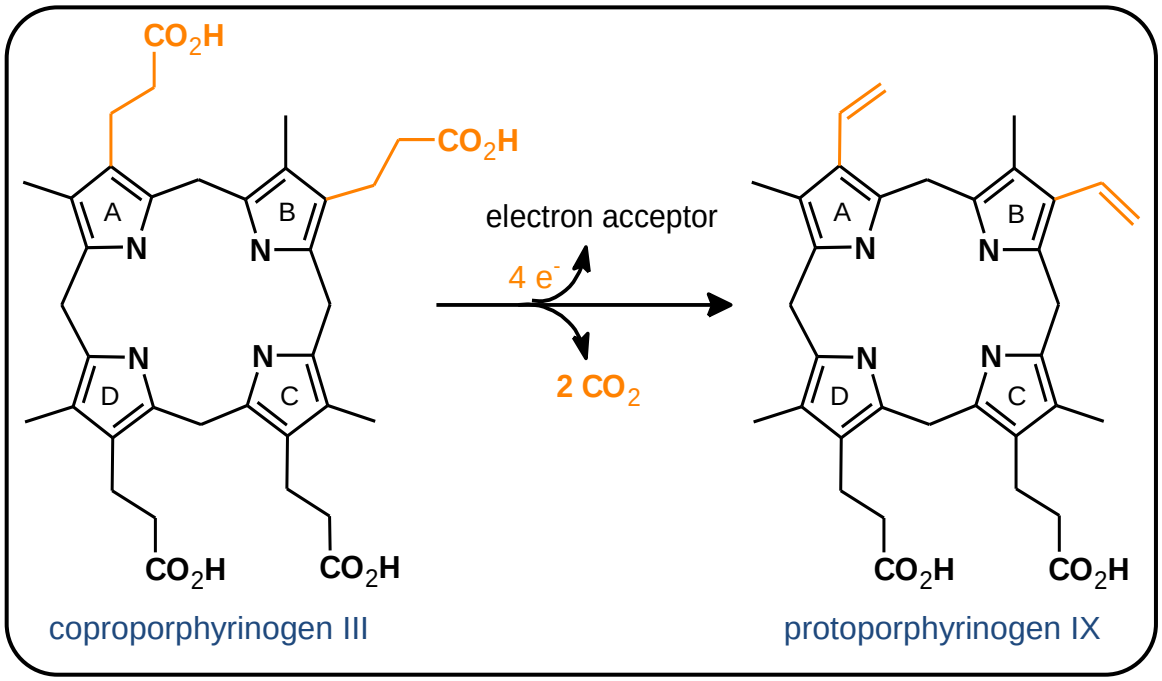

Figure 1-4: Reaction catalyzed by coproporphyrinogen III oxidases. Two propionate side chains on ring A and B of copro'gen are converted to vinyl groups yielding the product proto'gen. During the reaction, CO_2 is released. In addition, the reaction requires a terminal electron acceptor.

1.4.1 Oxygen Dependent Coproporphyrinogen III Oxidase

Mammalian CPO was described to be dependent on O_2 (Sano and Granick, 1961; Batlle *et al.*, 1965). The corresponding, oxygen-dependent CPO (HemF in *E. coli*) is well characterized; its crystallographic description includes enzymes from yeast, man, and *Leishmania* spp. (Phillips *et al.*, 2004; PDB entry: 1tk1; Lee *et al.*, 2005; PDB entry: 2aex and *inter alia* unpublished PDB entries 1vjn and 3ejo). Mutations in the human enzyme result in distinct porphyrias (either hepatic hereditary coproporphyria or erythropoietic harderoporphyria) (Schmitt *et al.*, 2005; Lee *et al.*, 2005). Despite numerous studies, the exact requirement for cofactors in different organisms is currently not resolved (Kohno *et al.*, 1996; Breckau *et al.*, 2003; Lash *et al.*, 1999). Several studies confirm that the propionate side chain of pyrrole ring A is converted prior to that of ring B (Cavaleiro *et al.*, 1973; Elder *et al.*, 1978; Jackson *et al.*, 1980) and that O_2 is essential. The precise mechanism of catalysis is, however, still unknown.

Heme-bearing cytochromes are also found in facultative anaerobe microorganisms indicating that ALA is also converted to proto' in the absence of molecular oxygen. An

oxygen independent CPO was hence inferred to exist for anaerobic bacteria and facultative anaerobes and a corresponding enzyme with a unique mechanism for the oxidative decarboxylation of copro'gen under anaerobic conditions was identified (Ehteshamuddin, 1968; Tait, 1969).

1.4.2 Oxygen Independent Coproporphyrinogen III Oxidase

First studies on the oxygen independent copro'gen oxidase were performed with cell free extracts from *Rhodobacter sphaeroides* (Tait, 1972) and the requirement of NADP, ATP, iron and L-methionine was suggested. Despite several further investigations, significant progress was only made in 1992 with the identification of the gene locus *hemN* which was proposed to be related to CPO activity under anaerobic conditions in *R. sphaeroides* and *Salmonella typhimurium* (Coomber *et al.*, 1992; Xu and Elliott, 1994). The *hemN* gene of *E. coli* could be cloned, the gene product HemN could be purified, and an enzyme assay for the recombinant purified enzyme could be developed (Troup *et al.*, 1995; Layer *et al.*, 2002). A characteristic CxxxCxxC amino acid motif, dependence on *S*-adenosyl-L-methione (SAM) as a cosubstrate of the reaction as well as the presence of a [4Fe-4S]-cluster were found to be important features of HemN (Layer *et al.*, 2002). Diverse spectroscopic analyses were performed to further characterize HemN. Coordination of the [4Fe-4S]-cluster, predominantly observed as a $[4Fe\text{-}4S]^{2+}$-cluster, by only three cysteines was deduced from Mössbauer spectroscopic data. The fourth iron atom was shown to be coordinated by a SAM molecule (Layer *et al.*, 2002). These findings are supported by the crystal structure of HemN presented in **Figure 1-5** (Layer *et al.*, 2003). HemN was shown to be a monomeric two-domain protein. The N-terminal domain comprises the cofactors and is also denoted as catalytic domain. The function of the C-terminal domain is yet unknown, but it is postulated to rearrange upon substrate binding to close the active site. The third structural feature is the so-called ‘trip-wire’ consisting of the N-terminal 35 amino acids that adopt an extended conformation without pronounced secondary structure and are partly disordered in the crystal structure. The ‘trip-wire’ is postulated to be involved in substrate recognition and induction of the C-terminal domain movement. The HemN crystal structure further allowed possible binding sites for the substrate, the electron donor, and electron acceptor to be proposed.

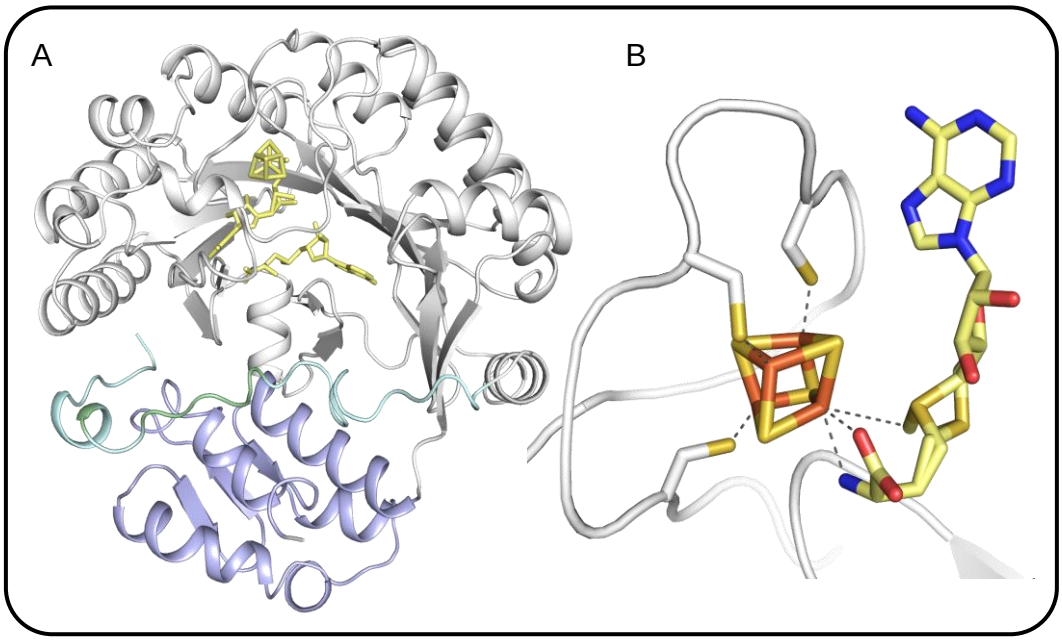

Figure 1-5: Crystal structure of HemN (PDB entry: 1olt). A: HemN is a monomeric two domain protein. Its N-terminal, catalytic domain (gray) is built around a twelve–stranded, largely parallel β–sheet surrounded on the convex side by α-helices. The C-terminal domain (blue) consists of a bundle of four roughly parallel α-helices and a small three stranded β-sheet. The first 35 amino acids adopt an extended conformation without pronounced secondary structure. They are referred to as a 'trip-wire' (amino acids not clearly defined in the electron density are shown in green, others in cyan). The [4Fe-4S]-cluster and two SAM-molecules are shown as yellow sticks. **B:** Coordination of the [4Fe-4S]-cluster by the CxxxCxxC-motif and the carboxylate and α-amino groups of SAM1.

EPR spectroscopy identified a substrate-based radical as part of the catalytic mechanism of HemN. Using synthetic, deuterated or [^{15}N]-labeled substrates, this radical was found to result from the abstraction of the pro-*S*-hydrogen atom from the β-carbon of the substrate propionate side chain (Layer *et al.*, 2006). The spin density of the corresponding allylic coproporphyrinogenyl radical is spread over the β-carbon of the propionate side chain and the α C-atom between methine bridge and pyrrole nitrogen. A reaction mechanism for HemN incorporating these data is presented in **Figure 1-6**. This stereospecific vinyl group formation needs to be repeated for both propionate groups on ring A and B of copro'gen and occurs both in aerobic and anaerobic reactions (Seehra *et al.*, 1983).

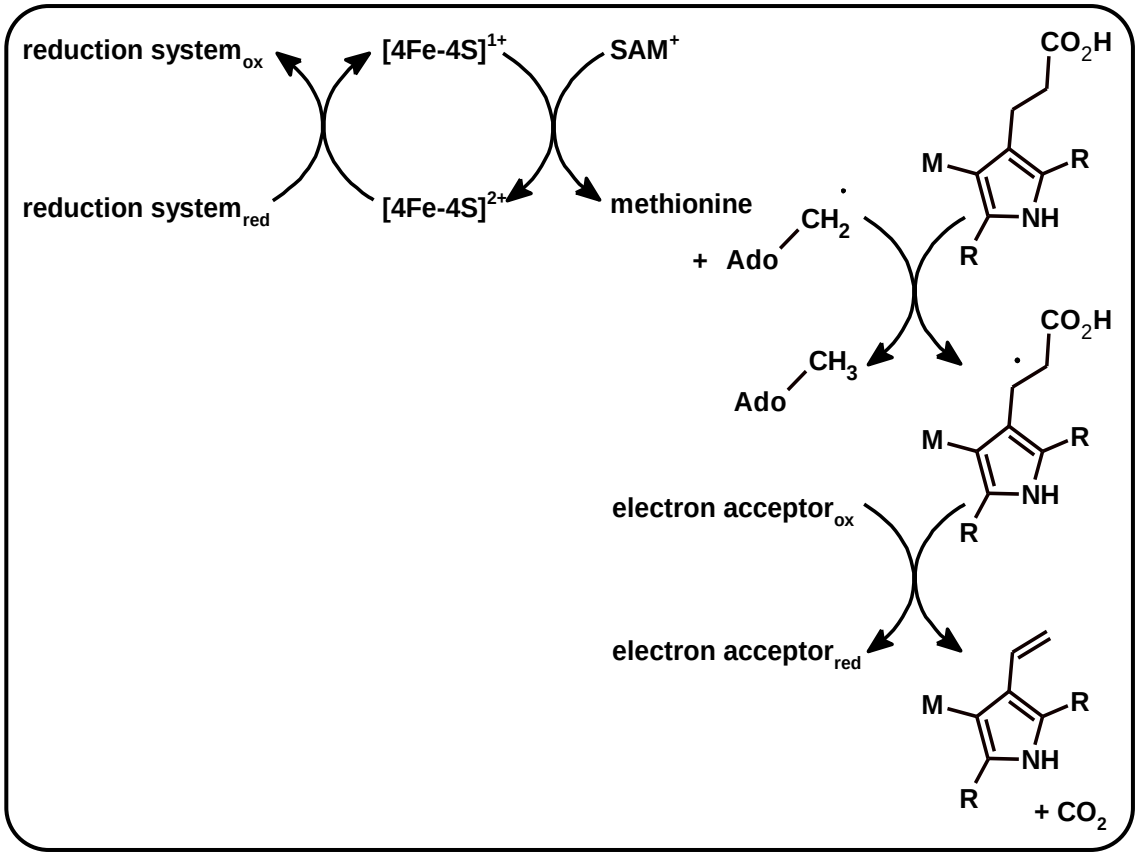

Figure 1-6: Proposed reaction mechanism for the oxidative decarboxylation of coproporphyrinogen III by HemN. First, the [4Fe-4S]-cluster is reduced by an as yet unidentified electron donor. The reduced cluster transfers an electron to SAM, which is cleaved to form methionine and a 5'-deoxyadenosyl radical. This radical abstracts a hydrogen atom from the β-carbon of the propionate side chain of pyrrole ring A or B of copro'gen resulting in 5'-deoxyadenosine and a substrate radical. In a concerted process CO_2 is released leaving the vinyl group of the product. (Modified from Layer (2004)). M: methyl group; R: tetrapyrrole.

In 2001 a bioinformatic classification identified HemN as a member of the Radical SAM enzyme superfamily together with 644 other enzymes. The family was divided into 31 subclasses. Features common to all enzymes include the dependence on *S*-(5-adenosyl)-L-methionine (SAM) and a radical based reaction mechanism (Sofia *et al.*, 2001). During the last few years, research on HemN and other Radical SAM proteins confirmed their membership to the Radical SAM family.

1.5 Radical SAM Enzymes Catalyze Chemically Difficult Reactions

The ancient family of Radical SAM enzymes is represented in all three kingdoms of life and catalyzes a diverse set of reactions in numerous pathways including biodegradation or the biosynthesis of DNA precursors, vitamins, or heme (Sofia *et al.,* 2001). The catalyzed reactions range from insertion of sulfur into unreactive carbon backbones (as in biotin synthase (BioB), liopoate synthase (LipA) or MiaB (Guianvarc'h *et al.*, 1997; Ollagnier-de Choudens *et al.*, 2000; Esberg *et al.*, 1999)), through glycyl radical generation (as in the activating enzymes (AE) of pyruvate formate lyase (PFL), anaerobic ribonucleotide reductase (ARNR), and glycerol dehydratase (GD) (Broderick *et al.*, 1997; Ollagnier *et al.*, 1997; Raynaud *et al.*, 2003)), to isomerization reactions (as in lysine-2,3-amino-mutase (LAM) (Lieder *et al.*, 1998)) or anaerobic oxidation (as in HemN). Of three maturating enzymes of [Fe]-hydrogenase (HydA), two (HydE and HydG) were found to be Radical SAM enzymes, but their exact functions remain to be elucidated (Posewitz *et al.*, 2004; Pilet *et al.*, 2009). Other examples include anaerobic sulfatase maturation enzymes (anSME) that post-translationally modify mammalian arylsulfatases (Benjdia *et al.*, 2007; Grove *et al.*, 2008), RimO, a MiaB-like Radical SAM enzyme (Anton *et al.*, 2008), or HMP-P synthase (ThiC) despite lacking the characteristic CxxxCxxC motif (Martinez-Gomez and Downs, 2008; Chatterjee *et al.*, 2008). ThiC catalyzes the complex intramolecular rearrangement from 5-aminoimidazole ribotide (AIR) to 4-amino-5-hydroxymethyl-2-methylpryimidine phosphate (HMP-P) in bacteria and plants during the thiamine pyrophosphate (vitamin B_1) biosynthesis. The need for a radical reaction mechanism often implies a complicated or chemically difficult reaction. This holds true for most Radical SAM enzymes.

Radical SAM family members have a conserved cysteine motif CxxxCxxC (CxxCxxxxC in ThiC), a glycine rich sequence involved in SAM binding, and a conserved core domain (Sofia *et al.*, 2001). They, furthermore, all use a low-potential $[4Fe\text{-}4S]^{1+}$-cluster to generate a strong reducing agent that reduces SAM causing it to split and giving rise to methionine and a 5'-deoxyadenosyl radical. The latter initiates the radical enzyme reaction (the first reaction steps in **Figure 1-6**). The [4Fe-4S]-cluster of Radical SAM

enzymes is special in that only three iron atoms are coordinated by cysteine residues namely those of the conserved cysteine-rich motif, whereas the fourth iron atom is ligated by a SAM molecule. This cofactor arrangement was structurally confirmed *inter alia* by the first Radical SAM crystal structure, the structure of HemN (see **Figure 1-5**). The characterization of Radical SAM enzymes has uncovered unexpected new functions of both iron-sulfur clusters (FeS-clusters) and SAM.

1.5.1 Iron-Sulfur Clusters and their Biosynthetic Machinery

FeS-clusters are ancient cofactors, ubiquitous to biological systems, and proposedly involved in the emergence of life on earth (Huber and Wächtershäuser, 1997). They actively participate in a broad range of functions such as electron transport in respiration or photosynthesis, redox and non-redox catalysis, iron or cluster storage, and gene regulation (for reviews see Cheek and Broderick, 2001 and Johnson *et al.*, 2005). The mammalian ferrochelatase, the enzyme catalyzing the last step in heme biosynthesis, is an appropriate example for the regulation of a protein by a [2Fe-2S]-cluster. In the presence of NO, the cluster of this enzyme is disassembled, leading to the inactivation of ferrochelatase. The reason for this is presumably to keep invading organisms from utilizing heme synthesized by the host (Sellers *et al.*, 1996). The finding, that [4Fe-4S]-clusters are also able to initiate radical catalysis as in the Radical SAM enzymes further expands the spectrum of functions of this prosthetic group.

Cysteines normally serve to complete the tetrahedral sulfur coordination of each iron site of FeS-clusters. In some proteins, cysteine ligands may, however, be replaced by histidine (as in all Rieske proteins), aspartate, serine or the backbone amide (Johnson *et al.*, 2005; Hou *et al.*, 2007). In the Radical SAM proteins and in aconitase, SAM and citrate respectively coordinate the fourth iron centre (Kennedy *et al.*, 1987). **Figure 1-7** presents the structure of a subset of FeS-clusters. The remarkable functional and structural diversity underlines the chemical versatility of the constituent elements iron and sulfur.

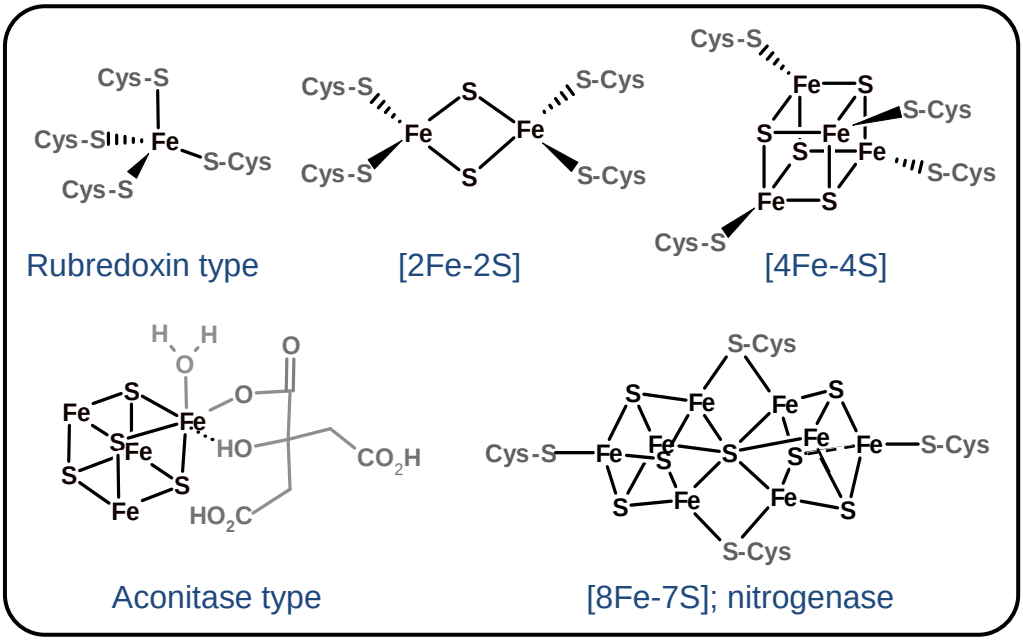

Figure 1-7: Representative iron-sulfur clusters in biological systems. The iron centers of [2Fe-2S]- and [4Fe-4S]-clusters are generally coordinated by cysteine ligands in proteins. In aconitase the fourth iron of the [4Fe-4S]-cluster is not coordinated by a cysteine. Its coordination sphere changes from tetragonal to octahedral on binding of citrate. The [8Fe-7S]-cluster (P-cluster) from nitrogenase is an example of more complex FeS-clusters. (Modified from Kiley and Beinert, 2003; Beinert, 2000; and Frazzon and Dean, 2003).

Although FeS-clusters can occasionally be reconstituted *in vitro* through the addition of sulfide and ferrous iron (Malkin and Rabinowitz, 1966), FeS-clusters do not form spontaneously in the cytosol. In particular, both Fe^{2+} and sulfide are toxic at concentrations required for *in vitro* cluster reconstitution. Instead, a complex biosynthetic machinery continuously synthesizes, disassembles, and rebuilds FeS-clusters. In eukaryotes, FeS-cluster biosynthesis predominantly takes place in mitochondria. Constituent elements or even entire FeS-clusters need to be transported across membranes with the help of a specialized machinery (Lill and Mühlenhoff, 2005).

Initial studies on bacterial FeS-cluster biosynthesis concentrated on enzymes catalyzing cluster formation in nitrogenase (Nif). This system is related to both the sulfur mobilization (Suf) and the iron-sulfur-cluster (Isc) systems. Each system requires a cysteine desulfurase (NifS/IscS) to provide sulfide and presumably FeS-cluster scaffold proteins (NifA/U or IscA/U) (Johnson *et al.*, 2005). The dynamic interaction of the desulfurase IscS and IscU and the scaffold function of the latter were validated for the Isc

system, encoded by the *iscRSUA* operon (Raulfs *et al.*, 2008), whereas IscR is required to regulate the process (Barras *et al.*, 2005). IscA presumably is an iron chaperone that recruits Fe^{2+} for FeS-cluster assembly under aerobic conditions (Yang *et al.*, 2006). Oxidative stress and iron starvation induce the Suf system in *E. coli* resulting in the production of a five-enzyme complex encoded by the operon *sufABCDSE* (Outten and Storz, 2004; Layer *et al.*, 2007).

1.5.2 *S*-(5-Adenosyl)-L-methionine is an Important Cofactor in Diverse Reactions

In the past, the role of *S*-(5-adenosyl)-L-methionine (SAM) was thought to be largely restricted to methylation reactions (Frey and Magnusson, 2003; Wang and Frey, 2007). The generation of radicals from SAM, first described in the 1980s (reviewed in Frey and Magnusson, 2003), was therefore rather surprising. As part of this process, SAM is homolytically cleaved. The resulting 5'-deoxyadenosyl radical invariably abstracts an appropriately positioned hydrogen atom generating either a substrate- or a protein radical (Layer *et al.*, 2004). In some enzymes, SAM acts as a true catalytic cofactor being regenerated at the end of the reaction. Examples of such enzymes include lysine 2,3-aminomutase (LAM) and spore photoproduct lyase (Wang and Frey, 2007). Mostly, however, SAM functions as a cosubstrate resulting in the release of methionine and 5'-deoxyadenosine after each turn-over. Enzymes of this type include ARNR-AE, PFL-AE, and biotin synthase (BioB) (Padovani *et al.*, 2001; Knappe *et al.*, 1984; Moss and Frey, 1990). HemN also belongs to the latter group as SAM is consumed as a cosubstrate during the reaction. In line with HemN having to generate two vinyl groups, it consumes two molecules of SAM per catalytic turn-over (Layer *et al.*, 2005a).

A related mechanism of generating 5'-deoxyadenosyl radicals is based on the homolytic cleavage of the Co-C5' bond of adenosylcobalamin. This mechanism does not require the transfer of an additional electron and the cofactor is invariably regenerated at the end of each reaction cycle. Though potentially representing a more elegant solution to an identical problem, adenosylcobalamin-dependent enzymes do not catalyze nearly as wide a range of reactions as Radical SAM family members, being largely restricted to isomerization reactions or the reduction of ribonucleotides (Frey and Magnusson, 2003).

1.5.3 Structural Information on Radical SAM Enzymes

Currently, crystal structures of eight distinct Radical SAM enzymes have been solved and published (**Figure 1-8**). The crystal structure of the first, HemN, in 2003 (Layer *et al.*, 2003) was rapidly followed by those of BioB and MoaA (Berkovitch *et al.*, 2004; Hänzelmann and Schindelin, 2004). These crystal structures confirm a common core domain of 200 amino acids for this family proposed on the basis of multiple sequence alignments (Sofia *et al.*, 2001), identifying this domain as an incomplete $(\beta/\alpha)_6$ TIM barrel (Layer *et al.*, 2004) extended to a complete $(\beta/\alpha)_8$ barrel in other enzymes (Nicolet and Drennan, 2004; Layer *et al.*, 2005b). More recent crystal structures of LAM, the tRNA modifying enzyme TYW1, HydE, PFL-AE, and of ThiC confirm this common $(\beta/\alpha)_6$-core for the Radical SAM enzymes (Lepore *et al.*, 2005; Chen *et al.*, 2006; Suzuki *et al.*, 2007; Goto-Ito *et al.*, 2007; Nicolet *et al.*, 2008; Vey *et al.*, 2008; Chatterjee *et al.*, 2008). This core domain invariably constitutes the catalytic domain bearing all elements required for radical generation. The architecture of the catalytic barrel reflects the size of the substrate with small ligands such as dethibiotin in BioB being bound in an uninterrupted $(\beta/\alpha)_8$-barrel, whereas larger substrates such as copro'gen in HemN or polypeptide chains in the activating enzymes require the lateral opening of the TIM-barrel. C-terminal extensions of the core domains are similarly highly variable again reflecting their role in binding a highly diverse set of substrates (Nicolet and Drennan, 2004). **Figure 1-8** presents the known crystal structures of Radical SAM enzymes.

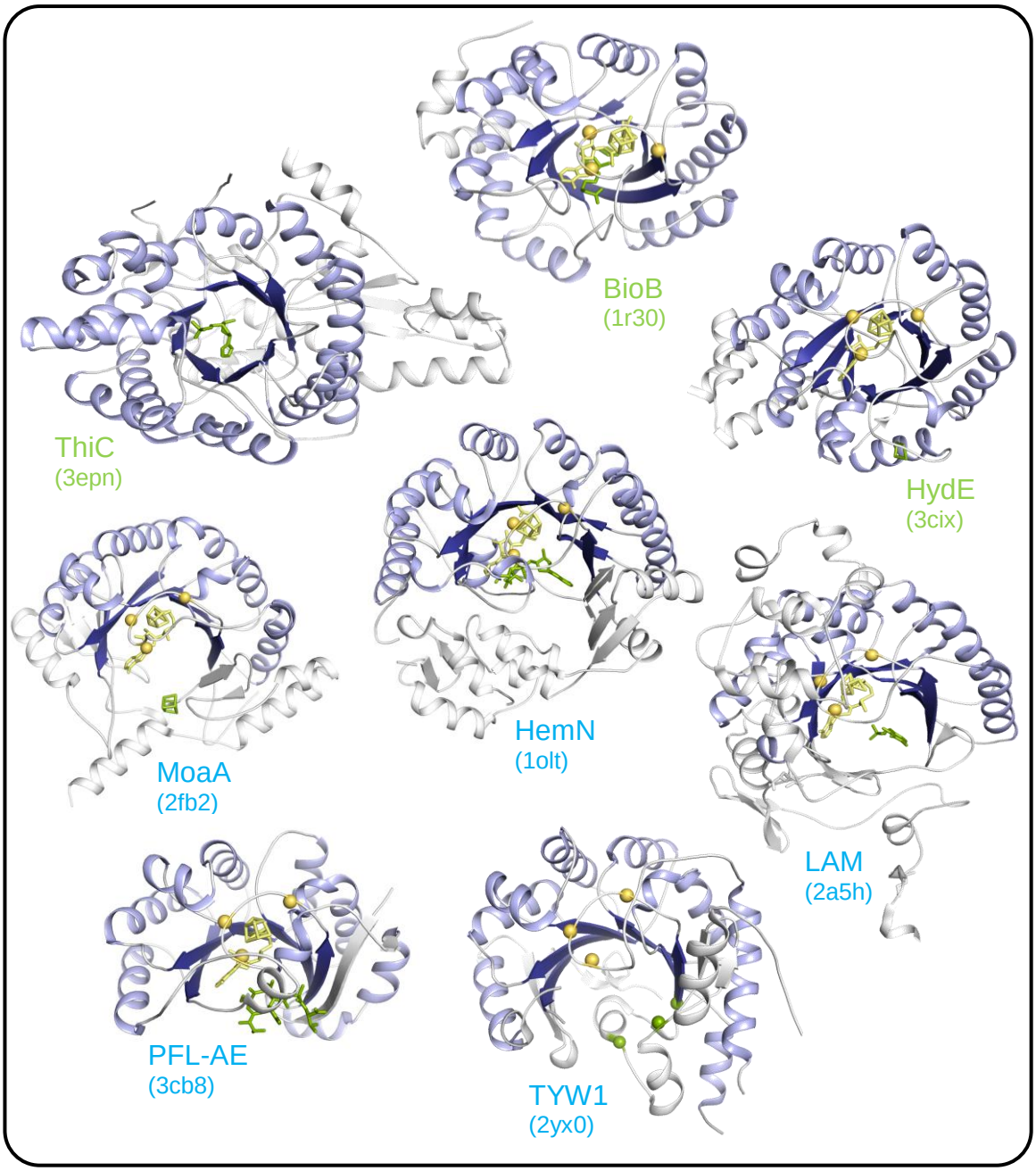

Figure 1-8: Crystal structures of Radical SAM enzymes. Crystal structures of monomeric HemN, HydE, TYW1, and monomers of homodimeric MoaA, PFL-AE, BioB, ThiC or homotetrameric LAM are shown as cartoon diagrams. The structural core of each protein is highlighted with β-sheets in dark blue and α-helices in light blue. Proteins with a complete $(\beta\alpha)_8$ barrel are labeled in green, those with a ¾-barrel (six βα-repeats) in blue. Additional domains of each protein are offset by their gray color. The [4Fe-4S]-cluster and the SAM molecule, common to all Radical SAM enzymes are shown as yellow sticks (if present in the crystal structure), while cysteines of the conserved CxxxCxxC-motif are marked by yellow spheres. Additional features of each structure are presented in green: a [2Fe-2S]-cluster and the substrate dethiobiotin in BioB; an imidazole ribonucleotide in ThiC, a [2Fe-2S]-cluster in HydE, a [4Fe-4S]-cluster in MoaA, a second SAM molecule in HemN, PLP in LAM, a peptide substrate in PFL-AE, and three conserved cysteines, probably involved in coordination of a [2Fe-2S]-cluster in TYW1. The CxxCxxxxC-loop involved in FeS-cluster coordination of ThiC is not resolved in the electron density.

In addition to common features of Radical SAM enzymes, biochemical and structural characterizations identified unique features for some family members. BioB, MoaA, AtsB, and RimO were found to bear a second or even a third FeS-cluster, proposedly to serve as a source of sulfur for the sulfur-insertion reactions catalyzed by these enzymes (Booker *et al.*, 2007; Hernández *et al.*, 2007). LAM was structurally found to bind an additional pyridoxal-5'-phosphate (PLP) cofactor (Lepore *et al.*, 2005), whereas HemN was found to bind a second SAM molecule (SAM2) (Layer *et al.*, 2003). This SAM2 of HemN is bound within the presumed substrate binding pocket, directly adjacent to the SAM molecule (SAM1) involved in cluster coordination. The presence of the second SAM molecule matches the requirement for two SAM molecules for the conversion of two propionate side chains per copro'gen substrate molecule. Mutational studies confirmed that some residues involved in SAM2 coordination are important for SAM-cleavage and HemN activity. Whether SAM2 is physiologically relevant has however not been finally investigated. MiaB similarly also consumes two SAM molecules per reaction, though the second SAM appears to serve as a more traditional methyl group donor (Pierrel *et al.*, 2004).

2 Aims and Scope

Despite an expanding set of crystal structures of Radical SAM enzymes, knowledge about the diverse reaction mechanisms of this enzyme class is still limited. HemN as member of this fascinating protein family functions in heme biosynthesis under anaerobic conditions. It catalyzes the oxidative decarboxylation of copro'gen converting it to proto'gen by oxidatively decarboxylating two propionate side chains on pyrrole rings A and B to the corresponding vinyl groups. The crystal structure of substrate-free HemN from *E. coli* had previously been solved while mutational and spectroscopic analyses have provided a wealth of functional data for HemN. Based on these data, a reaction mechanism was postulated involving the closure of the active site following substrate binding.

Numerous questions regarding the catalytic mechanism of HemN, however, remain to be answered. Two outstanding questions are the mode of substrate binding of HemN and the physiologic relevance of the second SAM molecule. Those were to be addressed *inter alia* by structural and biochemical characterization of HemN variants. At the beginning of this project, a crystal structure of HemN in complex with a substrate molecule was assumed to constitute a firm basis to provide deeper insights into enzyme and substrate arrangement and into the function of the second SAM molecule. Correspondingly one aim of this thesis was to generate a substrate-, intermediate- or product bound crystal of HemN from *E. coli* and to solve and refine the corresponding crystal structures. Techniques required to achieve this objective involved establishing an anaerobic working station in the laboratory as a basis for subsequent experiments. The expression and purification protocols of *E. coli* HemN and suitable mutants were to be improved to reproducibly ensure the availability of large amounts of intact and crystallizable protein. Co-crystallization experiments and soaking of pre-grown crystals with substrate were to be set up, while the substrate itself was to be generated both chemically and biochemically. Because procuring sufficient amounts of the substrate represented a major bottleneck to the project, its generation, characterization as well as those of potential intermediates and the product had to be established.

3 Materials and Methods

If not stated otherwise, all chemicals used were of '*pro analysis'* grade and were purchased from the companies Amersham Biosciences, Difco, Fluka, Hampton Research, Merck, Millipore, QIAGEN, Riedel de Haen, Roche, Roth, Sigma, and Stratagene. Molecular-biological methods used in this work are adapted from standard collections of methods and protocols (Sambrook and Russell, 2000; Coligan, 2003; Ausubel *et al.*, 2007). These methods will not be explained in detail. Only variations of standard protocols have therefore been described below.

3.1 Molecular Weight Standard

The 'Low Molecular Weight Marker' (SM0431) from Fermentas was used for SDS-PAGE analysis of proteins.

3.2 Bacterial Strains

Table 3-1 summarizes the bacterial strains used throughout this thesis.

Table 3-1: Bacterial strains.

E. coli strain	Genotype	Source
TOP10	F^-, *mcr* A Δ(*mrr-hsd*RMS-*mcr*BC) Φ80 *lacZ* Δ M15 Δ*lac*X74 *rec*A1 *ara*D139 Δ(*ara-leu*)7697 *gal* U *gal* K *rps*L *end*A1 *nup*G	Invitrogen
XL1-Blue supercompetent cells	*rec*A1 *end*A1 *gyr*A96 *thi-1 hsd*R17 *sup*E44 *rel*A1 *lac* [F´*pro*AB $lacI^qZ\Delta M15$ Tn*10* (Tet^r)].	Stratagene
BL21 (DE3)	F^- *dcm omp*T *hsd*S(r_B^- m_B^-) *gal* λ(DE3)	Stratagene
BL21 CodonPlus® (DE3)-RIL	B F^- *omp*T *hsd*S(r_B^- m_B^-) dcm^+ Tet^r *gal* λ (DE3) *end*A Hte [*arg*U *ile*Y *leu*W Cam^r]	Stratagene
Tuner™ (DE3)	F^-*omp*T *hsd*S_B (r_B^- m_B^-) dcm^+ dam^- *gal-lac*Y1 (DE3)	Novagen

3.3 Plasmids

The following expression plasmids were used throughout.

Table 3-2: Employed plasmids.

Plasmid	Description	Reference
pET-3a-*hemN*	pET-3a derivative encoding *E. coli* HemN	Layer *et al.*, 2003
pET-3a-*hemN*_R22A	Exchange of triplet CGA (nucleotides 64-66) for GCA, protein carries Ala instead of Arg in position 22	Grage, 2005
pET-3a-*hemN*_R22K	Exchange of triplet CGA (nucleotides 64-66) for AAA, protein carries Lys instead of Arg in position 22	this work
pET-3a-*hemN*_Q78A_H80A	Exchange of triplets CAG (nucleotides 232-234) for GCG and CAC (nucleotides 238-240) for GCC, protein carries Ala instead of Gln or His in position 78 or 80	this work
pET-3a-*hemN*_D87R	Exchange of triplet GCA (nucleotides 259-261) for CGC, protein carries Arg instead of Asp in position 87	this work
pET-3a-*hemN*_T247R	Exchange of triplet AGG (nucleotides 739-741) for ACC, protein carries Arg instead of Thr in position 247	this work
pET-3a-*hemN*_Q311N	Exchange of triplet CAG (nucleotides 931-933) for AAC, protein carries Asn instead of Gln in position 311	this work
pET-3a-*hemN*_R359A	Exchange of triplet CGT (nucleotides 1075-1077) for GCT, protein carries Ala instead of Arg in position 359	this work
pET-3a-*hemN*_R359K	Exchange of triplet CGT (nucleotides 1075-1077) for AAG, protein carries Lys instead of Arg in position 359	Grage, 2005
psD1	pET-14b derivative encoding *Bacillus megaterium* HemC	Raux *et al*., 2003
psD2	pET-14b derivative encoding *Bacillus megaterium* HemD	Raux *et al*., 2003
pHt#77	pAED4 with His-Tag from pET16b encoding human HemE	Phillips *et al.*, 1997
pGEX-2T:*CPO*_R401K	pGEX-2T derivative with GST fusion encoding human HemF with an aa exchange of Arg to Lys in position 401	Schmitt *et al*., 2005
pSL219	*E. coli iscS* gene subcloned from pSL209 (*Nco*I/*Bam*HI in pET15b) into *Bam*HI site of pACYC184	Leimkuhler and Rajagopalan, 2001; Hänzelmann *et al.*, 2004

3.4 Oligonucleotides

Oligonucleotides were used as primers for site-directed mutagenesis and PCR reactions. They were purchased from Invitrogen or Biozym (desalted and HPLC-purified). Site directed mutations in *hemN* were introduced by the QuikChange Mutagenesis^{TM}-Kit (Stratagene) according to the manufacturer's protocol and verified by DNA-sequencing by the company GATC. Sequencing was performed using the dye terminator method and the results were provided as ABI chromatogram files. Chromatograms were analyzed and compared using the program CONTIGEXPRESS from VECTORNTI (Invitrogen). Mutations and corresponding mutagenesis primers are summarized in **Table 3-3**.

Table 3-3: Primers used for mutagenesis reactions. Mutation sites are underlined and bold. Reverse primers are complementary to those of the corresponding forward-primers.

hemN-mutation	length [bp]	sequence (5'→3')
T247R	35	GCTGAGCAGCAAAAAT**CC**TCGGCAGATGCGCGTAG
D87R	32	CTTGCTCCAGCGCG**CG**CAGATACTGATCGGCC
Q78A_H80A	44	GATACTGATCGGCCTTG**GC**CTGC**GC**GCGAGTAACAATCT TATTG
Q311N	40	CGTGCTGCATCGTAACTTC**A**A**C**GGCTACACCACTCAGGGC
R359A	33	GGCAATGCGCTGTGG**GC**TGGTATTGCGCTAACG

3.5 Crystallization Screens

The following commercial screens (QIAGEN) were used to screen for initial crystallization conditions:

The Anions	The MbClass I + II	The pH-Clear I
The Cations	The Sparse Matrix 1-5	SFP (JCSG+)
The Classics I + II	The MPDs	PACT
The Cryos	The PEGs	

3.6 Buffers and Media

Media sterilized by autoclaving (121 °C, 2 bar, 20 min, Infection Control, Belimed). Heat-sensitive additives were sterile filtered (pore width 0.2 µm). Antibiotics were added after media had cooled to below 50 °C. Depending on the plasmid and bacterial strain, the following end concentrations of antibiotics were used: ampicillin (Amp) 100 µg/mL, kanamycin (Kan) 30 µg/mL, chloramphenicol (Cm) 34 µg/mL.

Buffers, which were used under anaerobic conditions, were de-aerated by alternating cycles of vacuum and nitrogen gassing (1 bar) using a home-made controller, kindly provided by Dr. Martina Jahn (TU Braunschweig). Smaller volumes were prepared from de-aerated stock solutions and de-aerated water.

Table 3-4: Media used in bacteria cultivation for protein production.

Medium	Composition
Lysogeny Broth (LB)	10 g/L tryptone; 7 g/L NaCl; 5 g/L yeast extract
Terrific Broth (TB)	12 g/L tryptone; 24 g/L yeast extract; 4 mL/L glycerol; 1 g/L casamino acids; after autoclaving: 100 mL/L KH_2PO_4/K_2HPO_4 (0.17 M/0.72 M); 20 mL/L 1 M glucose monohydrate; 50 µg/L thiamine chloride hydrochloride
MDG (non-inducing)	25 mM Na_2HPO_4; 25 mM KH_2PO_4; 50 mM NH_4Cl; 5 mM Na_2SO_4; 2 mM $MgSO_4 \cdot 7\ H_2O$; 0.2 x trace metal mixture; 0,5 % glucose; 0.25 % aspartate
ZYM502 (auto-inducing)	1 % tryptone; 0.5 % yeast extract; 25 mM Na_2HPO_4; 25 mM KH_2PO_4; 50 mM NH_4Cl; 5 mM Na_2SO_4; 2 mM $MgSO_4 \cdot 7\ H_2O$; 0.2 x trace metal mixture; 0.5 % glycerol; 0.05 % glucose; 0.2 % lactose
Trace metal mixture	13.52 g/L $FeCl_3$ x 6 H_2O; 2.2 g/L $CaCl_2$ x 2 H_2O; 1.98 g/L $MnCl_2$ x 4 H_2O; 2.88 g/L $ZnSO_4$ x 7 H_2O; 0.34 g/L $CuCl_2$ x 2 H_2O; 0.48 g/L $CoCl_2$ x 6 H_2O; 0.48 g/L Na_2MoO_4 x 2 H_2O; 0.048 g/L $NiCl_2$ x 6 H_2O; 0.25 g/L Na_2SeO_3; 0.12 g/L H_3BO_3; 60 mM HCl
SMM	2.0 g/L $(NH_4)SO_4$; 14.0 g/L K_2HPO_4; 6.0 g/L KH_2PO_4; 1.0 g/L Na_3 citrate x 2 H_2O; 0.2 mg $MgSO_4$ x 7 H_2O; 100 mL SMM mix, 10 mL trace elements, after autoclaving: 25 mg/L $(NH_4)_2Fe(SO_4)_2$ x 6 H_2O, 10 mM $NaNO_3$
SMM mix	0.005 g/L thiamine chloride hydrochloride; 100.0 g/L glucose monohydrate; 55.0 g/L Na-pyruvate; 1.0 g/L casamino acids
Trace elements	0.8 g/L $CaCl_2$ x 2 H_2O; 1.15 g/L $FeCl_2$ x 4 H_2O; 0.1 g/L $MnCl_2$ x 4 H_2O; 0.17 g/L $ZnCl_2$; 0.04 g/L $CuCl_2$ x 6 H_2O; 0.06 g/L $CoCl_2$ x 6 H_2O; 0.06 g/L Na_2MoO_4 x 2 H_2O

3.7 Protein Production and Purification

3.7.1 Test Expressions

Small-scale test expressions prior to preparative protein production were used to optimize the expression of novel gene constructs. Expression constructs were transformed into suitable bacterial expression hosts. 5 mL precultures from single colonies with appropriate antibiotics were grown over night at 37 °C. Expression test cultures of 50 mL medium/antibiotics were inoculated with the preculture (OD_{600} = 0.15) and incubated at 37 °C to an OD_{600} ~0.45, shifted to the expression temperature (20, 30, and 37 °C), and induced at OD_{600} ~0.6 with 0.4 mM IPTG (end concentration). Samples were taken after 2 h, 4 h, and after overnight induction and their OD_{600} was determined. Samples were centrifuged (21000 g, 1 min) and resulting cell pellets resuspended in 100 µL BugBuster® lysis buffer (0.2 mg lysozyme and 1 µL Benzonase® added per mL of BugBuster® solution) per 1 mL cell culture with an OD_{600} = 1. After 20 min incubation at room temperature the tubes were centrifuged (21000 g, 10 min) and the supernatant containing soluble proteins was removed and stored for analysis. Proteinaceous material remaining in the insoluble pellet was retrieved by resuspending the pellet in an equivalent volume of 8 M urea (50 mM Tris-buffered, pH 8). Aliquots of soluble and insoluble fractions were analyzed by SDS-PAGE

3.7.2 Recombinant Protein Synthesis

For aerobic protein production, cells carrying the desired plasmid were taken from a glycerol stock and grown in a 50 mL starter culture in LB-medium supplemented with the appropriate antibiotics at 37 °C and shaking at 180 rpm. Erlenmeyer flasks with 3-4 baffles were used to ensure sufficient aeration. After overnight incubation, the starter culture was used to inoculate 2 L of selective LB-medium with a starting OD_{600} of 0.15. This main culture was grown to exponential phase (OD_{600} 0.6–0.8) at 37 °C and 180 rpm, then shifted to the optimal expression temperature as determined by the test expression. Gene expression of HemN, HemC, HemD, and HemF was induced with IPTG. For HemE, the preculture was set up in MDG-medium and the main culture in ZYM505 medium. As ZYM505 is an autoinducing medium, no induction with IPTG was necessary in this case. As this medium contains both glucose and lactose, the bacteria first use glucose as carbon source, while glucose also serves to repress the lactose operon (catabolite repression). Once glucose has been exhausted, lactose serves as an inducer for expression of the target genes controlled by the LacI repressor. Lactose-induced gene expression is not as strong as that by IPTG such that the nascent target protein chain has more time to fold correctly. In theory the bacterium produces more biomass and proportionally more soluble target protein.

After expression all cells were harvested by centrifugation (6500 g, 10 min). If not used directly for protein purifications, resulting pellets were resuspended in an appropriate buffer, transferred into a reaction tube, and stored at -20 °C until use.

Table 3-5: Expression conditions for different protein expressions and main conditions for affinity chromatography.

Protein	Induction with IPTG [µM]	Expression temperature/ duration	*E. coli* strain for expression	Affinity matrix	Elution
HemN and its variants (aerobic)	50	25 °C / 4 h	BL21 (DE3)	Blue Sepharose™	0-2 M NaCl
HemN and its variants (anaerobic)	50	17 °C / o.n.	BL21 (DE3)	Blue Sepharose™	0-2 M NaCl
HemC	100	20 °C/ o.n.	BL21 (DE3) pLysS	Ni-NTA sepharose	0.4 M imidazole
HemD	100	20 °C/ o.n.	BL21 (DE3) pLysS	Ni-NTA sepharose	0.4 M imidazole
HemE	auto-induction	37 °C/ 8 h	BL21 (DE3) pLysS	Ni-NTA sepharose	0.4 M imidazole
HemF	50	25 °C/ o.n.	BL21 CodonPlus® (DE3)-RIL	GSH-sepharose	0.01 M glutathione
IscS	50	25 °C/ o.n.	BL21 (DE3) Tuner™	Ni-NTA sepharose	0.5 M imidazole

For anaerobic HemN production, anaerobic flasks were filled to 90 % with SMM minimal medium with all antibiotics and additives, inoculated under aerobic conditions, and tightly locked with a septum. For bacterial growth, the cultures were incubated at 37 °C and at 17 °C for protein production. Protein expression was induced at an OD_{600} of 0.35 and was performed o.n.. Rotation speed for anaerobic cultures was 100 rpm. Sample drawing and addition of IPTG were performed with a syringe and a cannula pierced through the septum. For cell harvesting the cultures were locked into the anaerobic chamber where centrifugation flasks were filled and balanced. After centrifugation for 10 min at 6500 g, cell pellets were anaerobically transferred into small anaerobic flasks and stored at -20 °C.

3.7.3 Cell Lysis

All steps were performed on ice or at 4 °C to prevent proteolytic degradation of the target. The cell pellet obtained by centrifugation was resuspended in the appropriate buffer (50 mM Tris pH 8.0; 3 mM DTT for HemN and 50 mM Tris pH 8.0; 150 mM NaCl; 3 mM DTT for other proteins) with 2 µL Benzonase® and protease inhibitor cocktail 'Complete EDTA-free' (Roche). For HemN purification, 0.1 % C_8E_4 (or 0.1 % Triton

X-100, if the protein was not used for crystallization setups) was added to the resuspension buffer. Cells were either disrupted by a single anaerobic passage through a French Press at 1500 p.s.i. or by ultrasonication (Bandelin Sonoplus HD 200) under aerobic or anaerobic conditions. For anaerobic protein purifications the ultra sonifier was locked into the anaerobic chamber. Cells were disrupted by 5 cycles of sonication at 50 % for 20 s each.

Cell debris and the insoluble protein fraction were removed by centrifugation for 60 min at 32000 g. The resulting supernatant was loaded onto the affinity chromatography matrix.

3.7.4 Preparation of *Escherichia coli* Cell-free Extract

E. coli cell-free extract is essential to restore enzymatic activity of purified, recombinant HemN. To prepare this cell-free extract, 2 L of *E. coli* BL21 (DE3) (inoculated from an anaerobically grown preculture) were anaerobically grown for 8 h and harvested by centrifugation. All further steps were performed under strictly anaerobic conditions. The sedimented cells were resuspended in 10 mL 50 mM Tris HCl, pH 8.0 with 3 mM DTT and disrupted by ultrasonication. Cell debris and all insoluble components were removed by centrifugation (15000 g, 90 min) and the resulting protein solution stored at -20 °C. The optimal amount of each cell-free extract used in an activity assay was determined by repeating standard activity assays with different amounts of extract. Ideally, the extract itself should have no copro'gen oxidase activity while HemN should convert all available copro'gen to proto'gen.

3.7.5 Protein Purification

Anaerobic Blue Sepharose™ Chromatography

The anaerobic purification of HemN from *E. coli* was adapted from a previous protocol (Verfürth, 1999). It relies on the specific binding of native HemN to Blue Sepharose™, the adenyl-like ligand of which allows adenyl-binding proteins to be selectively retained. HemN potentially binds this ligand through its SAM2 binding site allowing its efficient separation from other cell lysate proteins without purification tags being required.

A 40 mL Blue Sepharose™ XK26 column (Amersham Biosciences) was equilibrated with at least two column volumes (CV) of buffer A. If the protein was planned to be used in crystallization experiments, 0.01 % C_8E_4 was added to buffer A for the following steps. C_8E_4 was replaced by Triton X-100 if the protein was not used in crystallization experiments. After loading the supernatant of cell lysis onto the column (flow rate 0.5 mL/min), the column was washed with two CV of buffer A to remove unbound proteins (flow rate 1 mL/min). Retained proteins were eluted by a linear gradient from 0 to 2 M NaCl in buffer A at a flow rate of 1 mL/min. To lower the costs, C_8E_4 was omitted from buffer A with high salt concentrations for HemN elution. The eluate was collected in 4 mL fractions. Fractions containing HemN were identified by SDS-PAGE, pooled, dialyzed against buffer B when needed, and concentrated by ultrafiltration. The chromatography was performed in the anaerobic chamber using the BIORAD EconoSystem.

Buffer A:	50 mM Tris pH 8.0
	3 mM DTT
Buffer B:	10 mM Hepes pH 7.5
	150 mM NaCl
	3 mM DTT

Aerobic Blue Sepharose™ Chromatography

Once FeS-cluster reconstitution was established HemN and its different variants could be purified aerobically. The column with the Blue Sepharose™ matrix was used with an ÄKTA system in this case. Buffers, washing steps, and NaCl-gradient were adopted from the anaerobic purification protocol. Aerobically purified HemN was dialyzed against buffer A and further purified by ion exchange chromatography (IEC).

Ni-NTA Sepharose

HemC, HemD, HemE, and IscS were all produced with an N-terminal His_6-tag to allow for specific binding to Ni-NTA sepharose through the immobilized Ni^{2+}-ion. After incubating soluble cell extracts with 4 mL buffer-equilibrated beads for 1 h at 4 °C, the beads were washed extensively with the according buffer supplemented with 10 mM imidazole. It was checked for complete removal of proteinaceous material using a flow-through UV monitor at 280 nm. A second washing step with buffer containing up to 50 mM imidazole removed unspecifically bound proteins. Next, the fusion protein was eluted using buffer with 400 mM imidazole. The success of the purification was checked with SDS-PAGE. A dialysis against buffer without imidazole and concentration of the protein to ~1 mg/mL (6 mg/mL for IscS) followed.

Buffers for Ni-NTA Purification:

HemC: 50 mM Tris pH 8.0, 150 mM NaCl, 3 mM β-mercaptoethanol
dialysis: 50 mM Tris pH 8.0, 50 mM NaCl, 3 mM DTT
HemD: 2 x PBS + 120 mM NaCl, 5 mM β-mercaptoethanol
dialysis: 50 mM Tris pH 8.0, 150 mM NaCl, 5 mM DTT
HemE: 50 mM $NaPO_4$ pH 6.8, 300 mM NaCl, 10 % glycerol, 1 mM β-mercaptoethanol
dialysis: 50 mM Tris pH 7.5, 10 % glycerol, 100 mM NaCl, 5 mM DTT
IscS: 50 mM Tris pH 8.0, 50 mM NaCl
dialysis: 50 mM Tris pH 8.0, 50 mM NaCl, 5 mM DTT

GSH Sepharose

HemF was produced as a fusion protein with an N-terminal GST- (glutathione *S*-transferase) tag allowing its specific purification via glutathione (GSH) sepharose matrix. The first steps of the purification (cell lysis, incubation with beads, washing with buffer) are as described for the Ni-NTA purification. Purification was performed in 50 mM Tris pH 8.0, 100 mM NaCl, 3 mM DTT. The fusion protein was eluted using buffer supplemented with 10 mM reduced glutathione. Proteolytic cleavage was initiated

by adding 40 Units of thrombin and incubating the mixture for 24 h at 4 °C. Cleaved protein was dialyzed against salt free buffer and further purified via IEC.

Ion Exchange Chromatography (IEC)

During aerobic purification of HemN and HemF, affinity chromatography was followed by ion exchange chromatography (IEC) using a HR 10/10 column with the strong anion exchanger MonoQ (GE Healthcare) at a pH of 8.0 (with buffer A) on an ÄKTA^{TM}-FPLC system. The net charge of HemN and HemF at this pH is ~-13.7 and ~2.3, respectively (calculated with VECTOR NTI). After binding and washing, bound proteins were eluted using a linear 0-1 M NaCl gradient over 10 CV. Proteins were continuously monitored by measuring the absorbance at 280 nm. The quality of peak fractions was checked by SDS-PAGE. The purest fractions were pooled and concentrated (HemN to ~1 mg/mL; HemF to 4.7 mg/mL). The HemN solutions were then transferred to the anaerobic chamber and the FeS-clusters were reconstituted (see **section 3.8.3**).

3.7.6 Concentrating Protein Solutions

During anaerobic purification, wildtype and mutant HemN solutions were concentrated in a 10 mL stirred ultrafiltration cell with a cellulose membrane (YM10; MWCO of 10 kDa) at 200 kPa until a protein concentration of ~3 mg/mL was reached. If used for crystallization setups the protein was stored at 4 °C, otherwise at -20 °C.

Aerobically purified proteins were concentrated by ultracentrifugation using Vivaspin-2, -6, and -20 concentrators (MWCO: 10000). The absorption at 280 nm of the concentrate was checked against the flow-through until the desired protein concentration was attained.

3.8 Biochemical Protein Characterization

3.8.1 Determining Protein Concentrations

Concentrations of purified protein solutions were calculated on the basis of the Beer-Lambert law using the A_{280} against buffer. Molar extinction coefficients, ε_{280}, were calculated with the program VECTORNTI (Invitrogen) or the PROTEINCALCULATORTOOL (www.scripps.edu/~cdputnam/protcalc.html). As this method does not distinguish proteins in a mixture, it was only used when the target protein had largely been purified. For other protein fractions and in cases where Triton X-100 was present in the buffer, the protein concentration was determined using the BIORAD Protein Assay, following the manufacturer´s instructions and using BSA as a standard.

3.8.2 Determination of Iron Content

The iron content of recombinant, purified HemN was determined colorimetrically with *o*-phenanthroline (Lovenberg *et al.*, 1963). To 100 µL of each protein solution 10 µL of HCl (37 %) and 390 µL H_2O were added. Samples were incubated at 80 °C for 10 min to

denature the proteins and subsequently cooled on ice for 5 min. 100 µL of a 1 M hydroxylammonium chloride solution, 500 µL of an *o*-phenanthroline monohydrate solution (0.3 % (w/v) in 70 % EtOH) and 500 µL H_2O were added to each sample. Samples were mixed and incubated at RT for 30 min. After precipitation of the proteins and centrifugation (10 min, 14000 g) the absorption of the supernatant at 512 nm was measured. The iron content of the samples was determined via a calibration curve obtained from a series of dilutions of an iron standard (Merck).

3.8.3 FeS-Cluster Reconstitution

To reconstitute [4Fe-4S]-clusters, ~1 mg/mL aerobically purified, recombinant wildtype or mutant HemN was used under strict anaerobic conditions. The apo-protein was first incubated with 10 mM DTT for 10 min. A 10-fold molar excess of Fe^{II}-$(NH_4)_2(SO_4)_2$ was then added, followed by the addition of a 10-fold molar excess of Na_2S or a 20-fold molar excess of L-cysteine in the presence of 1.3 µM *E. coli* IscS. IscS is a 45 kDa, dimeric cysteine desulfurase (Flint, 1996). The reaction catalyzed by IscS is shown in **Figure 3-1**.

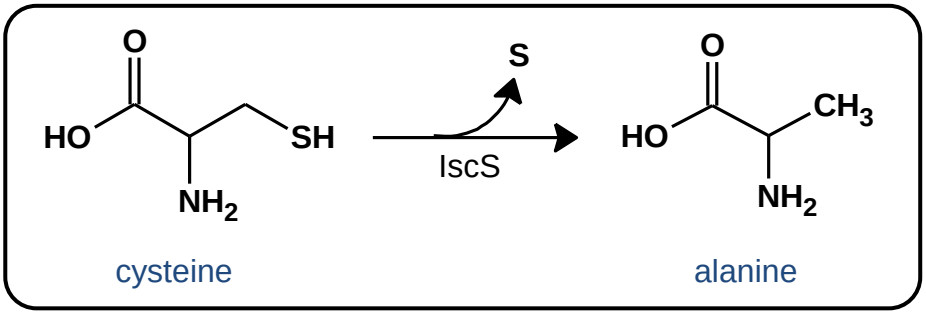

Figure 3-1: Reaction catalyzed by IscS. L-Cysteine is desulfurized to give alanine and free sulfur which can then be used for FeS-cluster assembly.

The described protein mixtures were incubated for at least 8 h at 4 °C under anaerobic conditions to allow [4Fe-4S]-cluster reconstitution. Thereafter, residual iron and sulfur were removed by NAP^{TM}-5 desalting columns previously equilibrated with anaerobized buffer and the reconstituted protein was concentrated as required.

3.8.4 Activity Assays for Recombinant HemB, HemC, HemD, and HemE

HemB and HemC

The activity of these two enzymes were checked by observing changes in color (from colorless to red) after adding 5 µg each of HemB and HemC, to a 1 mL reaction mixture containing 100 mM ALA, 5 mM $MgCl_2$, 100 mM KCl, 50 mM Tris pH 8.0 and incubating aerobically for 1 h at 37 °C.

HemD and HemE

To check the activity of HemD and HemE, the activity assays for HemB and HemC were supplemented with 5 µg each of HemD and HemE. As oxidation of tetrapyrrole intermediates had to be prevented, all buffers were replaced by the according anaerobized buffers using NAP^{TM}-5 or NAP^{TM}-10 desalting columns and the tests were performed in the anaerobic chamber. After 2.5 h incubation in the dark, synthesized tetrapyrroles were oxidized by transferring to aerobic conditions. 100 µL of each sample were mixed with 5 µL concentrated HCl and centrifuged for 10 min. 100 µL acetone:HCl (95.5:2.5) was added to the supernatant, filtered and 50 µL were injected onto the HPLC column and analyzed as described below (**section 3.8.9**).

3.8.5 Recombinant Oxygen Independent Coproporphyrinogen III Oxidase Activity Assay

The oxidase activity assay for O_2-independent copro'gen involves the conversion of copro'gen to proto'gen by HemN under strict anaerobic conditions in the presence of SAM and additional essential components such as electron donor and acceptor, NADH, and Triton X-100 (Layer *et al.*, 2002). Subsequent oxidation of porphyrinogens to the corresponding porphyrins allows for simple fluorometric detection.

In a total volume of 300 µL, a standard assay mixture consisted of 1.5 µM enzyme, 70 µL cell free extract, 500 µM SAM, 500 µM NADH, and 20 µM copro'gen.

After 90 min incubation at 37 °C in the dark, the reaction was stopped by adding 15 µL of 35 % (v/v) H_2O_2 (15 min) to oxidize both remaining copro'gen substrate and proto'gen product. Appropriate dilutions of the resulting porphyrins using buffer II were quantified by fluorescence spectroscopy by exciting at 409 nm and recording an emission spectrum between 570-680 nm (scan speed = 200 nm/min, excitation and emission slit widths = 5 nm, PerkinElmer fluorescence spectrometer).

Assay buffer:	50 mM	Tris HCl, pH 7.0;
	300 mM	NaCl
	0.3 %	Triton X-100
	3 mM	DTT
Assay buffer II:	500 mM	Tris HCl, pH 8.0
	2 % (v/v)	Tween 80

To identify and quantify potential reaction intermediates, the assay volume was increased to 1.6 mL and samples of 300 µL were taken after 15, 30, 45, 60, and 90 min, oxidized and stored at -20 °C for later analysis. 40 µL of each sample were used for fluorescence spectroscopy, 110 µL for HPLC analysis, and 150 µL for tetrapyrrole extraction and mass spectrometric analysis.

To assay SAM-cleavage [^{14}C]-SAM was used in the assay as described in **section 3.8.6**.

3.8.6 Assay for Cleavage of *S*-(5-Adenosyl)-L-Methionine (SAM)

HemN-mediated SAM cleavage was studied in the presence and absence of a terminal electron acceptor. As the electron acceptor is unknown, the assay relied on the addition of *E. coli* cell-free extract (**section 3.8.5**). 20 µM [^{14}C]-SAM were used in a total volume of 50 µL.

For analyses without *E. coli* cell-free extract (and hence without electron acceptor), sodium dithionite served as the electron donor: concentrations were 10 µM HemN, 80 µM [^{14}C]-SAM, 2 mM dithionite and 100 µM copro'gen in a total volume of 25 µL assay buffer (compare **section 3.8.5**). Assays were incubated for 90 min at 37 °C, stopped by addition of 10 % PCA and precipitated proteins were removed by centrifugation. Formation of [^{14}C]-methionine was determined by HPLC analysis of the supernatant (**section 3.8.9**).

3.8.7 Activity Assay of Recombinant HemF Variant R401K

The oxidase activity assay of HemF was performed similar to that of HemN. In a total volume of 1500 µL (50 mM Tris pH 8.0, 150 mM NaCl, 0.1 % Triton X-100) 20 µM chemically reduced copro'gen were mixed with 0.3 µM HemF under aerobic conditions. The reaction was performed in the dark at 37 °C for 90 min. Samples were taken at different time points and analyzed like the samples of the HemN activity assay.

3.8.8 UV-Visible Light Absorption Spectroscopy

UV-visible light absorption spectra (270-680 nm) of purified, recombinant HemN were recorded using a Lambda 2 (PerkinElmer) or an Ultraspec 3000 UV-visible Spectrophotometer (PharmaciaBiotech). Cuvettes were filled and tightly locked in the anaerobic chamber to allow for anaerobic conditions during the measurement. Absorption maxima at 320 and ~410 nm indicated the presence of a [4Fe-4S]-cluster (Lazazzera *et al*., 1996; Green *et al*., 1996, and Layer *et al*., 2002).

3.8.9 High Performance Liquid Chromatography (HPLC) Analysis

SAM Cleavage Assay

The samples for HPLC analysis were prepared as described in **sections 3.8.5** and **3.8.6.** After removal of the precipitated proteins the solution was filtered through a cellulose acetate membrane syringe filter with a pore width of 0.2 µm (Nalge Nunc International). 20 µL of the sample were loaded onto a 4.6 x 250 mm ODS Hypersil-C_{18} reversed phase column (Techlab) with a pore width of 120 Å. Separation was performed at 38 °C at a flow rate of 0.5 mL/min using 50 mM $(NH_4)H_2PO_4$ (pH 2.5) as mobile phase. [^{14}C]-SAM and [^{14}C]-methionine were detected by measuring the radioactivity using a flow through scintillation counter (Raytest Isotopenmessgeräte) and in parallel by photometric diode array analysis at 200-650 nm. The HPLC system was the JASCO 1500 series (JASCO, Gross-Umstadt, Germany).

Tetrapyrrole Detection

Samples were prepared as described by Layer *et al*. (2002) with minor modifications. To 110 µL of H_2O_2-oxidized assay mixtures (**section 3.8.5**) 7.5 µL undiluted HCl and 110 µL acetone/HCl (97.5 %/2.5 %) were added. Precipitated proteins were removed by centrifugation. The supernatant was filtered and 60 µL thereof injected onto a 250 x 4.6 mm Equisil™ BDS column (Dr. Maisch HPLC GmbH, Germany). Separation was performed at a flow rate of 0.5 mL/min using a 17:83 mixture of 1 M ammonium acetate, pH 5.2 and MeOH as mobile phase. Oxidized tetrapyrroles were detected by fluorescence measurements using an excitation wavelength of 409 nm and an emission wavelength of 630 nm and in parallel by photometric diode array analysis for 200-650 nm. Copro' and proto' were used as porphyrin standards. The HPLC system was the JASCO 1500 instrument (JASCO, Gross-Umstadt, Germany).

For HemE activity the following HPLC assay was used (Storbeck, TU Braunschweig, personal communication): 50 µL samples were loaded onto a 4.6 x 250 mm ODS Equisil™ column (Dr. Maisch HPLC GmbH, Germany) with a pore width of 120 Å. Separation was achieved with a flow rate of 0.5 mL/min using a linear gradient from 0:15:85 methanol:acetonitrile:(1 M ammonium acetate) ratio to 30:15:55 in 45 min and to 85:15:0 in 60 min. The latter ratio was maintained till the end of the run at 75 min. Tetrapyrroles were detected by fluorescence measurements using an excitation wavelength of 405 nm and an emission wavelength of 620 nm and in parallel by photometric diode array analysis for 200–650 nm. The HPLC system was a JASCO 2000 instrument (JASCO, Gross-Umstadt, Germany).

3.9 Protein Crystallization

Proteins were crystallized by hanging- and sitting-drop vapor diffusion methods. 2 h prior to crystallization HemN solutions were supplemented with 1 mM SAM. Without the addition of SAM the crystal growth was decelerated. Crystals were obtained after 2-3 weeks and 5-10 days without and with supplemented SAM, respectively.

Screening

To identify new crystallization conditions for wildtype and mutant HemN, protein solutions were screened for lead crystallization conditions using commercial screens (QIAGEN) in 96-well sitting-drop plates. Screen solutions in 96-well masterblocks (< 1 mL) were transferred to the anaerobic chamber at least three days prior to being used in crystallization experiments. To reduce the amount of dissolved oxygen in the screen solutions, the lid of each masterblock was opened several times to allow the gas layer above the solutions to exchange with the atmosphere of the anaerobic chamber. 1.4 µL drops containing equal amounts of protein- and crystallization solution were pipetted manually in the anaerobic box. The plates were sealed with Manco™ Crystal Clear tape (Jena Bioscience), transferred to the MiniMACS™ anaerobic box (Whitley DG250 Work-station, DonWhitley Scientific) in a sealed plastic bag, and incubated in the dark at 23 °C.

Optimization

Initial crystallization conditions were optimized manually in 24-well hanging drop plates, using drop volumes of 2-3 µL and varying the salt/precipitant concentration, the pH value or the protein concentration to optimize crystal quality for X-ray diffraction experiments. All crystallization experiments were set-up under anaerobic conditions.

Microseeding

To improve HemN crystallization, existing crystals were transferred to a 1.5 mL reaction tube together with 100 µL reservoir solution and thoroughly vortexed for 5 min to break the crystals into pieces. These crystal fragments were used in new crystallization setups to provide crystallization nuclei. 50 µL of the crystal/reservoir-solution were diluted with another 50 µL of reservoir-solution and thoroughly mixed. Dilutions of up to 2^{14} were prepared in this way. The standard reservoir solutions for a 24-well crystallization plate were prepared. Crystallization drops were pipetted using 1 µL of protein solution plus 1 µL of dilutions 2^{8}, 2^{10}, 2^{12}, or 2^{14} replacing the reservoir solutions.

Co-crystallization

Several attempts were undertaken to co-crystallize HemN with its substrate or product. This included the strategy to let the enzymatic substrate synthesis occur *in situ* to allow it to directly bind to the active site of HemN or to co-crystallize with chemically reduced copro'gen or proto'gen.

For the first strategy, the enzymes preceding HemN in heme biosynthesis HemB, HemC, HemD, and HemE were purified (**section 3.7.5**). The buffer of each of these aerobically purified proteins was exchanged by NAP^{TM}-5 or NAP^{TM}-10 desalting columns with anaerobic buffer. The pH of a 100 mM ALA stock solution was adjusted to ~8 with 10 M NaOH. 5 µg of each enzyme and 10 µL ALA-solution were added to ~300 µL of HemN solution 0-120 min before crystallization drops were set up.

Alternatively, following another approach by Phillips *et al*. (2003), a protein mixture was prepared containing 50 µg/mL of each protein and 100 µL ALA solution and incubated for 30 min to 3 h. 5 µL of HemN were then mixed with 15 µL of enzyme mixture directly on the cover slip for crystallization, incubated for 5 min and finally mixed with 8 µL of reservoir solution.

Chemically reduced copro'gen was added in a 4 fold molar excess to the protein solution and the mixture was incubated for 0-4 h either at RT or on ice before crystallization drops were set up. To some wildtype solutions containing copro'gen, Na-dithionite was also added in a final concentration of 2 mM.

Crystal Soaking

A range of chemicals was used for soaking experiments including tetrapyrroles (substrate and product) as well as an artificial electron donor and an artificial electron acceptor.

Solutions of tetrapyrroles were placed in the anaerobic chamber two days prior to use. Protected from light, the lids of the reaction tubes were left open to allow for exchange of dissolved gasses. Due to evaporation, resulting tetrapyrrole concentrations were higher than originally determined. Tetrapyrrole solutions were either mixed with reservoir solution and the cryoprotectant to allow a single transfer of crystals during harvest. Alternatively, these solutions were directly added to the crystallization droplet containing crystals (0.2 µL added to 2 µL drop).

Na-dithionite or phenazine methosulfate (PMS) were added as artificial electron donor or electron acceptor, respectively. Na-dithionite was added to a final concentration of 2 mM. PMS was added either as solution in a ten-fold molar excess to the protein or added in the solid state directly to the crystallization droplet.

3.10 X-ray data Collection

Protein crystals larger than 30 µm in the smallest dimension were harvested from their mother liquor and flash-cooled in liquid nitrogen. 10-15 % PEG 400 or 15 % glycerol was used as cryoprotectant for wildtype HemN and I329A mutant crystals. X-ray diffraction data were collected on an in-house rotating copper anode generator (RINT-2000 series RU-H3R) and an R-AXIS IV^{++} image plate detector (Rigaku) or at synchrotron beamlines BW7A, X11, X12, and X13 (EMBL, DESY, Hamburg), MX-14-1 (BESSY, Berlin), and ID14-1 and ID14-2 (ESRF, Grenoble) using charge-coupled device detectors (MarCCD or MAR555 Flatpanel from MarResearch or ADSC).

3.11 Data Processing and Structure Solution

X-ray diffraction data were indexed and integrated with DENZO (Otwinowski and Minor, 1997), XDS (Kabsch, 1988), or with MOSFLM (Leslie, 1992). Images were scaled using SCALEPACK or SCALA (Otwinowski and Minor, 1997). Further data processing and manipulation was performed using the CCP4 SUITE of software (Collaborative Computational Project Number 4, 1994). PHASER (McCoy *et al.*, 2005; Storoni *et al.*, 2004) was used for maximum-likelihood based molecular replacement with wildtype HemN (PDB entry: 1olt) as the search model. Structures were refined by alternating cycles of manual fitting in COOT (Emsley and Cowtan, 2004) and restrained refinement including TLS-protocols using REFMAC5 (Murshudov *et al.*, 1997). PROCHECK (Laskowski *et al.*, 1998) was used to check the quality of the structure including analyses by Ramachandran plot. Structural differences were quantified by calculating r.m.s. displacements between superposed structures using LSQKAB (Kabsch, 1976; Krissinel and Henrick, 2004). Graphical depictions were generated using PYMOL (DeLano, 2002).

3.12 Tetrapyrrole Extraction

To identify and quantify tetrapyrroles in solutions after activity assays and to detect possible reaction intermediates of HemN, tetrapyrroles were extracted from 150 µL of a particular assay sample (see **section 3.8.5**). The extraction described by Wang *et al.* (2008) was adapted slightly. Briefly, 1.5 mL of 3:7 acetic acid:ethyl acetate was added and the resulting mixture vortexed for 30 s and centrifuged at 12000 g for 3 min. The top 650 µL of supernatant were transferred to a new 1.5 mL reaction tube containing 650 µL of sodium acetate (3 % (w/v)). The mixture was vortexed and centrifuged as described. Again the topmost 200 µL ethyl acetate layer was transferred to another reaction tube with 200 µL of distilled water, again vortexed and centrifuged. The top 100 µL of ethyl acetate were transferred to another tube and 20 µL of 15 % HCl (w/v) were added to separate the tetrapyrroles from the ethyl acetate. The tetrapyrrole samples were subsequently analyzed by mass spectrometry.

3.13 Tetrapyrrole Reduction

Chemical Reduction

For standard activity assays and first co-crystallization experiments, copro'gen was prepared by reducing copro' (Paesel + Lorei, Duisburg) with freshly prepared 3 % sodium amalgam (Grandchamp and Nordmann, 1982). DTT (50 mM) was added to the copro'gen solution and the pH adjusted to 7-8 with 20 % (v/v) phosphoric acid. The copro'gen solution was stored in the dark at -20 °C.

Alternatively, a new technique of using palladium and H_2 to achieve tetrapyrrole reduction was established. Following the protocol of Bergonia *et al.* (2009), 2 mg of copro' and 5 mg palladium catalyst (10 % Pd on charcoal, hydration catalyst, Merck, Germany) were placed in a small flask together with a small magnetic stirrer bar. After flushing the flask with argon, 100 µL Ar-bubbled H_2O and 1.8 mL Ar-bubbled MeOH were added. Under constant stirring a H_2-filled balloon was attached to the flask to start the reaction. The flask was wrapped in foil to protect the reaction from light. The progress of reduction, indicated by the loss of fluorescence, was intermittently monitored by exposing the mixture to UV-light for some seconds. The reaction was usually complete after 50-60 min. To remove the methanol from the reaction mixture, the flask was shaken under vacuum until the volume was clearly reduced (~1 min). The remaining solution was removed from the flask with a syringe and filtered (Schleicher and Schüll, Dassel, Germany) directly into another flask with 200 µL of Ar-bubbled 50 mM KOH and 800 µL buffer (20 mM Tris pH 7.5; 10 mM DTT). The reduced copro'gen was transferred to the anaerobic chamber, fractioned under dim light, and stored at -20 °C until used.

Enzymatic Reduction

The enzymatic production of copro'gen from the precursor ALA was also established using the four preceding enzymes from heme biosynthesis under strict anaerobic

conditions. HemC, HemD, and HemE were expressed and purified (**section 3.7.5**) and buffers exchanged by de-aerated buffers using NAP^{TM}-5 and NAP^{TM}-10 columns. 5 µg each of purified HemB, HemC, HemD, and HemE were mixed with appropriate buffers to make up a total volume of 1 mL with 1 mM ALA, 5 mM $MgCl_2$, 100 mM KCl, 50 mM Tris pH 8.0. The mixture was incubated at 37 °C for at least 4 h in the dark. Tetrapyrroles were detected by HPLC as described (**section 3.8.8**). Enzymatic substrate synthesis for co-crystallization experiments is described in **section 3.9**.

3.14 Mass Spectrometry

Tetrapyrrole samples were analyzed by mass spectrometry (MS) by Dr. Manfred Nimtz and Anja Meier (HZI, Braunschweig): tetrapyrroles were extracted from activity assay samples as described (**section 3.12**). Samples were diluted 1:3 with MeOH, loaded onto a prespotted anchor chip (PAC) target with an α-cyano-4-hydroxycinnamic acid matrix and dried at RT. The molecular masses were determined in the positive-ion mode on a Bruker Ultraflex time-of-flight mass spectrometer (Bruker Daltonics GmbH, Bremen) using a nitrogen UV laser with a wavelength of 323 nm and an acceleration voltage of 25 kV.

4 Results

Most experiments described in the following had to be performed under strictly anaerobic conditions because of the oxygen sensitivity of the [4Fe-4S]-cluster of HemN and the intermediates of the heme biosynthesis pathway. Work initially commenced at the Technical University (TU) in Braunschweig where anaerobic facilities were kindly provided by Prof. Dieter Jahn. Only after suitable infrastructure had been acquired and established at the home institute, most activities could move to the Helmholtz Center for Infection Research (HZI) campus.

4.1 Installation of an Anaerobic Working Station

HemN and many intermediate products of heme biosynthesis are highly sensitive to molecular oxygen. Anaerobic facilities were therefore set up to be able to undertake the planned project. For most operations such as protein purification, activity assays, and general protein handling a glove box (Coy Systems) proved optimal. Initially an ÄKTA^{TM}-Basic liquid chromatography system was integrated into the anaerobic chamber to permit protein purification under strictly anaerobic conditions. Due to space limitations, only elements in direct contact with buffers or protein fractions were physically placed within the anaerobic chamber, while the main instrument, gradient mixer, and detectors remained outside the anaerobic chamber. Only the tubing connecting the two parts were allowed to pass through the anaerobic chamber wall (**Figure 4-1**). The redox-indicator resazurin was used to check that anaerobic conditions were maintained by this setup during purification. A change in the color of the indicator, however, clearly demonstrated the presence of oxygen in the buffers after having passed through the ÄKTA^{TM} system. As even traces of oxygen are sufficient to destroy the FeS-cluster of HemN, the ÄKTA^{TM} (Basic) system could not be used to perform HemN purification like at the Technical University, where the compact ÄKTA^{TM}-Prime system was used for HemN purifications within the anaerobic chamber. The ÄKTA^{TM}-Basic chromatography system was therefore replaced by the Econo-System from BIORAD. This combines a small

programmable peristaltic-pump with a UV-monitor, and a small fraction collector, all of which are more easily accommodated within the anaerobic chamber. A simple glass gradient mixer allowed linear salt-gradients to be generated for protein elution. To minimize the number of steps outside the anaerobic chamber, cells were not disrupted by French Press, as described (Layer *et al.*, 2002). Instead, repeated cycles of ultrasonication using a Sonoplus HD200 (Bandelin) were used for cell disruption as the ultrasonic probe head could be introduced into the anaerobic chamber, when required. Using these facilities, protein purification under strictly anaerobic conditions was possible.

Delicate procedures such as preparing crystallization setups are difficult or impossible to achieve using heavy rubber gloves that are normally attached to glove boxes. For such purposes, an anaerobic box was connected to the glove box. To monitor and document crystal growth, yet a third anaerobic box (Whitley DG250 Workstation (miniMACS), DonWhitley Scientific) equipped with a digital video microscope (VHX 100, Keyence) was installed. This box features a two-door system allowing crystal mounting under anaerobic conditions.

To remove molecular oxygen from solutions, Dr. Martina Jahn (Institute of Microbiology, TU Braunschweig) kindly provided a non-commercial de-aeration device that applies alternating cycles of vacuum and nitrogen onto solutions in anaerobic flasks. All plastic disposables and glass devices were introduced into the anaerobic chamber 24 and 2 h prior to use, respectively, to exclude residual oxygen. The laboratory with the anaerobic working station was air conditioned to 20 ± 0.5 °C to ensure stable conditions for crystal growth. For experiments involving light-sensitive tetrapyrroles, all windows were covered with aluminum foil while a small lamp to which a red filter was fitted served as the sole source of light to avoid light-induced oxidation of tetrapyrroles. Some images of the working station as developed as part of this thesis are presented in **Figure 4-1**.

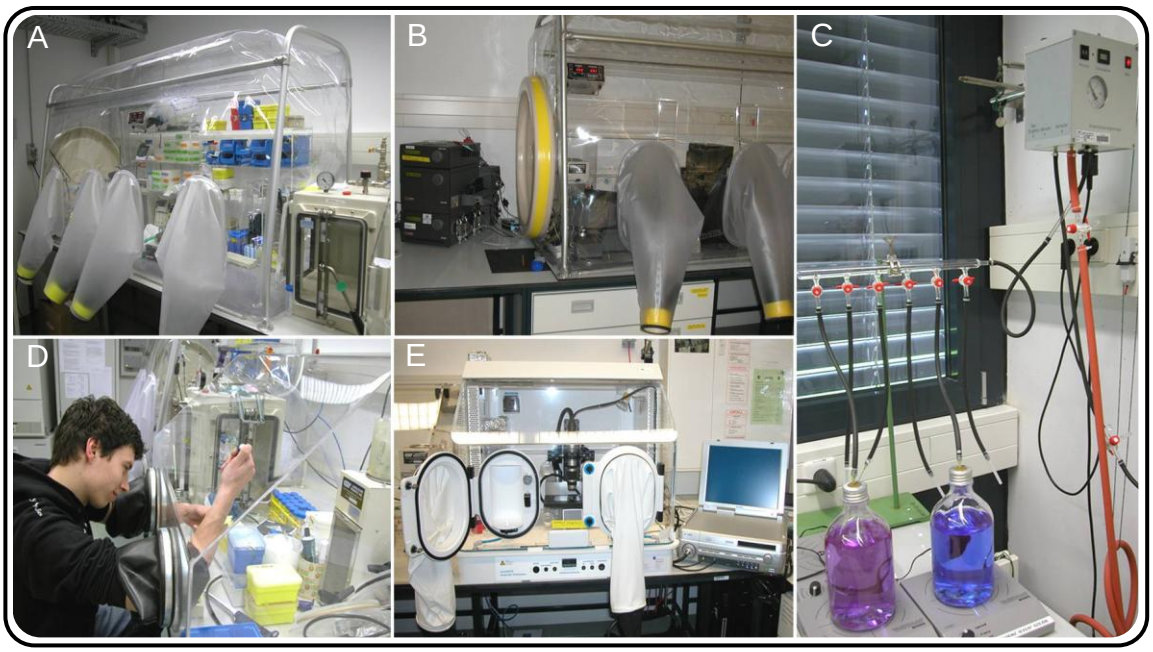

Figure 4-1: Anaerobic working station. A: Anaerobic chamber. A sluice to transfer buffers and equipment into the anaerobic chamber is located on the right hand side. **B**: ÄKTA-system (Basic) adapted to anaerobic chamber. Buffers, injection valve, and fraction collector were positioned in the anaerobic chamber whereas all other parts of the ÄKTA were left outside of the chamber. **C**: Buffers with redox-indicator resazurin. Darker colors indicate the presence of molecular oxygen in the solution. Oxygen is removed by alternating cycles of vacuum and nitrogen gassing (1 bar) controlled by the de-aeration device on the right hand side. **D**: Crystallization experiments are manually pipetted in an anaerobic box. **E**: Anaerobic box with two door system. Crystal growth can be monitored and documented via the video microscope.

4.2 Reconstitution of the HemN Iron-Sulfur Cluster Yields Enzymatically Active and Crystallizable Protein

An intact [4Fe-4S]-cluster is essential for HemN catalysis, in common with other Radical SAM enzymes. Because the FeS-cluster in all such enzymes is only coordinated by three cysteines, the fourth iron is particularly labile (Broderick, 2000). As a result, it is particularly challenging to purify these enzymes with a homogeneously intact cluster. Repeated anaerobic purification of HemN resulted in highly variable amounts of bound iron ranging from 0.26 to 4.22 mol iron/mol HemN. Even trace amounts of oxygen in plastic disposables or glass ware during or after purification led to FeS-cluster destruction accompanied by the loss of their characteristic brown color. As an iron-content of at least 1.8 mol iron per mol HemN is essential for crystallization, obtaining sufficient intact HemN was critical for all later experiments. Using an ÄKTA^{TM}-Prime system at the TU Braunschweig, the HemN elution chromatogram of the first column (Blue Sepharose^{TM}) was closely analyzed (**Figure 4-2**).

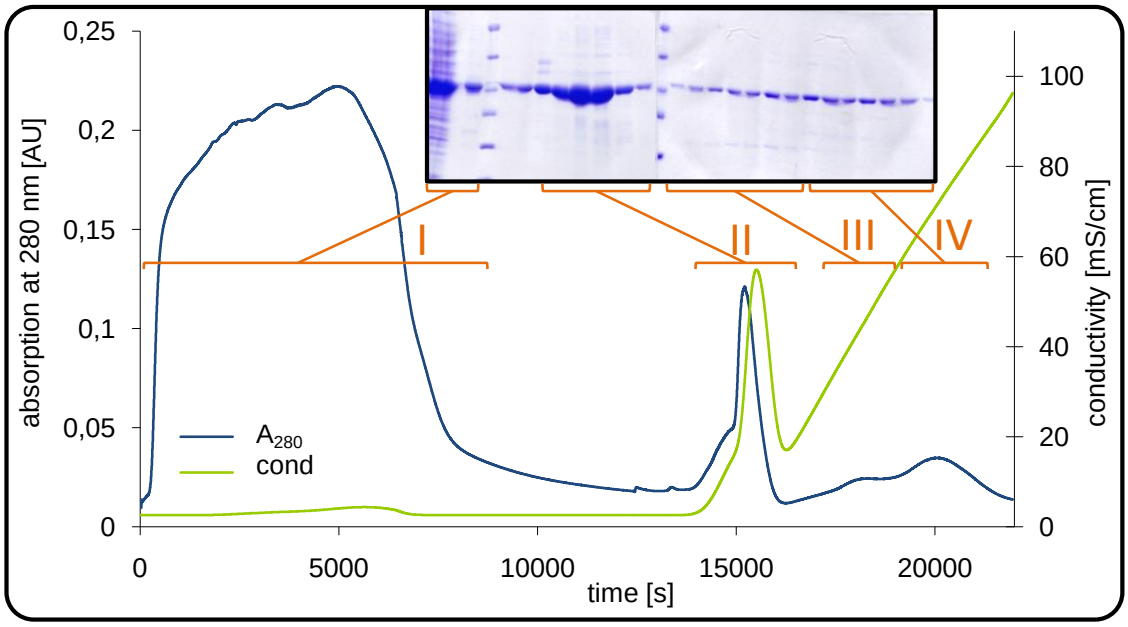

Figure 4-2: Purification of wildtype HemN. Protein was purified under anaerobic conditions via a blue sepharose column. After washing out unbound protein, HemN was eluted with a linear NaCl gradient (up to 2 M). Flow through of column (I), pooled protein fractions (II – IV), corresponding SDS-gel fractions, and peaks of the chromatogram are labeled. Pool IV displayed a light brown color whereas all other fractions were colorless.

This indicates that HemN elution corresponds to four distinct peak regions. The iron contents of fractions in peaks II to IV were analyzed. Fractions in peak IV were distinctly brown in color, which was confirmed by an iron content of 3.13 mol iron per mol HemN. Fractions corresponding to peak II and III were not noticeably brown and yielded values of 0.17 and 0.71 mol iron per mol HemN. Clearly, only a small fraction of purified HemN contains/retains sufficient iron for successful crystallization. Overall, the analysis emphasized the need for a more efficient and reproducible HemN purification.

To reconstitute the [4Fe-4S]-cluster in aerobically purified HemN, $Fe(NH_4)_2(SO_4)_2$ and Na_2S or alternatively L-cysteine and the enzyme IscS (Flint, 1996; Leimkuhler and Rajagopalan, 2001; Hänzelmann *et al*, 2004) were added (**section 3.8.3**). The plasmid encoding *E. coli* IscS for the production in *E. coli* cells was kindly provided by Dr. Sandrine Ollagnier de Choudens (Université Joseph Fourier, Grenoble, France). IscS was purified very efficiently by a single step using a Ni-NTA column (**Figure 4-3**, **A** and **B**). As the pyridoxal-5-phosphate (PLP) cofactor of IscS was lost during extensive dialysis after the affinity chromatography, IscS was reconstituted with a 50 fold molar excess of PLP. Surplus PLP was subsequently removed by dialysis.

Using Na_2S as sulfur source for the reconstitution did not result in cluster reconstitution. Strong formation of dark brown iron-sulfur-complexes other than the expected cluster, which could not be removed from the protein solution after the reconstitution, occurred in this case. In contrast, the combination of L-cysteine and IscS as sulfur source reproducibly yielded in a golden-brown HemN solution, typical for HemN with intact [4Fe-4S]-cluster, indicating successful FeS-cluster reconstitution (**Figure 4-3**, **D**, shown for HemN variant T247R). The reconstitution solution slowly turns golden-brown after ~15 min and after two h reconstitution is complete.

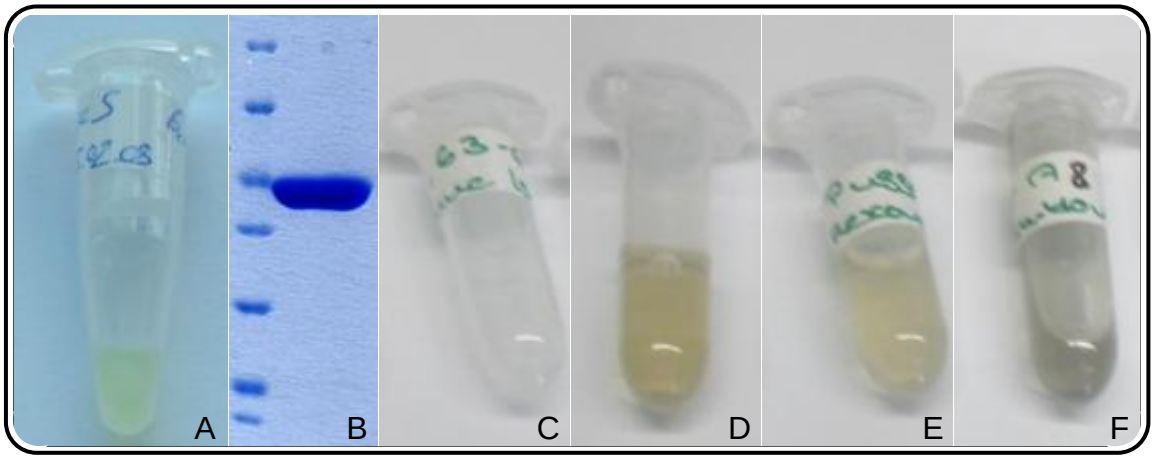

Figure 4-3: Concentrated IscS from *E. coli* and Fe-S-cluster reconstitution. IscS was purified in a single step with a Ni-NTA column. Concentrated protein is slightly yellow in color due to the cofactor PLP (**A**) and is observably pure on an SDS-PAGE gel (**B**). **C**-**F**: cluster-reconstitution. **C**: control without added iron and sulfur, **D**: reconstitution of HemN variant T247R at 1.6 mg/mL, five- and ten-fold molar excess of iron and sulfur, respectively, and 1.3 µM IscS under strict anaerobic conditions, **E**: control without IscS after 15 min, **F**: control without IscS after 2 h.

Reconstitution is crucially dependent on IscS. In the absence of IscS the HemN solution also turns brown after ~15 min (**Figure 4-3, E**) but turns dark gray/brown after 2 h indicating that other FeS-complexes than the [4Fe-4S]-cluster are formed (**Figure 4-3, F**). These complexes could not be separated from HemN after the reconstitution. Reconstitution was equivalent for wildtype HemN and all variants. The calculated iron content for wildtype HemN and variant T247R was 0.1 and 4.2 mol iron/mol HemN prior and after reconstitution, respectively. For the variant Q311A the iron content was 2.8 mol iron/mol HemN after reconstitution.

Reconstituted wildtype HemN was analyzed to ensure that reconstitution results in an active and crystallizable protein indicating an intact [4Fe-4S]-cluster (**Figure 4-4**).

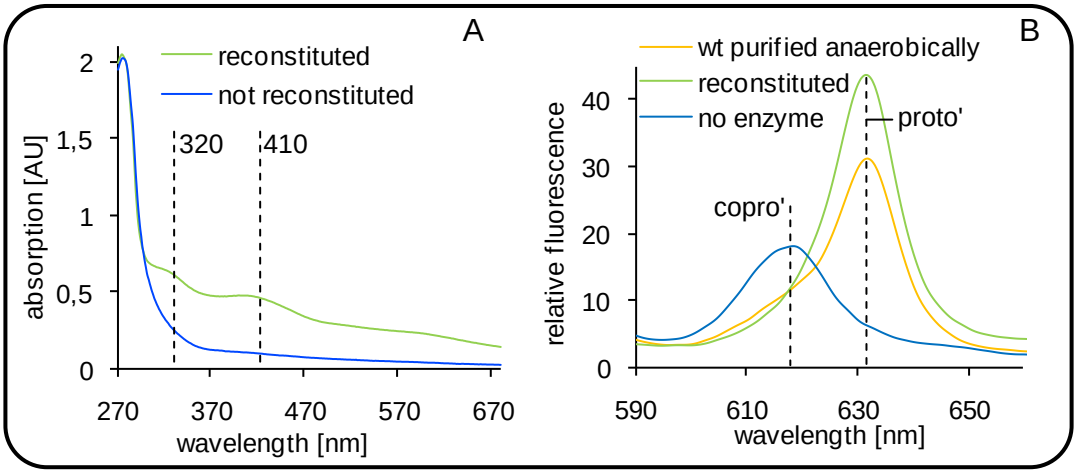

Figure 4-4: UV-visible light absorption spectra (A) and activity assays (B) of wildtype HemN prior to and after reconstitution. A: UV-visible light absorption spectra were recorded at a concentration of 0.8 mg/mL. Shoulders at 310 nm and 420 nm in the case of reconstituted HemN indicate an intact iron-sulfur cluster. **B**: For the activity assays, 1.5 µM wildtype HemN was used. Sodium amalgam reduced copro'gen was added to start the reaction. A fluorescence peak at 618 nm is typical for copro', while a peak at 633 nm indicates the product proto'. In the control-reaction no HemN was added to the substrate.

Spectra were recorded for reconstituted wildtype HemN. Peak shoulders at 320 nm and ~410 nm (missing in the unreconstituted protein) and a value of 0.24 for the ratio of A_{410}/A_{280} after reconstitution (0.05 prior to reconstitution) clearly indicate the presence of a [4Fe-4S]-cluster per HemN molecule in the reconstituted HemN-sample. According to the calculations of Green *et al*. (1996) and Hernández *et al.* (2007) an A_{410}/A_{280} ratio of ~0.25 is expected for one cluster per HemN molecule.

The enzymatic activity of reconstituted wildtype HemN is comparable or better than that of anaerobically purified enzyme while it is essentially inactive prior to reconstitution (data not shown).

Crystallization conditions optimized for anaerobically purified wildtype HemN, similarly produced crystals of reconstituted HemN within one week. The hexagonal crystals were harvested and flash-cooled and X-ray diffraction data up to 2.25 Å resolution were collected at beamline ID 14-2 (ESRF, Grenoble). Indexing revealed an isomorphous space group with equivalent unit cell dimensions. After restrained refinement no noticeable differences to anaerobically purified wildtype protein were observed. Reconstituted HemN is thus functionally and structurally indistinguishable from anaerobically purified enzyme, but more easily produced and purified.

4.3 Characterization of HemN Variants Probably Involved in SAM2- and Substrate Binding

Prior to this thesis, the role of an N-terminal extension of the catalytic domain and of other amino acid residues potentially involved in substrate- and SAM2-binding had been investigated by mutational analyses (Grage, 2005; Layer *et al.*, 2005a). To extend these analyses, additional HemN variants were produced by site-directed mutagenesis. Protein production and characterization were performed under anaerobic conditions as described (Grage, 2005).

Analyzed residues included Gln311, which has been implicated in SAM2-binding (Layer *et al.*, 2003), Arg359, potentially involved in substrate binding, and Arg22, located in the 'trip-wire' and also postulated to be involved in substrate recognition and binding. The listed residues are all highly conserved among different HemN enzymes (Grage, 2005). Substitutions of these residues included Q311N (Gln311 replaced by asparagine), R359A, R22A and R22K. The HemN variants Q311A and R359K had already been characterized by Katrin Grage. The positions of the amino acid substitutions are shown in **Figure 4-5**.

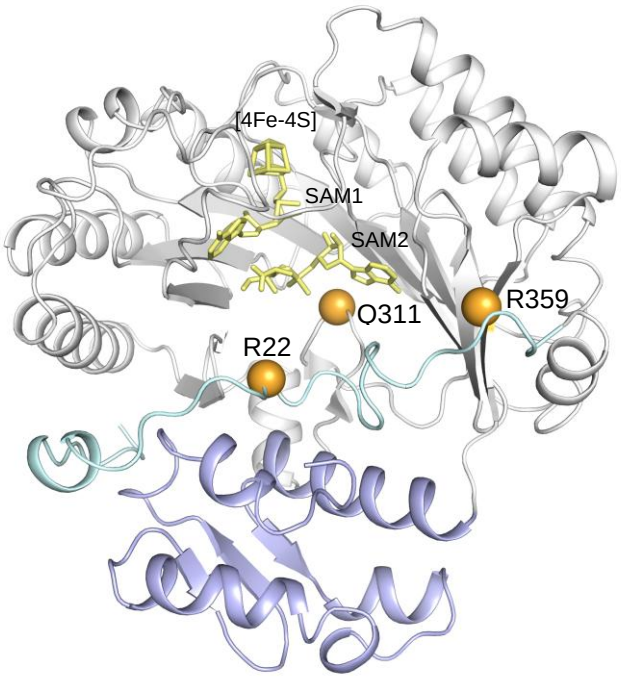

Figure 4-5: Positions of substituted residues of HemN. The catalytic domain is shown in gray, the C-terminal domain in blue, the 'trip-wire' in cyan, and the cofactors in yellow. Parts of the 'trip-wire' not well-defined in the initial electron density have been included in this figure for clarity. Residues potentially involved in SAM2- or substrate-binding and hence substituted as part of this analysis are marked by orange spheres.

Elution fractions resulting from a standard wildtype purification are shown on SDS-PAGE gels in **Figure 4-6**. These SDS-PAGE gels are also representative for the purification results of Q311A and R22K.

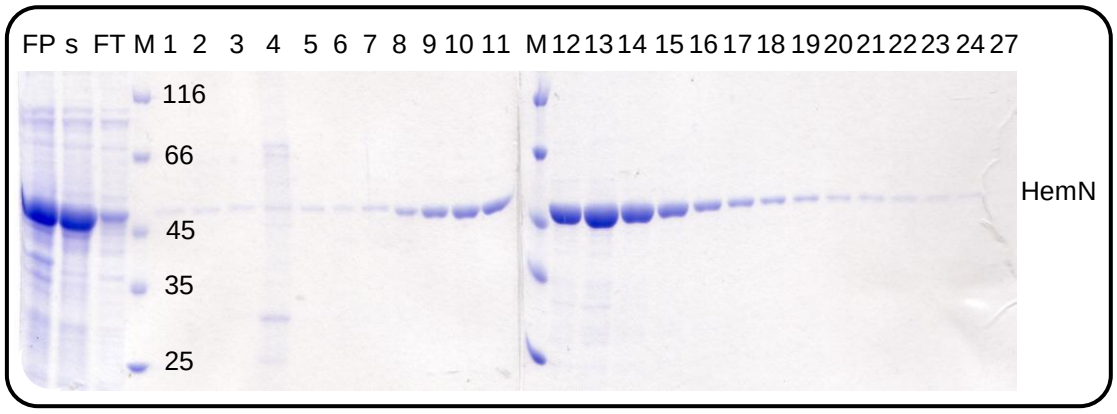

Figure 4-6: SDS-PAGE of the production and the affinity chromatography of wildtype HemN under strictly anaerobic conditions. Protein was produced in and purified from *E. coli* BL21 cells. Elution fractions containing HemN (here 7-24) were pooled and used for further experiments. M: marker (molecular weights for marker proteins are denoted in kDa), FP: cell lysate after French Press disruption; s: soluble fraction; FT: flow-through; 1-27: elution fractions.

Most *E. coli* proteins had been removed from the column prior to elution. The linear NaCl gradient resulted in the elution of HemN in fractions 9-17. Only a small fraction of HemN was lost in the flow-through and other elution fractions. HemN-containing fractions were pooled and concentrated.

HemN binding to the Blue Sepharose™ matrix was adversely affected by mutations R359A and R22A. **Figure 4-7** illustrates the purification of variant R359A.

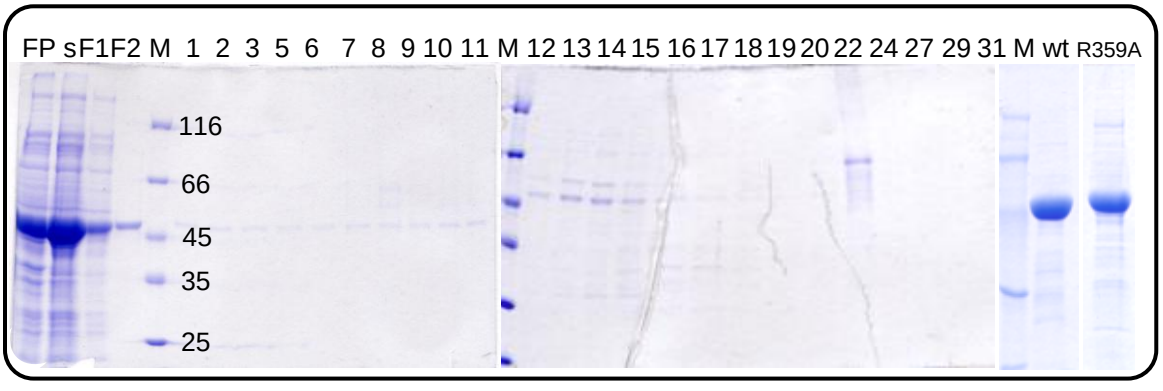

Figure 4-7: SDS-PAGE of HemN variant R359A production and its purification by affinity chromatography under strictly anaerobic conditions. Protein was produced in and purified from *E. coli* BL21 cells. HemN did already elute in the flow-through and was not eluted by the NaCl gradient. M: marker, FP: cell lysate after French Press disruption; s: soluble fraction; F: flow-through, 1-31: elution fractions; wt: pooled wildtype HemN fractions after purification and concentration (6.8 µg); R359A: flow-through 2 after purification and concentration (16.1 µg).

The elution fractions contain almost no HemN variant R359A. As a large amount of this variant was detected in the flow-through, the latter was split into two fractions. Whereas the first such fraction included most other *E. coli* proteins in addition to HemN, the second fraction comprised mostly HemN variant R359A. Thus the second flow-through fraction was used for further experiments. A similar effect was observed during purification of the HemN variant R22A, though in this case a small fraction of HemN variant R22A was eluted by the NaCl-gradient and could be used for subsequent experiments. Protein from the flow-through was similarly pure as protein that derived from later NaCl-eluted fractions (see **Figure 4-7**).

All HemN-variants were concentrated to 3 mg/mL and analyzed for their FeS-cluster content and their copro'gen oxidase (CPO) activity. Additionally their ability to cleave SAM was tested with different electron donors and their total iron-content was determined both colorimetrically and by UV-visible spectroscopy. The results of the UV-visible spectrometry and of a representative CPO activity assay are presented in **Figure 4-8**. In **Figure 4-8 A** UV-visible spectra of the purified HemN variants are shown. The dark blue trace recorded from wildtype HemN presents a typical UV-visible spectrum for a [4Fe-4S]-cluster containing protein. In addition to the peak at 280 nm present for all proteins, a shoulder at 320 nm and a broader shoulder or peak at ~410 nm are observed for these proteins. The characteristic peak pattern is also clearly present for the variants Q311N, R22K, and R359A. Only for the R22A variant the absorption at 320 nm and at ~410 nm is reduced. A slight shoulder at 410 nm, however, is still visible. The results of the UV-visible absorption spectra are in good agreement with the observed colors of concentrated protein solutions. Whereas the Q311N-variant exhibited the typical yellow-brown color of wildtype HemN, the R359A and R22K variants were only colored at higher protein concentrations and the R22A variant appeared colorless. In **Table 4-1** the iron contents, calculated from the iron concentration relative to the protein concentration are provided and support the results.

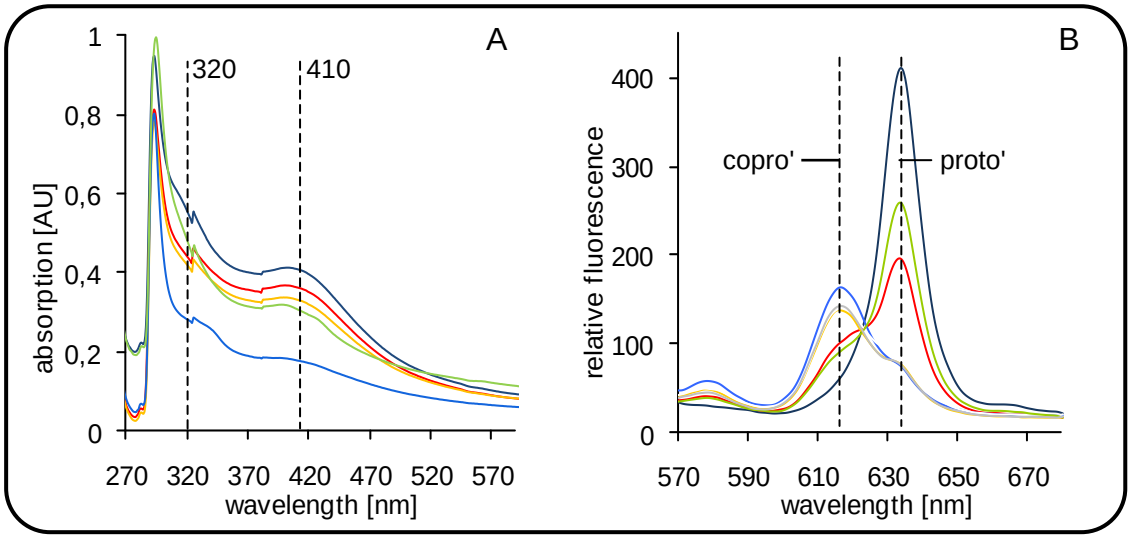

Figure 4-8: UV-visible light absorption spectra and CPO activity of purified HemN variants (3 mg/mL). A: UV-visible spectra of purified variants were recorded under anaerobic conditions. The presence of an iron-sulfur cluster was indicated by an absorption maximum at 410 nm and a shoulder at 320 nm **B**: CPO activity was determined as described (**section 3.8.5**). One of three experiments is shown; average activities are given in **Table 4-1**. Expected peaks are at 618 nm for copro' (substrate) and 633 nm for proto' (product). Wildtype HemN_wt (—), HemN variant Q311N (—), HemN variant R22K (—), HemN variant R22A (—), HemN variant R359A (—), blank (—). AU: absorbance unit.

CPO activities of wildtype HemN and its variants are shown in **Figure 4-8 B**. The dark blue trace again represents wildtype activity. A single peak at 633 nm indicates the complete conversion of copro'gen to proto'gen in the setup. All HemN variants exhibited reduced CPO activity compared to the wildtype. The variants R359A and Q311N are still able to convert copro'gen, but a shoulder at 618 nm results from residual copro'gen in the experimental setup hence indicating a reduced CPO activity of these variants compared to wildtype. A complete loss of activity was observed for the two Arg22 variants with similar fluorescence spectra like in the negative control. Average results of three activity assays, the iron content per HemN-molecule, and the results of a SAM-cleavage assay are provided in **Table 4-1**.

Table 4-1: Properties of HemN variants compared to wildtype enzyme

HemN variant	total iron content [mol iron/ mol HemN]	SAM-cleavage [%][1]		CPO activity [%][4]
		+ electron acceptor[2]	- electron acceptor[3]	
wildtype	2.7	100	100	100
Q311A	1.9	--	--	0
Q311N	2.5	100	62	42
R22K	1.3	4	88	4
R22A	1.1	0	13	1
R359K	2.0	--	--	100
R359A	1.4	60	62	71

[1] SAM-cleavage was determined using [^{14}C]-SAM and different electron acceptors. The amount of [^{14}C]-methionine formed during a reaction was determined after HPLC-separation of [^{14}C]-SAM and [^{14}C]-methionine. Fractions of the methione-peak area of the total peak area were calculated, fractions of wildtype activity were set to 100 % and variant activities related to that. Denoted are the results of a single experiment.

[2] SAM-cleavage with terminal electron acceptor was determined using *E. coli* cell-free extract (compare **section 3.8.6**)

[3] SAM-cleavage without terminal electron acceptor was determined using Na-dithionite as reductant for the Fe-S-cluster (compare **section 3.8.6**).

[4] CPO activity was determined using non-labeled SAM and *E. coli* cell-free extract. Maximum peak height at 633 nm of wildtype CPO was set to 100 % and the activities of the HemN variants were related to that. Denoted are the average activities from three independent experimental setups.

Green: HemN variants characterized by Katrin Grage

The enzymatic activity of wildtype and variant HemN does not correlate particularly well with the rate of SAM-cleavage. R22K, for instance, cleaves SAM even without a terminal electron acceptor, despite a low iron-content and despite a near complete absence of product. The enzymatic activity of Q311N is similarly strongly reduced being comparable to wildtype HemN in iron content and SAM cleavage in the presence of extract.

4.4 Detection of a Reaction Intermediate of HemN

Oxygen dependent copro'gen oxidase (HemF) has been shown to first oxidatively decarboxylate the propionate side chain of pyrrole ring A to the corresponding vinyl-group, giving rise to the intermediate product harderoporphyrinogen (hardero'gen). In the case of HemN, such an intermediate product has not as yet been demonstrated. To detect

the potential intermediate hardero'gen, an activity assay using the fluorescence spectrophotometer is not useful because the spectroscopic features of harderoporphyrin (hardero') (a single fluorescence peak at 630 nm) are not sufficiently different from those of the reaction product proto' with a fluorescence peak at 633 nm. Instead it proved possible to separate the tetrapyrroles by HPLC analysis. Samples from HemN activity assays, taken at different times, were oxidized and the tetrapyrroles analyzed by HPLC (**sections 3.8.5** and **3.8.9**; **Figure 4-10**).

To get a hardero' standard for HPLC analysis, purified variant R401K of human oxygen dependent copro'gen oxidase (HemF) was also used in an activity assay (**section 3.8.7**). This mutant is known to accumulate its intermediate product hardero'gen during catalysis (Schmitt *et al.*, 2005). A plasmid coding for this HemF variant was kindly provided by the group of Prof. Jean-Charles Deybach (Centre Français des Porphyries, Université Paris VII, Hôpital Louis Mourier, France). Fluorescence spectra of an activity assay of this HemF variant are presented in **Figure 4-9**.

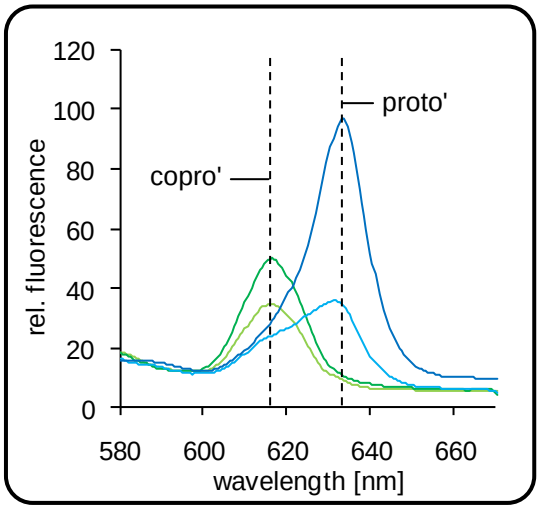

Figure 4-9: Activity assay of HemF variant R401K. The product spectra of R401K after 5 and 90 min are shown in light and dark blue, respectively, the corresponding controls without HemF in light and dark green.

The second possible intermediate of HemN, isoharderoporphyrin (isohardero'; vinyl group on ring B), is not available as a standard.

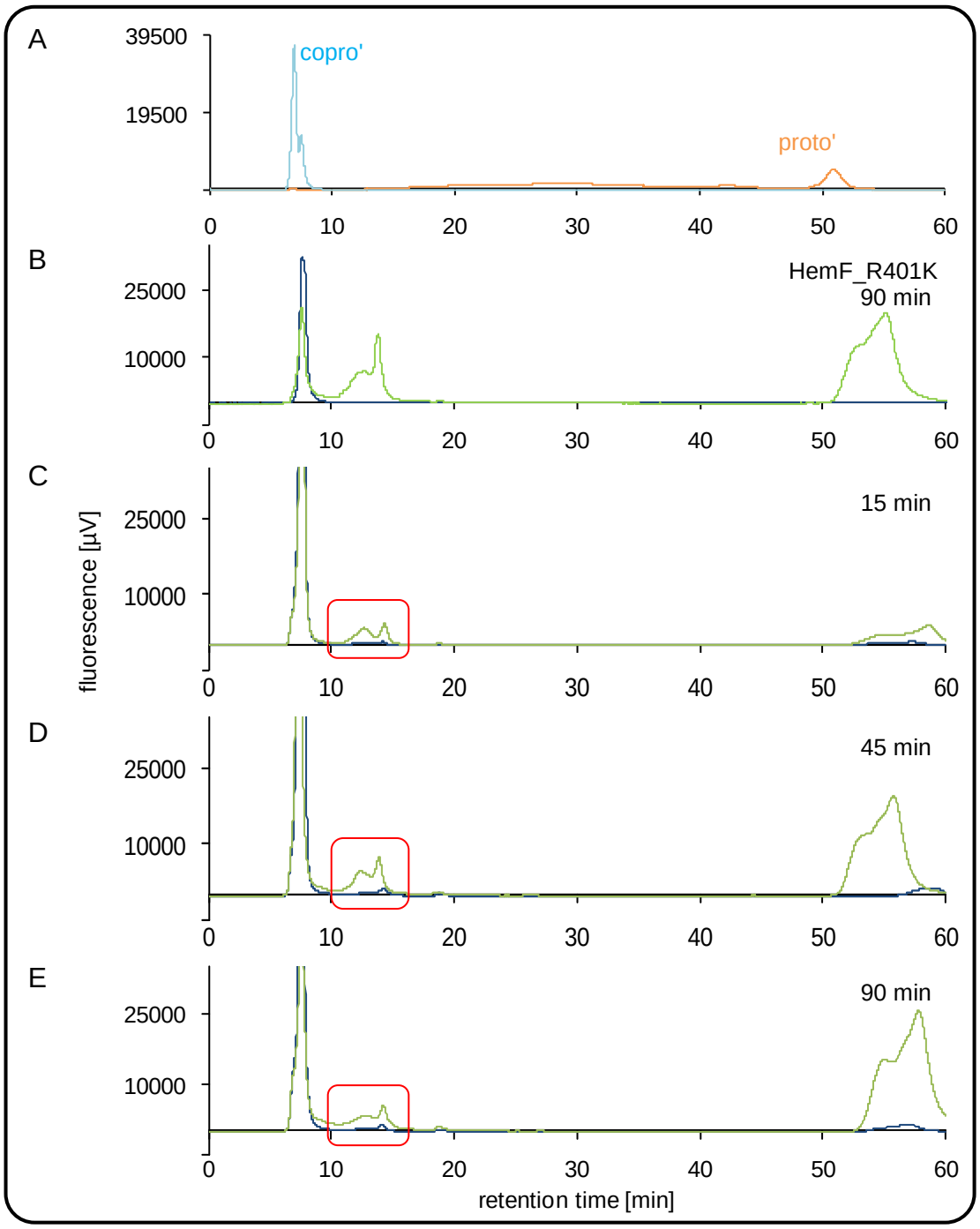

Figure 4-10: HPLC analysis of oxidized tetrapyrroles after wildtype HemN and HemF variant R401K activity. A: commercially available copro' and proto' were used as standards. Samples were taken from the activity assay of HemF variant R401K (**B**) and wildtype HemN (**C-E**) after different times of incubation. The green trace in each case shows the set up with the corresponding enzyme, the blue line corresponds to the control reaction where everything but the enzyme was added. For the HemN reactions two yet unknown peaks, running at 12.1 and 13.7 min, are marked with red boxes. Shown are the results of one of three separate setups each.

Figure 4-10, A indicates that copro' and proto' are nicely separated by the applied HPLC system shown here for the commercially available standards. The copro' peak was

reproducibly found at a retention time (rt) of 7.5 min. Retention times proved inconsistent for longer retention times. As a result, the peak resulting from proto' was observed between 52 and 58 min, often as a broad peak. In addition to the peaks corresponding to copro' and proto', two peaks were observed for the hardero' accumulating HemF variant at retention times of 12.3 and 13.8 min probably corresponding to hardero' (**Figure 4-10, B**). Interestingly peaks with retention times of 12.1 and 13.7 min were also observed as a result of wildtype HemN activity indicating hardero' to be synthesized during the HemN reaction. Maximum heights of these peaks were observed after 30, 45, and 60 min HemN reaction (45 min shown in **Figure 4-10, D**), being smaller after 15 and 90 min. In the corresponding control reactions without HemN respective peaks were smaller or absent. During the 90 min of reaction the peak corresponding to copro' is gradually reduced by HemN with the proto' peak accordingly increasing. In the control reactions copro'gen is not converted to proto'gen. Only after 90 min of reaction time a small peak corresponding to proto' is detected most probably due to some extract activity (**Figure 4-10, C-E**).

Tetrapyrroles were extracted from activity assays as described (**section 3.12**) and analyzed by mass spectrometry. Mass peaks could be observed that correspond to copro' (655.2 Da), hardero'/isohardero' (609.2 Da), and proto' (563.1 Da) (**Figure 4-11**).

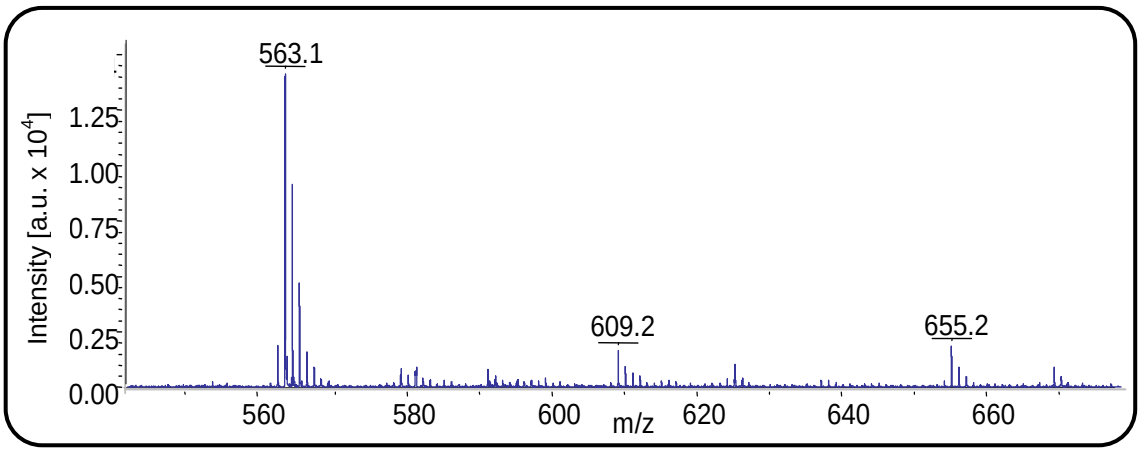

Figure 4-11: MALDI spectrum of extracted tetrapyrroles from a wildtype HemN activity assay. The sample was taken after 30 min reaction. Calculated masses for tetrapyrroles are 563.27 Da for protoporphyrin IX, 609.27 Da for harderoporphyrin/isoharderoporphyrin, and 655.28 Da for copro'.

4.4.1 Chemically Synthesized Harderoporphyrin

In cases where enzyme-substrate complexes are difficult to crystallize, the use of a reaction intermediate has occasionally proved useful. In the case of HemN, hardero'gen could represent such an intermediate. As hardero'gen or its oxidized counterpart hardero' are not available commercially, a collaboration was initiated with the group of Prof. Markus Kalesse (Department of Organic Chemistry, Biological Chemistry and Natural Product Synthesis; Leibniz University Hannover). In the course of this collaboration, hardero' was chemically synthesized and provided for biochemical analyses. **Figure 4-12** provides a simplified representation of the complex synthesis performed by Claudia Noll.

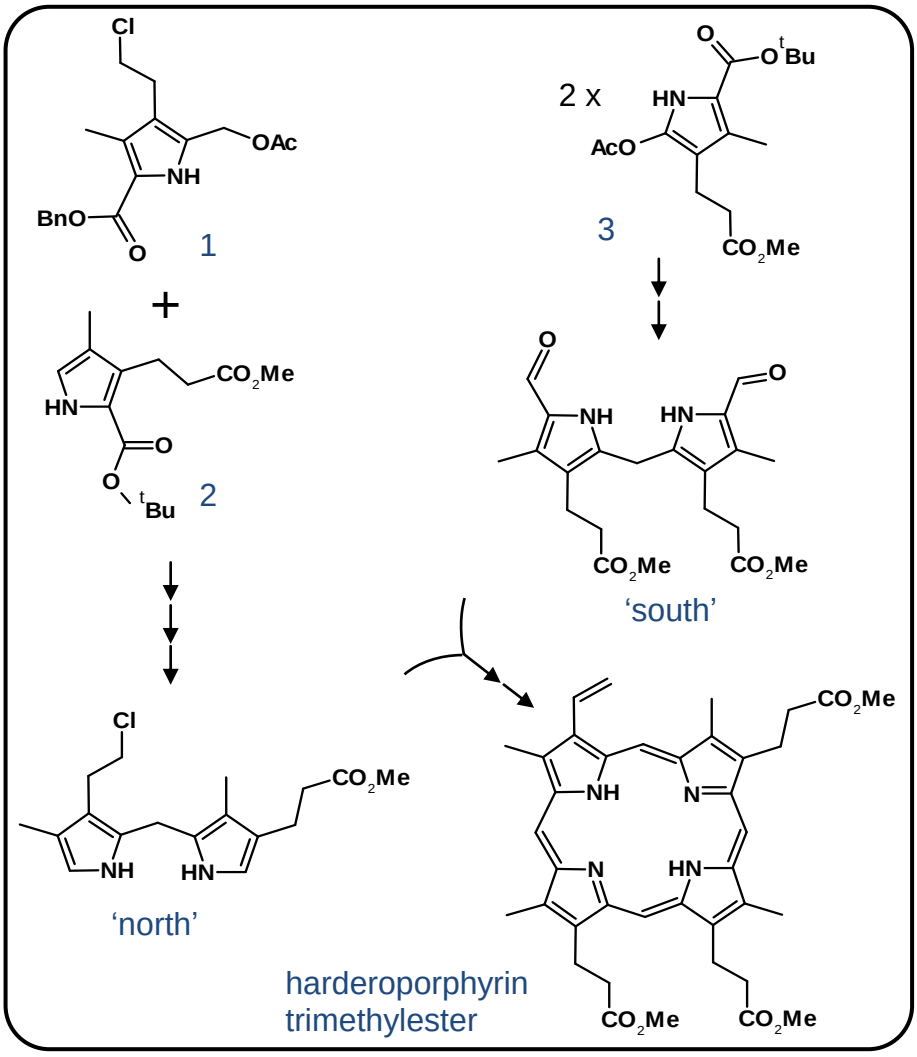

Figure 4-12: Simplified harderoporphyrin trimethylester synthesis performed by Claudia Noll. Four single-pyrrole fragments developed by retrosynthesis were synthesized separately (1-3). Fragment 1 was combined with fragment 2 to generate the 'north'-fragment, while two copies of fragment 3 yielded the 'south'-fragment. These dipyrrolic fragments were then coupled to produce a hardero'-trimethylester. Bn: benzyl; tBu: tert-butyl; Ac: acetyl; Me: methyl.

The synthesis involved 19 steps. Four pyrrole-based fragments of hardero', developed by retrosynthesis (Arsenault *et al.*, 1960), were separately synthesized and later combined into two different dipyrrolic intermediates (denoted as ‘north’ and ‘south’ fragments, **Figure 4-12**). The ‘north’ and ‘south’ fragments were finally coupled to yield the complete hardero' backbone (**Figure 4-12**). The synthetic reactions were performed as described with minor changes (Carr *et al.*, 1971; Cavaleiro *et al.*, 1974; Lash *et al.*, 1999; Chen *et al.*, 1999; Ludwig and Lehr, 2004). The overall yield, especially for coupling the ‘north’ and the ‘south’ intermediates (here the yield was 36 %), was low (Claudia Noll, personal communication). As final purification by HPLC saw further losses, this step was omitted in later rounds of synthesis. The final yield was 1.3 mg of HPLC-purified or 18.3 mg of non-purified hardero’. In each case hardero’ was provided as the trimethylester.

Working with the synthesized hardero’ entailed some problems. The dark red, oily hardero’ trimethylester was difficult to be dissolved in water or methanol. Only mixtures of methanol and acetone could keep it in solution. First attempts to reduce it with Na-amalgam resulted in a yellow solution that could not be used in HemN activity assays. As hardero' was provided as methylester, hydrolyzation was necessary to give the propionate side chains of hardero' before the chemical reduction and further experiments could be set up. As the hydrolyzation could not be optimized in the timeframe of this thesis, the synthesized hardero' was handed to Dr. Gunhild Layer, our cooperation partner at the TU Braunschweig.

4.5 Crystallographic Analysis of Potential HemN Substrate Complexes

4.5.1 Modeling Coproporphyrinogen III into Electron Density of Wildtype HemN

Wildtype HemN was purified (**section 3.7.5**) and successfully crystallized using published crystallization conditions (Layer *et al.*, 2003). In initial trials, copro'gen, produced by reducing copro' with Na-amalgam, was added to the crystallization drops in a four-fold molar excess to allow co-crystallization of the substrate with the protein. Hexagonal crystals grew in the presence and in the absence of substrate. Crystals were cryoprotected with 15-20 % PEG 400. Copro'gen was added to some cryodrops to allow the substrate to diffuse into the crystals and potentially bind to the active site.

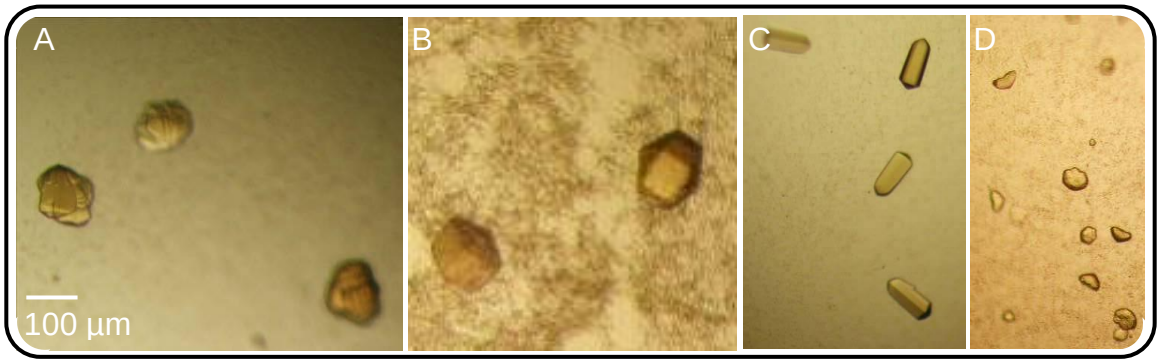

Figure 4-13: Crystals of wildtype HemN in hanging drop crystallization trials. Crystals were grown in 18 % PEG 4000, 10 % isopropanol, and 100 mM Hepes pH 7.0 or 7.2. Crystals were obtained by the microseeding technique using 2^{8}, 2^{10}, and 2^{12} dilutions (**A**-**C**) as well as without microseeding (**D**) (**section 3.9**). In **A** and **B,** the concentration of copro'gen in the crystallization drop was 100 µM. Crystals of **A** were additionally soaked for 1 min in 40 µM copro'gen solution. In both **C** and **D** no substrate was present during the crystallization experiment.

Data were collected for two crystals (dataset 1 from condition **A**; dataset 2 from condition **B** of **Figure 4-13)** at beamline X13 (DESY, Hamburg, Germany). Data collection statistics are provided in **Table 4-2.** The structures were solved by molecular replacement (using PHASER from the CCP4 Suite) using the published HemN structure (PDB entry: 1olt) as searching model.

Table 4-2: Data collection statistics for two datasets of wildtype HemN crystals. Dataset 1 was collected from a crystal from **Figure 4-13**, A; dataset 2 from **Figure 4-13**, B, respectively. All data were processed using XDS and SCALA.

Dataset	1	2
Beamline	DESY X13	DESY X13
Wavelength [Å]	0.8015	0.8015
Space group	$P6_3$	$P6_3$
Resolution [Å]	32.8 - 2.5 (2.64 - 2.5)	37.8 - 3.1 (3.27 - 3.1)
Unit cell axis a=b, c [Å]	111.4 , 75.6	111.6 , 75.5
Unique reflections	18591 (614)	9844 (322)
Completeness [%]	99.9 (98.8)	99.9 (97.0)
Redundancy	14.6 (12.6)	11.3 (11.5)
Mosaicity [°]	0.81	0.66
Wilson B-factor [$Å^2$]	45.0	63.5
I/σI	8.3 (2.0)	6.0 (1.7)
R_{merge} [%]	7.2 (38.9)	12.3 (45.0)
Values in parentheses refer to shell of highest resolution.		

As a possible aim of this thesis was the analysis of the complex between the substrate copro'gen and HemN by X-ray structural analysis, data were all processed but structure refinement only proceeded to that point where residual difference electron density would allow a potential tetrapyrrole to be identified. In cases where electron density for the substrate could not be seen, structure refinement was discontinued in favor of investigating alternative conditions that would allow substrate binding to the active site of HemN. **Table 4-3** provides the refinement statistics for the two wildtype HemN crystals.

Table 4-3: Refinement statistics for wildtype HemN crystals. Datasets are labeled according to **Table 4-2**. For dataset 2, additional refinement statistics for two models are provided where copro'gen was added in two distinct positions into the structure of dataset 2. For dataset 2 statistics for a model with both SAM molecules and copro'gen are given in A, statistics for a model in which copro'gen replaces SAM2 in B. The corresponding statistics result from ten cycles of likelihood restrained refinement in REFMAC5**.**

Dataset	1	2		
	without copro'gen	without copro'gen	A	B
R_{work} [%]	26.7	24.3	24.3	24.5
R_{free} [%]	30.8	30.7	33.8	34.4
Number of atoms				
Protein	4066	3568	3568	3568
Solvent	0	6	6	6
FeS	8	8	8	8
SAM	65	57	57	30
Coproporphyrinogen III	0	0	47	47
Cl	0	0	2	2
Ramachandran plot regions				
Favored [%]	89.7	87.1	84.5	83
Allowed [%]	8.5	12.1	14.4	15.7
Generously allowed [%]	1.0	0.3	0.5	0.8
Disallowed [%]	0.8	0.5	0.5	0.5
r.m.s.d. from ideal				
Bond lengths [Å]	0.020	0.012	0.013	0.013
Bond angles [°]	2.56	1.46	1.86	1.88
R_{free} test set size is 5 %				

For both datasets, the overall structure of HemN was unchanged. The r.m.s. displacement between equivalent atom positions of the published structure and the potential substrate complex are 0.48 Å for dataset 1 and 0.40 Å and dataset 2, indicating a largely unchanged structure. In the case of dataset 2, some difference electron density features were observed in the active site cleft that are not accounted for by the published model of HemN (**Figure 4-14**).

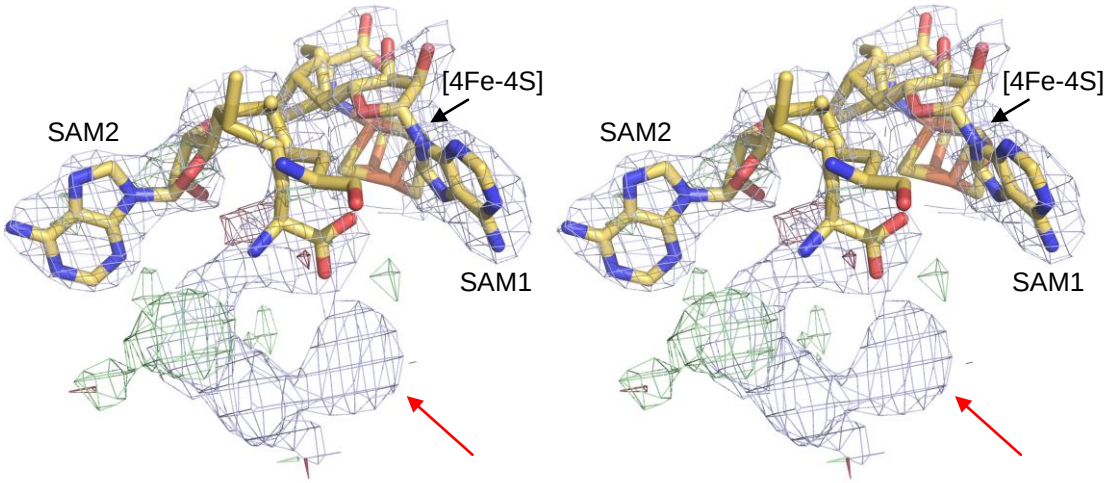

Figure 4-14: Stereo view of the cofactors of wildtype HemN as refined using dataset 2 together with observed electron density. HemN cofactors are shown as yellow sticks. Electron density is shown for the cofactors and for the active site cleft after major likelihood restrained refinement. Electron density (blue) unexplained by the model is marked by a red arrow. $|2F_o\text{-}F_c|$-electron density is shown in blue, $|F_o\text{-}F_c|$-maps in green (positive) and red (negative). Contour levels are 1σ and 3σ, respectively.

Copro'gen could be modeled into the density. As the reduced forms of tetrapyrroles are very flexible, the exact positions of the pyrrole elements and the side chains can only be estimated. One possible conformation is shown in **Figure 4-15**. The positions of pyrrole rings A and B might be interchanged and the pyrrole side chains might be positioned in a different way during catalysis. As the pyrrole ring A and its propionate side chain occupy the same electron density previously assigned to the methionine part of the second SAM molecule (SAM2), this methionine moiety had to be moved away by modifying the torsion angles of SAM2 (**Figure 4-15**). Only one of the possible conformations is shown here for the SAM2.

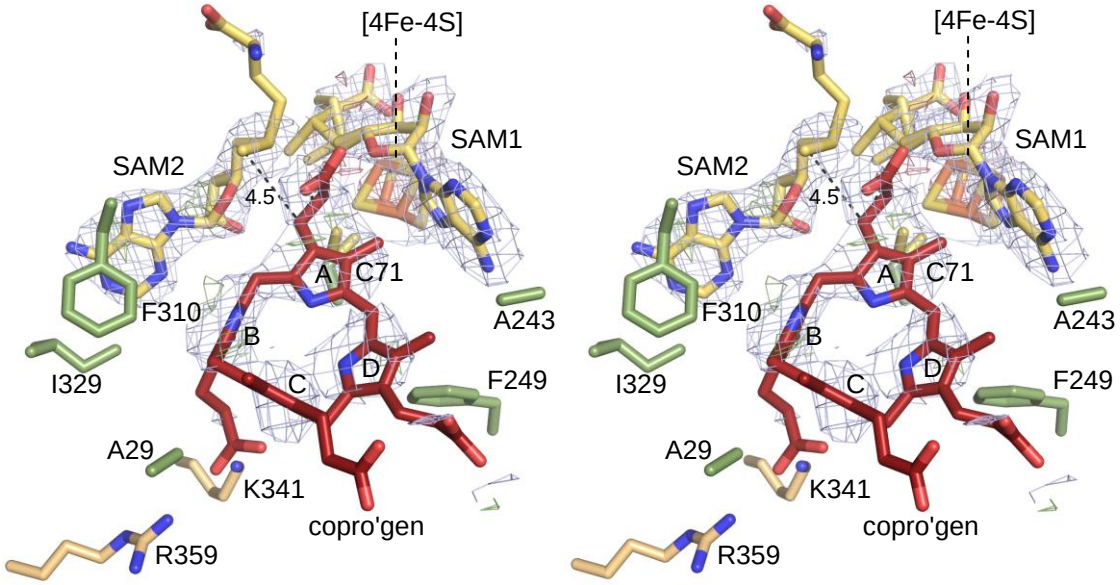

Figure 4-15: Stereo view of the active site of wild-type HemN (dataset 2) with modeled coproporphyrinogen III and modified methionine of SAM2. SAM cofactors and [4Fe-4S]-cluster are shown in yellow, the modeled copro'gen in red. Amino acids that could coordinate copro'gen in the modeled conformation are rendered in green for hydrophobic interactions and in light orange for hydrogen bonds. The distance of the β-carbon to the S-C5' bond of SAM2 where the 5'-deoxyadenosyl radical is postulated to be generated is marked with a dashed line and given in Å. The distance of the β-carbon to SAM1 is 5.1 Å). Electron density ($|2F_o\text{-}F_c|$, 1σ) is shown in blue after 10 cycles of restrained refinement, weighted difference maps ($|F_o\text{-}F_c|$) in green (3σ) and red (-3σ).

In the modeled position in **Figure 4-15** the propionate side chain of pyrrole ring B of copro'gen would be hydrogen bridged by residues Arg359 and Lys341 with distances of 2.9 and 3.0 Å, respectively. The pyrrole rings would be stabilized by hydrophobic interactions provided by Ala29, Cys71, Phe249, Phe310, Ile329, and Ala243. In the given position the distances between the 5'-deoxyadenosyl radical and the β-carbon, from which a hydrogen atom is abstracted during HemN activity would be 5.1 Å to SAM1 and 4.5 Å to SAM2. As the 5'-deoxyadenosyl radical might move after SAM cleavage, hydrogen abstraction on pyrrole ring A would be possible in this model. For the propionate side chain of pyrrole ring B the distance to both SAM molecules would be too long for the hydrogen abstraction by the radical. A rearrangement of HemN or copro'gen, or the formation of an intermediate HemN radical (for example at Cys71 like postulated by Layer (2005)) would thus be indispensable for the second decarboxylation.

Presuming that binding of SAM2 is an artifact of crystallization and not of physiological relevance, allows copro'gen to be positioned in its place significantly closer to SAM1 and the [4Fe-4S]-cluster (**Figure 4-16**). The distance from the β-carbon of pyrrole ring A to

the 5’-deoxyadenosyl radical would be 4.4 Å in this model.

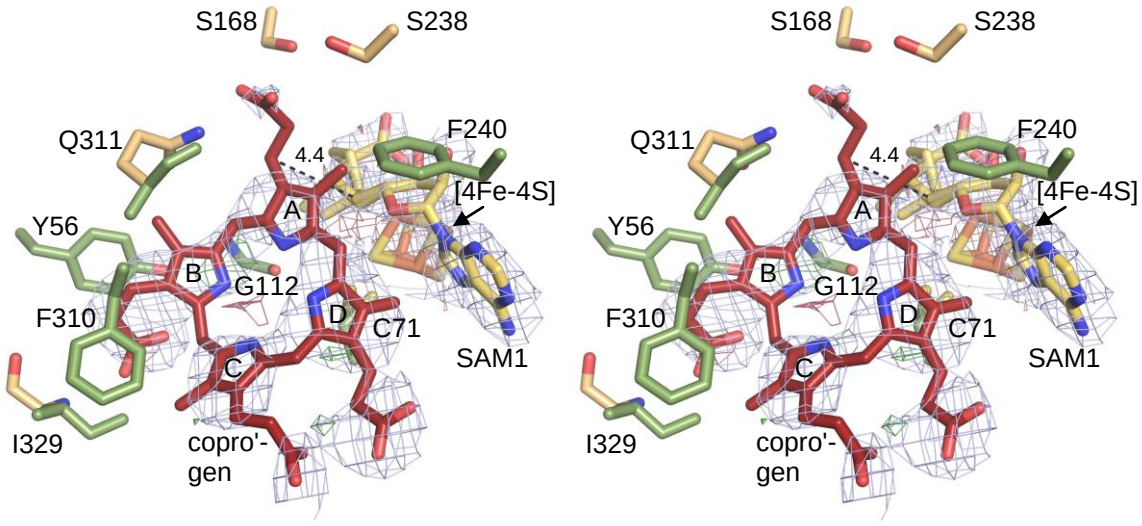

Figure 4-16: Stereo view of the active site of wildtype HemN (dataset 2) including coproporphyrinogen III but without SAM2. SAM1 and the [4Fe-4S]-cluster are shown in yellow, the modeled copro’gen in red. Electron density ($|2F_o\text{-}F_c|$, 1σ) is shown in blue after 10 cycles of restrained refinement, weighted difference density ($|F_o\text{-}F_c|$) in green (3σ) and red (-3σ). Amino acids that could coordinate copro'gen in the modeled conformation are rendered in green for hydrophobic interactions and in light orange for hydrogen bonds. The distance of the β-carbon to the S-C5’ bond of SAM2 where the 5’-deoxyadenosyl radical is postulated to be generated is marked with a dashed line and given in Å.

In this model Ile329, Gln311, Ser168, and Ser238 are positioned to form hydrogen bonds with the carboxyl groups of the propionate side chains of pyrrole rings A and B. Hydrophobic interactions again stabilize the pyrrole rings. Whereas the β-carbon of the propionate side chain A would be appropriately positioned for hydrogen abstraction (the distance to the postulated 5’-deoxyadenosyl radical is 4.4 Å before SAM cleavage) rearrangements of copro'gen or the formation of an intermediate HemN based radical would again need to occur for the second oxidative decarboxylation on pyrrole ring B.

Both models were refined using REFMAC5 (Murshudov *et al.*, 1997). 10 cycles of restrained refinement were performed with the modeled copro'gen in the different positions to check how the modeled copro'gen would affect the calculated electron density. Refinement statistics for each model are given in **Table 4-2**. Neither the obtained R-factors nor the electron density confirmed the modeled position or were suggestive of an alternative position or conformation of copro'gen. Accordingly neither of the modeled copro'gen positions is favored by the obtained electron density and no clear evidence for the reaction mechanism is yielded.

As the HemN copro'gen complex could not be determined unambiguously different routes were pursued to get a higher occupancy of a binding tetrapyrrole. These experimental setups are elucidated in the subsequent paragraphs.

4.5.2 Crystallizing HemN with Enzymatically Synthesized Substrate

Synthesizing Coproporphyrinogen III with Four Enzymes of the Heme Biosynthesis Pathway

Reducing porphyrins by Na-amalgam is an established technique since the late 1950s (Falk, 1964). Nevertheless, anecdotal evidence indicates that corresponding products are not necessarily suitable for co-crystallization experiments. Thus uro'gen decarboxylase, another tetrapyrrole modifying enzyme, could not be co-crystallized with Na-amalgam reduced uro'gen, apparently because of the high pH of Na-amalgam reduced substrate (Phillips *et al.*, 2003). Analogously, repeated attempts to crystallize HemN with Na-amalgam reduced copro'gen yielded only low binding occupancy of substrate (previous section). In the case of uro'gen decarboxylase, successful co-crystallization with its product was achieved instead by enzymatic substrate synthesis using the precursor porphobilinogen and the two preceding enzymes added to the crystallization solution (Phillips *et al.*, 2003).

Following this approach, the enzymatic synthesis of copro'gen was attempted starting from ALA, the first common tetrapyrrole precursor. Porphobilinogen synthase (HemB) from *Pseudomonas aeruginosa* was provided by Nicole Frankenberg-Dinkel (Ruhr-University Bochum). The following three enzymes, porphobilinogen deaminase (HemC; *Bacillus subtilis*), uro'gen synthase (HemD; *Bacillus subtilis*), and human uro'gen decarboxylase (HemE) were recombinantly produced and purified by affinity chromatography. Whereas this proved relatively simple for HemC and HemD, HemE could not be expressed as soluble protein in a number of different *E. coli* strains and under diverse expression conditions as revealed by test expressions (data not shown). Switching to HemE of *Thermosynechococcus elongatus* did not significantly improve the yield. Soluble expression was only yielded when autoinducing medium was used, which allowed significant amounts of human HemE to be produced. Using this medium the

induction occurs with lactose and proceeds slower than with IPTG (Studier, 2005). In addition, the cell density was observed to be significantly higher than using LB medium (OD_{600} of 14.8 rather than 5.0) resulting in a corresponding increase in the protein yield of 15 mg/L compared to 3 mg/L (Phillips *et al.*, 1997).

The enzyme activities of HemB and HemC were tested by combining the enzymes in a buffer containing Mg^{2+}, K^{+}, and Cl^{-}, crucial for HemB activity, and adding ALA. A linear tetrapyrrole (namely pre-uroporphyrinogen) is synthesized that spontaneously cyclizes to uroporphyrinogen I. As this assay is performed under aerobic conditions, uroporphyrinogen I is immediately oxidized to red uroporphyrin I.

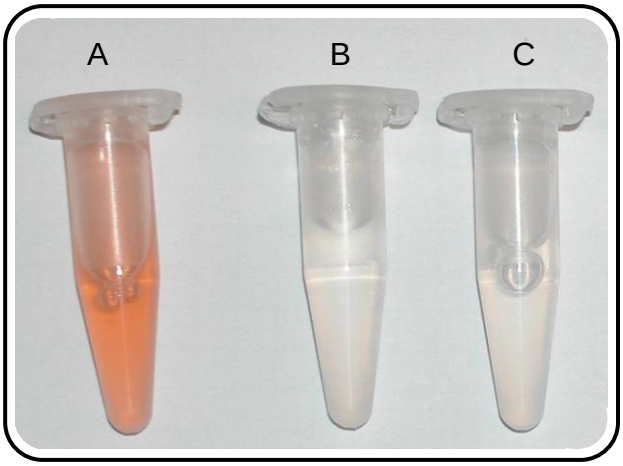

Figure 4-17: Activity assay for HemB and HemC. Shown are the mixtures of ALA with purified HemB and HemC (**A**), without HemC (**B**), and without HemB (**C**) after incubation (1 h, 37 °C).

When HemB, HemC and ALA are present together, the reaction solution turns bright red, whereas it remains colorless when either HemB or HemC is omitted (**Figure 4-17**) indicating that both enzymes are active and are required to produce the intermediate.

The activity of the remaining enzymes in the heme biosynthesis pathway cannot be easily analyzed, as all intermediate products share a similar red color when oxidized and cannot be distinguished easily. Instead, the activity of the enzymes was analyzed by distinguishing the production of oxidized tetrapyrroles by HPLC after combining all enzymes – or leaving away HemE, as a control (see **Figure 4-18**) (HPLC analysis was performed by Sonja Storbeck, group of Dr. Gunhild Layer, TU Braunschweig). Commercially available copro' was used as a standard.

Copro' has a rt of 60.6 min (**Figure 4-18, A**). In the absence of HemE, this peak is not detected (**Figure 4-18, B**), while peaks at rt of 10.1 and 6.6 min presumably correspond to uroporphyrin I and uroporphyrin III. When HemE is added, the peak expected for copro' was indeed observed (**Figure 4-18, C**).

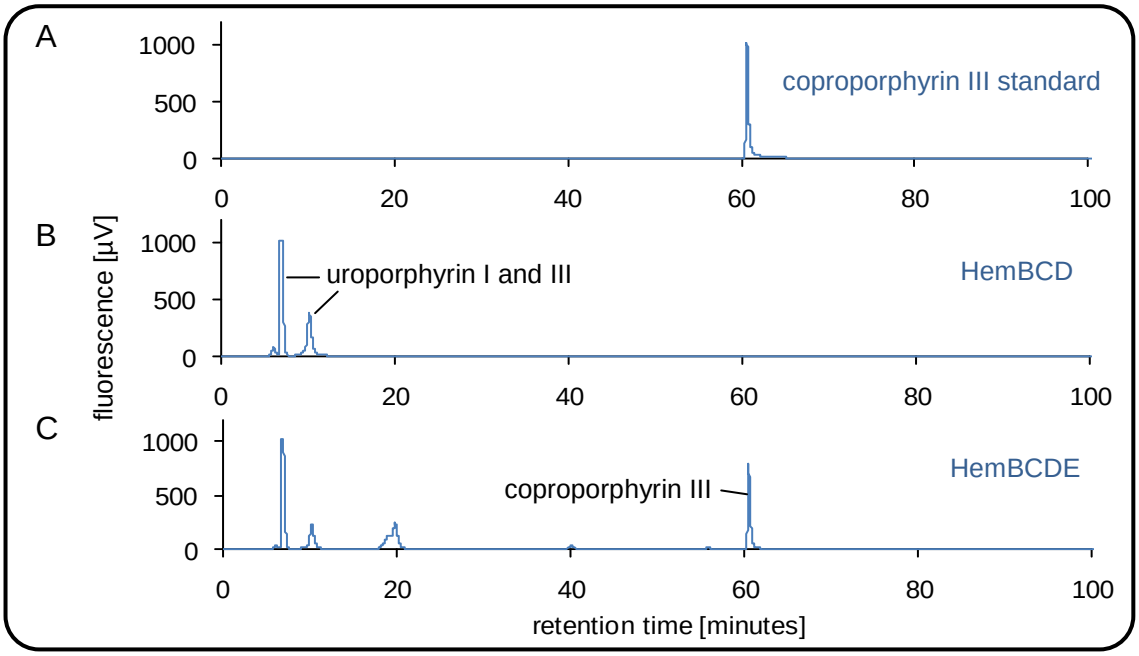

Figure 4-18: HPLC analysis of enzymatically synthesized tetrapyrroles during copro' synthesis. A: commercially available copro'. **B**: porphyrins after activity of HemB, HemC, and HemD, **C**: porphyrins after activity of HemB, HemC, HemD, and HemE.

Co-Crystallization of HemN and Enzymatically Synthesized Substrate

Commercial screens were used to identify new crystallization conditions that would allow the co-crystallization of enzymatically synthesized copro'gen and HemN variant I329A under anaerobic conditions. After 21 days, small hexagonal crystals were found in four conditions: 0.1 M MES, pH 6.5 and 25 % PEG 3000, PEG 4000, PEG 6000, PEG 8000 or PEG 10000 (PEGs Screen, QIAGEN, conditions C7 – C10). However, no electron density indicating a bound tetrapyrrole was found in these crystals.

4.5.3 Co-crystallization of HemN with H_2/Pd-reduced Coproporphyrinogen III

As the substrate concentration of enzymatically synthesized substrate is potentially too low for co-crystallization with HemN, another technique of reducing commercially available copro' with H_2 in the presence of the catalyst Pd was used (Bergonia *et al.*, 2009). In particular this method avoids the problems associated with the use of Na-amalgam. The experimental setup and an activity assay of wildtype HemN and the H_2/Pd reduced copro'gen are presented in (**Figure 4-19**).

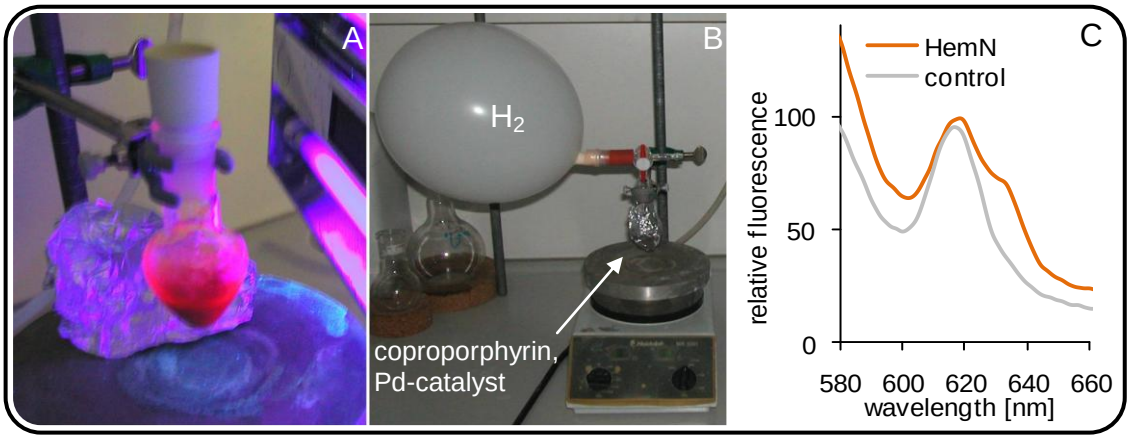

Figure 4-19: Coproporphyrin III-reduction with hydrogen and palladium-catalyst. A: oxidized copro' in the reaction mix prior to reduction exhibits strong fluorescence. **B**: experimental setup for reduction. The reaction mix is shielded from light by aluminum foil. **C**: HemN activity assay performed with palladium-reduced copro'gen. A fluorescence peak at 633 nm indicates HemN activity.

After ~1 h of H_2/Pd-reduction of copro' to copro'gen, fluorescence was no longer detectable indicating that reduction was complete. The reduced copro'gen, however, proved highly unstable, rapidly re-establishing a red color during the steps of removing the catalyst by filtering and methanol evaporation. Despite this observed re-oxidation of the copro'gen, an activity assay with freshly reduced copro'gen indicated that sufficient substrate remained and that HemN could convert this to proto'gen (small peak at 633 nm in **Figure 4-19**, **C**).

Modifying the technique by adding 2 mL of argon-bubbled 100 mM Tris/HCl pH 8.0 with 50 mM DTT and applying a vacuum to the reaction vessel for ~10 min to remove most of the methanol, yielded a solution of copro'gen that remained colorless for several weeks at -20 °C. The nature of the produced compound is not entirely clear, however, as this presumed copro'gen could not be converted to proto'gen by HemN in an activity assay. This reduced copro'gen was nevertheless used in crystallization experiments. However, neither co-crystallization nor soaking experiments resulted in crystals containing the substrate although crystallization itself was not visibly affected by the presence of added substrate.

4.5.4 Co-crystallization Setups and Soaking of Protoporphyrinogen IX

Additionally to the setups with the substrate copro'gen, some co-crystallization experiments were also performed with the product proto'gen. Na-amalgam reduced proto'gen was kindly provided by the group of Prof. Dieter Jahn (TU Braunschweig), but no crystals were obtained under these conditions. In addition proto' was reduced with H_2/Pd. In this case crystals grew from wildtype HemN in setups with and without SAM being added to the crystallization drop (**Table 4-5**). Data were collected of both conditions at the beamline 14-1 at the BESSY. However, in each case no electron density fitting for a tetrapyrrole was found in the structures of these crystals and no significant differences to the already known wildtype HemN structure were observed. In fact, even when SAM was omitted from crystallization setups both SAM1 and SAM2 were well defined by the electron density (shown for SAM2 in **Figure 4-20**). This result is especially interesting for SAM2 as its involvement in HemN activity is still under discussion. Its presence in the HemN crystal structure without excess SAM in the crystallization condition argues for its physiological relevance.

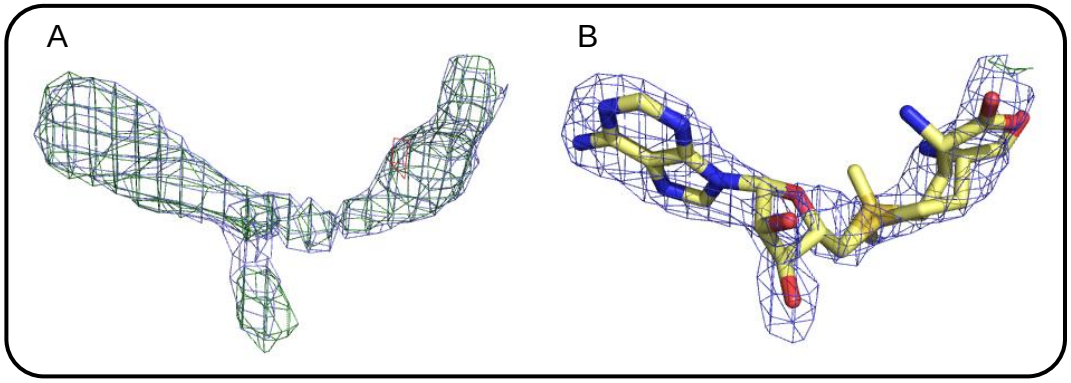

Figure 4-20: Electron density of SAM2 in wildtype HemN crystal where SAM was omitted from the crystallization condition. A: Electron density ($|2F_o\text{-}F_c|$, 1σ) obtained when SAM2 was omitted from the HemN model is shown in blue after 1 cycle of restrained refinement. Weighted difference density ($|F_o\text{-}F_c|$) is shown in green (3σ) and red (-3σ). A SAM molecule could easily be fitted into this density and the electron density obtained after restrained refinement further confirmed the presence of a SAM molecule at this position (**B**).

4.5.5 Co-crystallization Setups and Soaking of an Artificial Electron Donor

Soaking and co-crystallization experiments were also performed with wildtype HemN and the addition of copro'gen in combination with the reducing agent Na-dithionite. The idea behind these experiments was to add an electron donor together with the substrate to

get the reaction started. As there was no electron acceptor present in these setups, the reaction could not be completed and the substrate or already an intermediate product might be trapped in the active site of HemN. Some crystals were obtained that grew under the same conditions like wildtype HemN crystals and shared the same morphology like those. The overall structure of HemN, however, was again unchanged compared to the published HemN structure in these crystals.

4.5.6 Co-crystallization Setups and Soaking of an Artificial Electron Acceptor

The physiologic electron acceptor of HemN is yet unknown. By soaking experiments of wildtype HemN crystals with an artificial electron acceptor we aimed for some information about the electron acceptor binding site of HemN. For this purpose phenazine methosulfate (PMS) was utilized. PMS is an electron acceptor and carrier in enzyme systems being yellow in its oxidized and colorless in its reduced form. For soaking experiments, both solid PMS and freshly prepared PMS-solutions were used. In **Figure 4-21** one soaking experiment is documented.

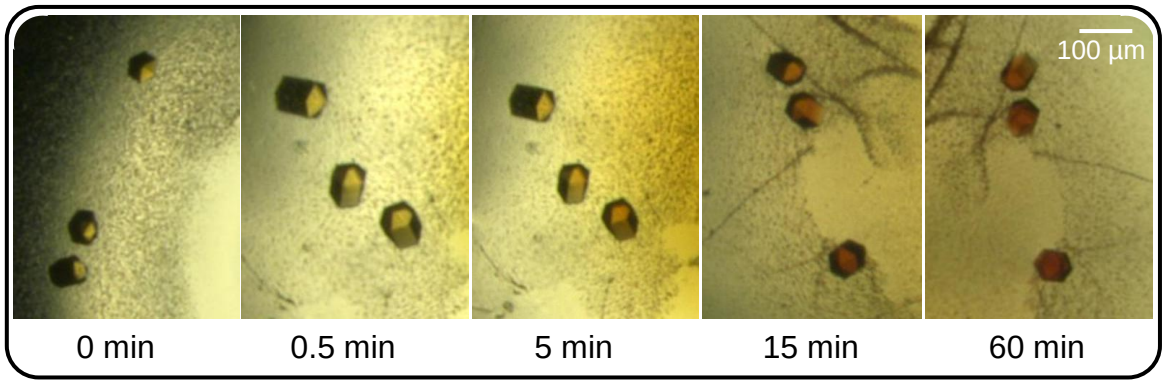

Figure 4-21: Soaking of PMS into wildtype crystals. A crumb of solid PMS was added directly to the crystallization droplet. The droplet turned to a dark yellow/orange color, whereas the crystals turned red. No changes in the crystals (shape, cracks) were noticed. Pictures were taken after the indicated times and crystals were mounted at different time points.

Despite the clear change of color of the crystals in this drop, no changes in the crystals (especially no damages) were observed even after one hour of incubation with PMS. In the structure of a crystal harvested and flash-cooled after 60 min no electron density could be observed that indicated the presence of PMS. As expected, the overall structure of HemN did not change in the presence of PMS.

4.6 Crystallizing the SAM2 Binding Site Variant I329A

Mutational and functional analyses of the SAM2 binding site had previously indicated residues Ile329 and Gln311 being crucial for SAM2 binding (Grage, 2005; Layer *et al.*, 2005a). Despite an intact [4Fe-4S]-cluster, HemN mutants I329A and Q311A are unable to convert copro'gen to proto'gen. Whereas the addition of substrate, electron donor, and electron acceptor results in enzymatic activity in wildtype HemN, variants I329A and Q311A were observed to cleave only one SAM per HemN under these conditions. As SAM-cleavage is dependent on prior substrate binding, the observed partial cleavage of SAM led to the hypothesis that substrate binding is not completely abrogated by the described mutations. The HemN variants were furthermore concluded to bind only a single SAM-molecule resulting in the pre-termination of catalysis. Solving the crystal structure of these variants that would potentially trap a reaction intermediate in the conversion of copro'gen appeared an attractive starting point in gaining new insight into the reaction mechanism of HemN. As an intermediate protein conformation would furthermore potentially be trapped by this procedure, crystal contacts may be changed. Consequentially a new crystal packing arrangement would perhaps be achievable by this route.

The HemN variants I329A and Q311A were produced and purified anaerobically as described for wildtype HemN. The variants did not reveal any obvious differences to wildtype HemN during purification. After purification the iron content was 1.8 and 1.2 mol iron/mol HemN for I329A and Q311A, respectively. Several crystallization experiments were set up using these enzymes in combination with wildtype HemN crystallization conditions. In addition to the use of these crystallization conditions screening for new crystallization conditions with a possibly new crystal packing was performed.

The ability of the I329A variant to bind substrate was analyzed using H_2/Pd-reduced copro'gen in a 3.3 fold molar excess. The light red color of the substrate solution indicated that only marginal re-oxidation of the substrate had occurred previously. Alternatively, the heme precursor ALA as well as the intermediate enzymes HemB, HemC, HemD, and HemE were added to the HemN-solution for simultaneous enzymatic substrate synthesis (compare **sections 3.9** and **4.5.2**).

Independent of the presence or absence of copro'gen in the crystallization setups, crystals grew within 4-10 days. **Figure 4-22** presents some representative crystals grown from the I329A variant. Crystals depicted in **Figure 4-22 E** and **F** grew under identical reservoir conditions, but copro'gen was only added to the crystallization droplet presented in **Figure 4-22 E**. These crystals appear of a slightly darker color than crystals grown without substrate. **Figure 4-22 D** and **H** show crystals grown in commercial screens under conditions yet unknown for wildtype HemN crystallization. To these crystallization droplets ALA and enzymes for substrate synthesis had been added.

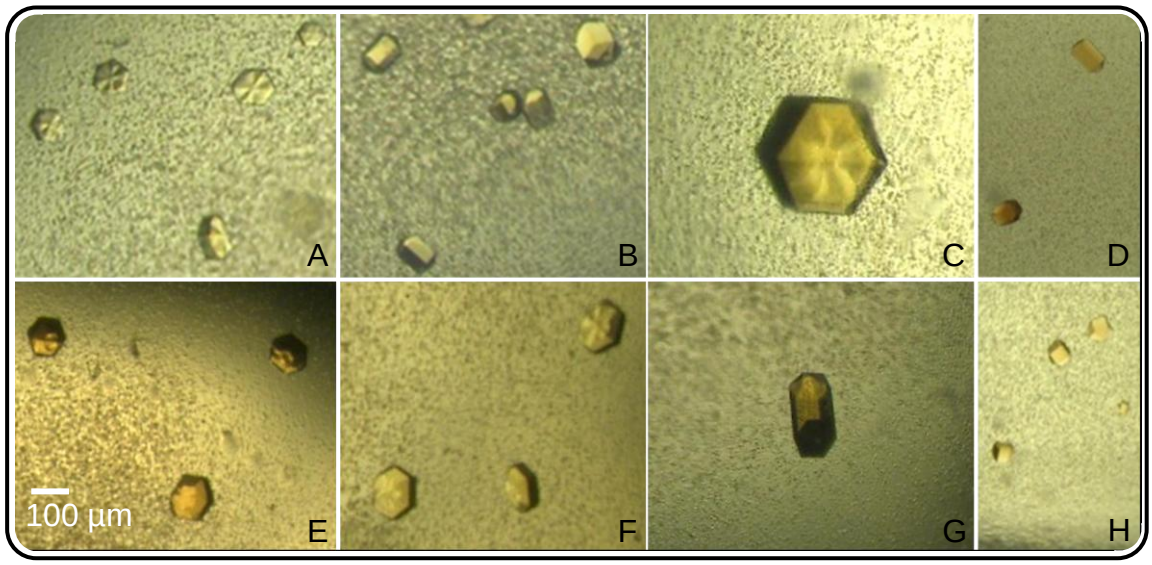

Figure 4-22: Representative hexagonal crystals of HemN variant I329A grown in 0.1 M Hepes pH 7.0 – 7.4; 20 % PEG 3350 (**A**), 20 % PEG 4000 (**B**), 19 % PEG 3350 (**C**, **E**, **F**), or 17 % PEG 3350 (**G**). Crystals in **D** and **H** grew under reservoir conditions with 0.1 M MES pH 6.5 and 25 % PEG 3000 and 8000 (PEGs, QIAGEN, C7 and C10), respectively. H_2/Pd-reduced substrate (**section 4.5.3**) was added to the protein-solution used in **E** and **G**. Crystals in **E** and **F** grew on the same cover slide in different drops. ALA in combination with all proteins for enzymatic substrate synthesis was added in drops **D** and **H**.

Independent of the crystallization condition and the presence or absence of substrate all I329A crystals share a hexagonal shape already described for wildtype crystals. Crystals were harvested using 15-20 % PEG 400 as cryoprotectant and employed in X-ray diffraction experiments. In terms of diffraction, no significant difference between crystals of wildtype HemN and I329A – whether with or without substrate – was observed. **Table 4-4** lists the statistics of three such datasets. Data reduction, molecular replacement and structure refinement were performed as described in **section 4.5.1.**.

Table 4-4: Diffraction statistics for three HemN variant I329A crystals. All data were processed with XDS and SCALA.

Dataset	Coproporphyrinogen III		
	None	H_2/Pd-reduction	Enzymatic synthesis
Data collection statistics			
Beamline	DESY X11	DESY X12	DESY X12
Wavelength [Å]	0.81500	0.97777	0.97777
Space group	$P6_3$	$P6_3$	$P6_3$
Resolution [Å]	33.48 – 2.1 (2.21 – 2.1)	40 - 2.05 (2.16 - 2.05)	40 - 2.65 (2.79 - 2.65)
Unit cell axis a=b, c [Å]	114, 76	113, 76	114, 76
Unique reflections	32962 (1086)	34752 (5072)	16223 (2354)
Completeness [%]	100 (100)	99.9 (100.0)	100.0 (100.0)
Redundancy	6.6 (6.7)	4.3 (4.3)	6.6 (6.6)
Mosaicity [°]	0.56	0.55	0.47
Wilson B-factor, [$Å^2$]	21.7	26.5	50.1
I/σI	6.2 (2.2)	7.0 (2.0)	6.2 (2.0)
R_{merge} [%]	10.1 (35.4)	8.3 (38.0)	10.3 (36.9)
Refinement statistics			
R_{work} [%]	22.3	25.7	22.9
R_{free} [%]	27.9	28.0	26.7
Number of atoms			
Protein	4066	4066	3703
Solvent	0	0	396
FeS	8	8	8
SAM	65	65	65
Ramachandran plot regions			
Favored [%]	90	92.8	91.3
Allowed [%]	9.3	6.7	8.2
Generously allowed [%]	0.3	0	0
Disallowed [%]	0.5	0.5	0.5
r.m.s.d. from ideal			
Bond lengths [Å]	0.020	0.014	0.006
Bond angles [°]	3.414	2.14	0.94
Values in parentheses refer to shell of highest resolution; R_{free} test set size is 5 %			

All structures were analyzed for the presence of copro'gen and other structural differences compared to the wildtype structure. Particular attention was paid to SAM2 as this was proposed to be absent in the variant I329A (Layer *et al.*, 2005a). **Figure 4-23** shows a superposition of the structures of variant I329A and wildtype HemN.

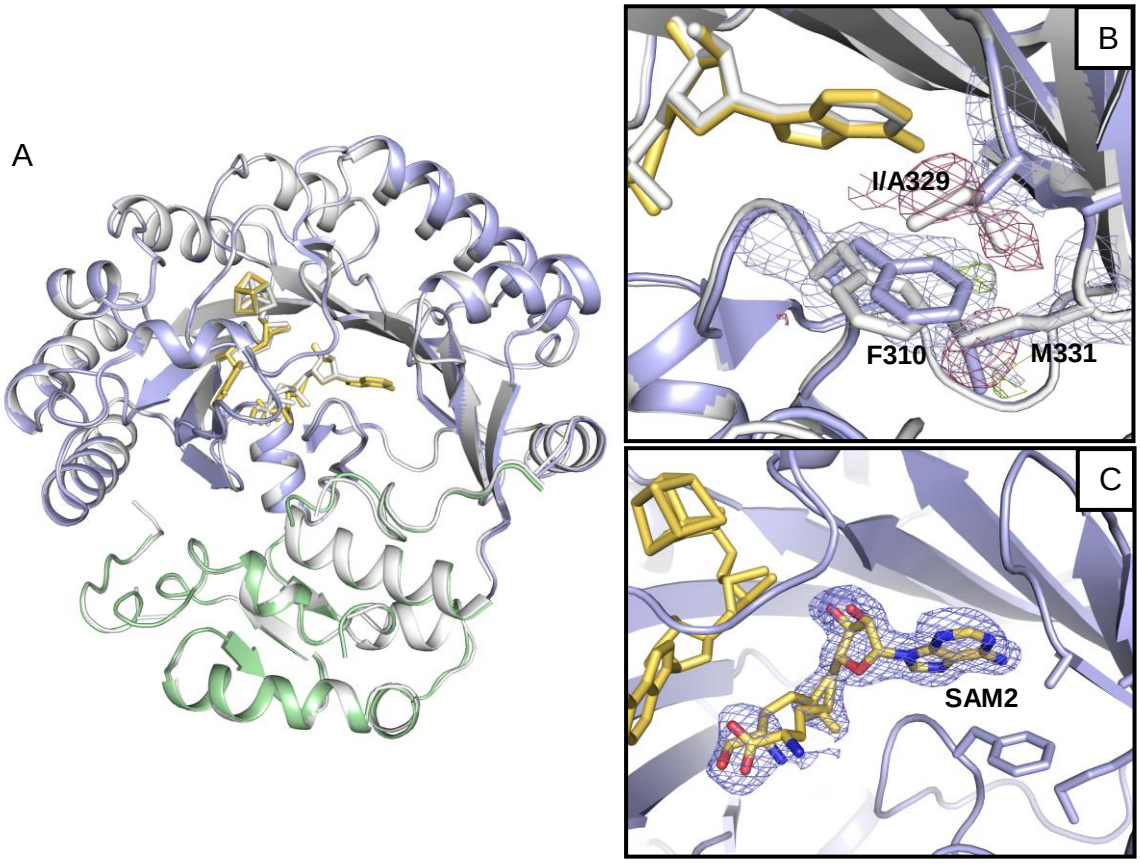

Figure 4-23: Superposition of wildtype HemN and variant I329A. The wildtype structure is rendered in gray. The C-terminal domain and trip-wire of HemN_I329A are shown in green, the catalytic domain in blue, and cofactors in yellow. Residues affected by the mutation (I329A) are shown in stick-representation and labeled in the upper zoom-box (**B**). Electron densities and difference electron densities for those residues are presented. In the lower zoom-box (**C**) the electron density of omit-map ($2F_o$-F_c), contoured at 3σ is shown for SAM2.

In all crystal structures of I329A (also in complex with either enzymatically produced or H_2/Pd-reduced substrate), negative difference electron-density (red) confirmed the successful substitution of Ile329 by alanine. Due to the shorter side chain of alanine, the side chains of Phe310 and Met331 reorient themselves towards SAM2, ~1.7 Å for the C_ζ-atom of Phe310 or 2.6 Å for the terminal methyl-group of Met331. Apart from these slight adjustments, no other differences between mutant and wildtype structure are observed. Instead, as documented by **Figure 4-23**, SAM2 is clearly present in the I329A variant. Mirroring the situation in the wildtype structure, the adenosine nucleoside is clearly defined in the electron density, whereas density for the methionine moiety is fragmented indicating more flexibility for this part of the molecule. Replacing isoleucine by alanine thus does not modify the coordination of SAM2. Phe310 still stacks upon the adenine of SAM2 and the hydrogen bonds remain intact as the back bone atoms of Ile329

do not move. Clearly, the observed changes of this variant concerning SAM cleavage and overall activity are not caused by the loss of SAM2 as postulated before (Layer *et al.*, 2005a), but by a different factor that is not accounted for by the present crystal structure of the I329A variant.

In **Table 4-5** the experimental setups described in the previous sections are summarized.

Table 4-5: Summary of experimental setups performed to get a tetrapyrrole bound/closed HemN-structure. Presented are setups from which diffracting crystals were obtained. PMS: Phenazine methosulfate.

HemN variant	Tetrapyrrole added	Additive	Data collected up to [Å]	Results
wt	Co-crystallization with and soaking of Na-amalgam reduced substrate copro'gen	SAM	2.0	No e^--density indicative of a present tetrapyrrole; no differences to apo-structure
wt	Co-crystallization with Na-amalgam reduced substrate copro'gen	SAM	3.0	Despite some unexplained e^--density, no tetrapyrrole could be unambiguously modeled into e^--density; no differences to apo-structure
wt	Co-crystallization with the product proto'gen	SAM	2.4	No e^--density indicative of a present tetrapyrrole; no differences to apo-structure
wt	Co-crystallization with the product proto'gen	no SAM	2.2	No e^--density indicative of a present tetrapyrrole. Both SAM molecules present; no differences to apo-structure
wt	Co-crystallization with H_2/Pd-reduced substrate copro'gen	SAM + artificial e^--donor Na-dithionite	2.5	No e^--density indicative of a present tetrapyrrole or any other additional molecule; no differences to apo-structure
wt	No tetrapyrrole added	SAM + artificial e^--acceptor PMS	2.7	No e^--density indicative of an additional molecule; no differences to apo-structure
I329A	Substrate synthesized enzymatically by addition of HemB, HemC, HemD, HemE, and ALA	SAM	2.7	No e^--density indicative of a present tetrapyrrole; no differences to apo-structure
I329A	Co-crystallization with H_2/Pd-reduced substrate copro'gen	SAM	2.0	No e^--density indicative of a present tetrapyrrole; no differences to apo-structure
I329A	Co-crystallization with and soaking of H_2/Pd-reduced substrate copro'gen	SAM	1.9	No e^--density indicative of a present tetrapyrrole; no differences to apo-structure

4.7 Rational Engineering of HemN Crystal Contacts

Due to the large size of the putative substrate binding site and the lid-like appearance of the C-terminal domain, HemN was proposed to undergo a conformational change upon substrate binding, resulting in a closed or spherical conformation being essential for catalysis (Layer *et al.*, 2003). Although HemN crystals were grown under a range of conditions, all retained the original hexagonal morphology, as well as similar unit cell dimensions and identical space group. Analyses performed in this thesis addressed the question whether the present crystal packing arrangement allows for the proposed closed substrate bound conformation of HemN. A closer look at the crystal packing of HemN revealed that it is dominated by HemN trimers packed into alternating layers in which trimers are rotated by 60° with respect to each others. Two such HemN trimers, in fact, constitute one unit cell. **Figure 4-24** depicts the dominant crystal contacts of wildtype HemN crystals. Crystal contacts can thus be subdivided into intratrimer and intertrimer interactions.

Near the three-fold crystallographic axis, neighboring HemN molecules interact by a π-π stacking between the carboxylate of Glu78 and the imidazole of His80. Due to the three-fold symmetry this interaction is repeated three times, resulting in a ring-like set of interactions, stabilizing the HemN trimer. The intratrimer interaction is further stabilized by a short bidentate salt bridge between Asp87 and Arg77 (N···O distances of 2.8 and 2.9 Å), additive salt bridges involving Lys64 and Glu90 (2.7 and 3.5 Å) as well as Lys128 and Asp187 (2.6 Å), and some hydrogen bonds.

Substantially fewer contacts stabilize intertrimer interactions: These involve a single salt bridge between Lys256 and Asp294 (2.4 Å), two hydrogen bonds between Arg253 and Gln279 (3.0 Å) and Ala230 to Thr247 (2.5 Å) and a number of van der Waals contacts.

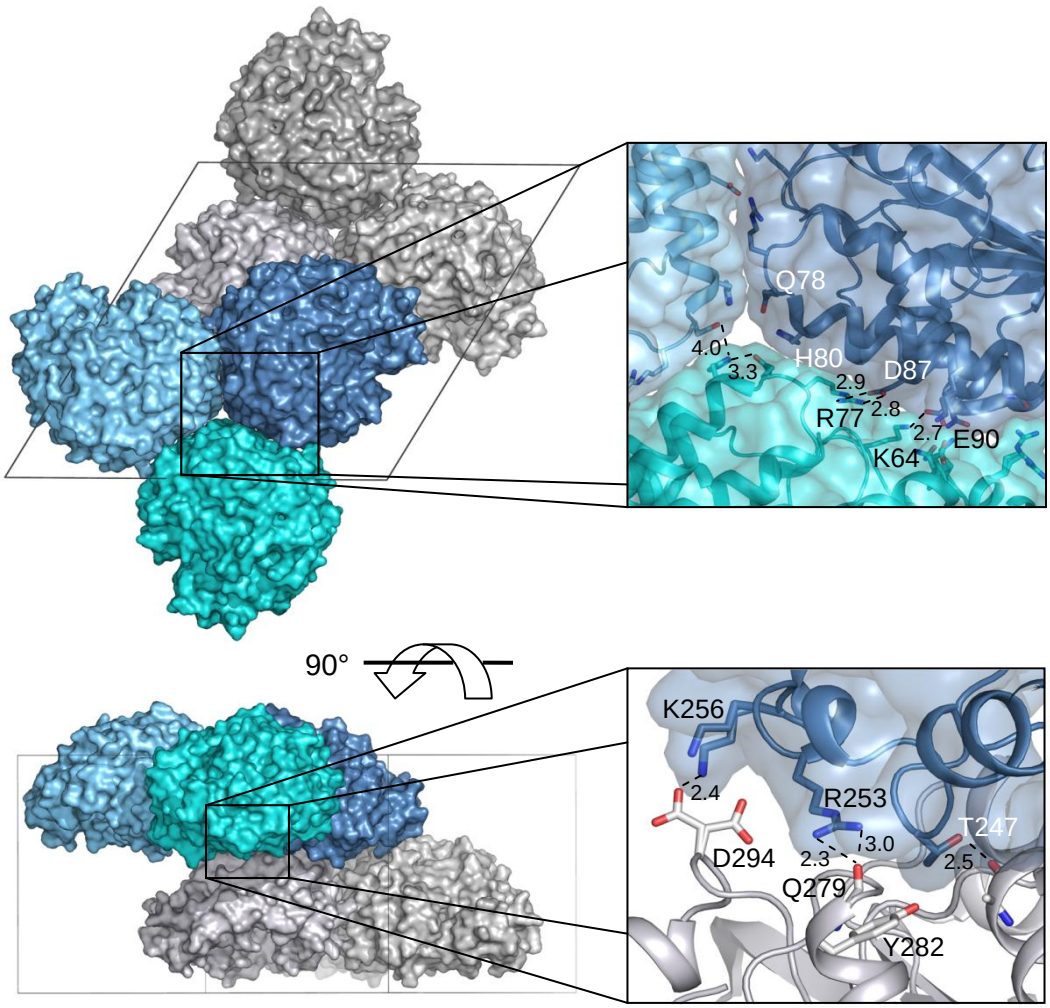

Figure 4-24: HemN crystal packing. All six HemN molecules in one unit cell are shown from two different perspectives. One trimer is colored in different shades of blue, the second trimer in shades of gray. Main contact areas with amino acids as stick representation and important distances between atoms labeled are shown in zoom boxes. Residues that were mutated in this work are colored white. Distances are given in Å.

A detailed analysis of the crystal packing arrangement of HemN indicates that although the C-terminal domain is only marginally involved in crystal packing contacts (one hydrogen bond between Ala138 and Lys405 with an N···O distance of 2.8 Å), the predicted movement of the C-terminal domain is physically prevented by the catalytic domain of a neighboring molecule within the crystal. In particular, α-helices α6 and α7 (nomenclature of Layer *et al.*, (2003)) of the adjacent molecule fill the space proposedly required for the C-terminal domain (see **Figure 4-25**).

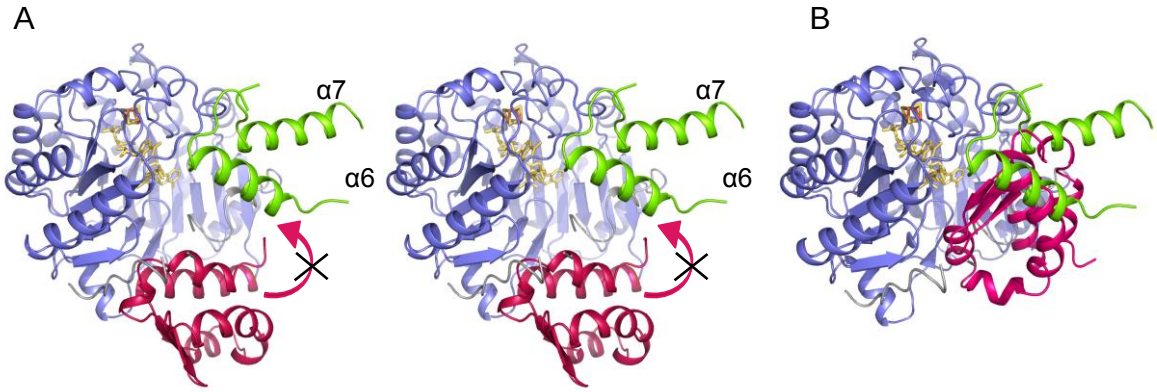

Figure 4-25: Proposed movement of C-terminal domain of HemN and its interaction with helices α6 and α7 of the adjacent HemN-molecule. A: stereo view of HemN as it is present in the crystal structure in $P6_3$ (PDB entry: 1olt) and the two helices of its symmetry equivalent. The crossed arrow marks the direction of the postulated movement of the C-terminal domain. **B**: Model of HemN in the closed form. The C-terminal domain was rotated as a rigid domain into a position where it would close the active site of HemN. Colors: C-terminal domain: pink, catalytic domain: blue, trip-wire: gray, cofactors: yellow, helices α6 and α7 of adjacent catalytic domain: green.

To prevent HemN molecules from repeatedly adopting the described packing arrangement that inhibits the putative closed substrate-bound conformation to be adopted, four residues involved in crystal contacts were substituted with the aim of enabling a novel packing arrangement (**Figure 4-26**):

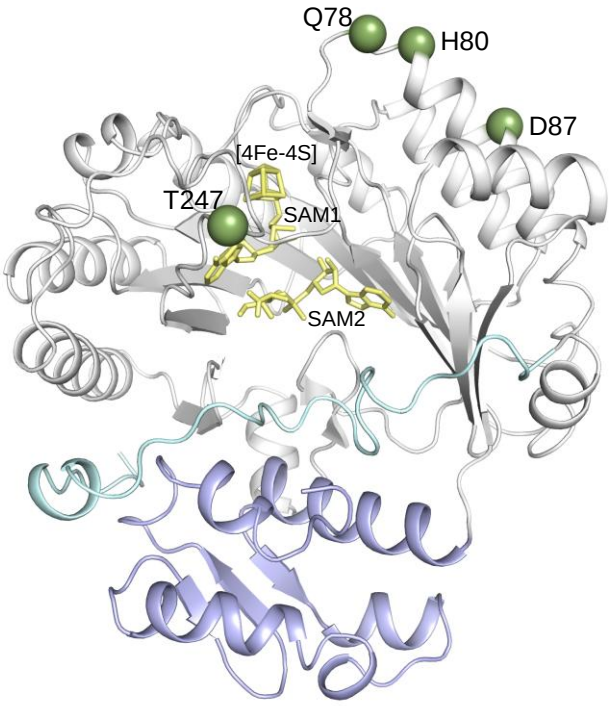

Figure 4-26: Positions of amino acid exchanges of crystal contacts in HemN. The catalytic domain is shown in gray, the C-terminal domain in blue, the N-terminal 'trip-wire' in cyan, and the cofactors in yellow. The positions of the substitutions are shown as green spheres. For the sake of clarity, amino acids of the trip wire that were not defined in the crystal structure are modeled in this figure.

To sterically prevent the intertrimer crystal contacts involving Thr247, this residue was replaced by the large, positively charged amino acid arginine, creating the variant T247R. In the same manner the variant D87R was constructed to sterically prevent intratrimer crystal contacts. The relevance of the π-π interaction between Glu78 and His80 to HemN-trimer formation was investigated by replacing both residues by alanine, creating the HemN-variant Q78A-H80A.

The three HemN variants were purified aerobically by Blue Sepharose™ affinity chromatography and by anion exchange chromatography (**section 3.7.5**). The [4Fe-4S]-clusters of all variants could be reconstituted under anaerobic conditions (**section 4.2**). An enzyme activity assay indicated that the three HemN variants are able to convert copro'gen to proto'gen. However, the efficiency is ~5 times lower than that of the wildtype enzyme. In **Figure 4-27, A** the oxidase activity of the T247R variant is compared to wildtype HemN. Whereas the wildtype completely converts copro'gen to proto'gen, activity of T247R results in a broad peak from 618 to 633 nm indicating that despite synthesized proto'gen some copro'gen remained.

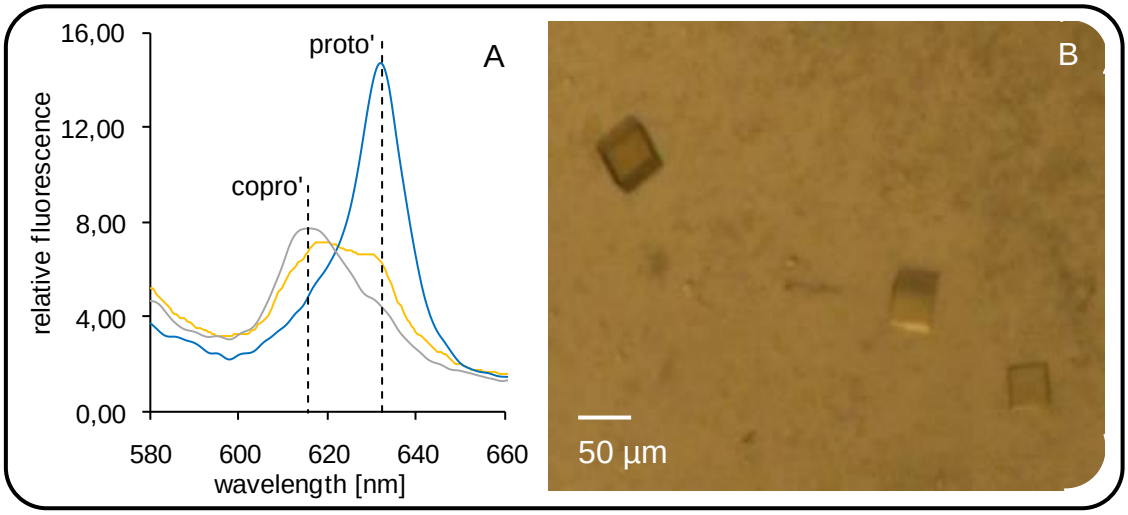

Figure 4-27: Activity assay and crystals of HemN variant T247R. A: The CPO activity assay was performed as described (**section 3.8.5**). The results from one representative activity assay are shown. Whereas wildtype HemN (—) completely converts copro'gen to proto'gen, HemN variant T247R (—) only performs partial conversion. In the control reaction without enzyme (—) copro'gen is not converted. **B**: Crystals of HemN variant T247R grown in 0.1 M KSCN, 30 % PEG 2000 MME.

All three crystal-packing variants of HemN were used in crystallization experiments. As variations of the wildtype HemN crystallization conditions did not yield crystals and a

new crystal packing may only be possible under new crystallization conditions, commercial crystallization screens were used to screen for new crystallization conditions. In the case of variant T247R, crystals were obtained after 20 days from two conditions of the Classics II-Screen (QIAGEN): 30 % PEG 2000 MME, 0.1 M KSCN or 0.15 M KBr, (**Figure 4-27, B**). These cubic crystals do not share the hexagonal shape described for wildtype HemN and the I329A variant (**section 4.6**).

The high concentration of PEG 2000 MME allows these crystals to be harvested and flash-cooled directly, without requiring an additional cryoprotectant. A dataset of one such crystal was successfully collected at beamline ID 14-1 of the ESRF, though the diffraction limit was only 4.5 Å (**Table 4-6**).

Table 4-6: Diffraction and refinement statistics for a crystal of the T247R variant of HemN

Data collection statistics			
Beamline	ESRF ID14-1	Redundancy	12.6 (12.9)
Wavelength [Å]	0.9340	Mosaicity [°]	0.61
Space group	F23	Wilson B-factor [$Å^2$]	161
Resolution [Å]	40 - 4.5 (4.66 - 4.5)	I/σI	30.5 (4.1)
		R_{sym} [%]	9.7 (84)
Unit cell axis a=b=c [Å]	240.2	Refinement statistics	
Unique reflections	6918 (675)	R_{work} [%]	29.0
Completeness [%]	100 (100)	R_{free} [%]	44.6
Values in parentheses refer to shell of highest resolution. R_{free} test set size is 5 %			

The autoindexing routine of DENZO (HKL2000 package) determined the space group to be F23. Data were integrated and scaled in this space group. Crystal packing analyses indicate two molecules of T247R per asymmetric unit, resulting in a solvent content of 55.0 % and a V_M of 2.73 $Å^3$/Da – compared to one molecule per asymmetric unit in the hexagonal crystal packing of wildtype HemN (solvent content: 52.9 %; V_M: 2.61 $Å^3$/Da) (Matthews, 1968). Using wildtype HemN as a search model in molecular replacement with the program PHASER yielded two clear solutions with an overall Z-score of 12.86, indicating the successful placement of the molecule. Only rigid body refinement was possible with this dataset, as the limited resolution does not allow for full-matrix

refinement. Following rigid body refinement the crystal packing arrangement was analyzed (**Figure 4-28**).

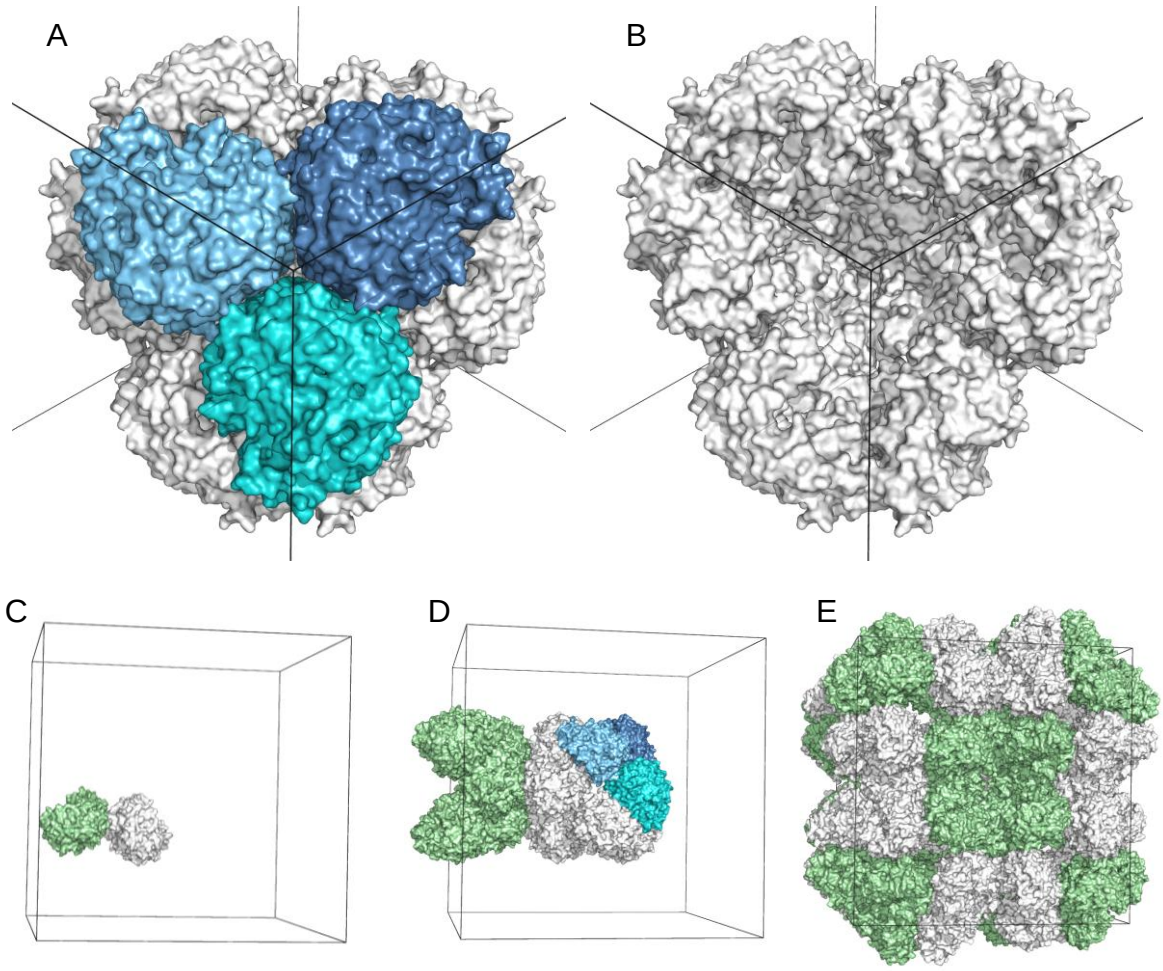

Figure 4-28: Crystal packing arrangement of HemN variant T247R in F23. A: Molecules forming one crystallographic trimer are shown in different shades of blue (compare **Figure 4-24**). Four crystallographic trimers arrange together to build a hollow sphere (the blue colored trimer is omitted in **B**). The other three crystallographic trimers are shown in gray. **C**: Two molecules are present in the asymmetric unit (shown in gray and green, respectively). **D**: Symmetry mates of each monomer of the asymmetric unit arrange to a sphere of twelve molecules. **E**: Eight spheres fill the unit cell. For clarification, surfaces were generated using the amino acid side chain positions as calculated by molecular replacement.

The analysis of the crystal packing arrangement revealed I) that the trimerization of HemN molecules previously observed for the hexagonal crystal packing is maintained in the cubic crystal; II) instead of alternating layers of trimers, a tetrahedral arrangement of four trimers creates a large sphere (diameter ~150 Å), surrounding a solvent filled centre with a diameter of ~50 Å. Eight such HemN spheres or a total of 96 HemN molecules serve to fill the unit cell.

5 Discussion

The crystal structure of oxygen-independent copro'gen oxidase (HemN), the first structure of a radical SAM enzyme, revealed many details about this family of enzymes, in particular about the cofactor arrangement and about the common reaction steps i.e. electron transfer and SAM cleavage. Spectroscopic investigations identified a substrate radical to be created during HemN catalysis and a reaction pathway could be postulated. This reaction pathway included a substantial movement of the C-terminal domain upon substrate binding. However, detailed knowledge about the substrate binding mode, the physiologic electron donor and acceptor as well as the exact reaction mechanism is still lacking for HemN and most other Radical SAM enzymes. In this thesis, distinct methods were used to get more insight into the HemN reaction mechanism. Several variants of HemN had been constructed to either delineate the substrate and/or SAM2 binding. As the favored hexagonal crystal packing arrangement observed for wildtype HemN and the I329A variant did not allow postulated domain movements, further HemN variants were designed to change the crystal packing arrangement. In addition to the construction of diverse HemN variants, functional and structural characterization of HemN was performed in the presence of an electron acceptor or donor. The substrate copro'gen was obtained by diverse approaches including chemical reduction and enzymatic synthesis. Most experiments were performed by utilizing an anaerobic working station that was newly established at the institute as part of this thesis. The purification protocol of HemN and its variants had to be altered and adapted to this new working station.

5.1 [4Fe-4S]-Cluster Reconstitution is a Convenient Tool for HemN Purification

The sensitivity of some FeS-clusters towards molecular oxygen is frequently described (Imlay, 2006). In nature this sensitivity is utilized for gene regulation or catalytic regulation of some proteins like *E. coli* dihydroxy-acid dehydratase, fumarase A, or glutamine 5-phosphoribosyl-1-pyrophosphate amidotransferase from *Bacillus subtilis*

(Flint *et al.*, 1993a; Flint *et al.*, 1993b; Smith *et al.*, 1994). A prominent example is the global oxygen-responsive regulator FNR in *E. coli*. Its dimerization and DNA binding depends on an intact [4Fe-4S]-cluster which is lost upon exposure to oxygen. Consequently the transcription of genes in response to oxygen deprivation is strictly regulated (Lazazzera *et al.*, 1996). In mammalian aconitase and members of the Radical SAM enzyme family the [4Fe-4S]-cluster is only coordinated by three cysteine ligands (compare **Figure 1-7** and **Figure 1-5, B**). The fourth iron atom is coordinated by citrate or SAM, respectively, and is especially labile towards oxygen. Accordingly for those enzymes loss of the [4Fe-4S]-cluster during purification was frequently described (Gardner and Fridovich, 1991; Broderick, 2000; Ollagnier-de Choudens *et al.*, 2000). Reconstitution of Radical SAM enzymes has been successfully performed *inter alia* with HydE, ARNR-AE, GD-AE, PFL-AE, and MiaB (Rubach *et al.*, 2005; Tamarit *et al.*, 1999; O'Brien *et al.*, 2004; Yokoyama *et al.*, 2007; Ollagnier-de Choudens *et al.*, 2000; Hernández *et al.*, 2007). It was described either with $Fe(NH_4)_2(SO_4)_2$ or $FeCl_3$ as iron source and Na_2S or L-cysteine (in combination with the cysteine desulfurase IscS) as sulfur source. Reconstitution resulted in 0.5 - 0.9 iron/polypeptide chain prior to and 3.7 – 4.2 iron/polypeptide chain after reconstitution for biotin synthase and lipoate synthase, respectively (Ollagnier-de Choudens *et al.*, 2000). Similar results were described for MiaB, where in addition to the common Radical SAM FeS-cluster a second [4Fe-4S]-cluster could be reconstituted (Hernández *et al.*, 2007). However, until recently HemN could not be successfully reconstituted (Layer *et al.*, 2005a). In this work, both systems described above were used to reconstitute the FeS-cluster of HemN, but only the use of IscS and L-cysteine resulted reproducibly in reconstituted protein. HemN-samples turned brown within 2 h and UV-visible spectra, activity assays, and the crystal structure of reconstituted wildtype HemN revealed the presence of an intact [4Fe-4S]-cluster (see **Figure 4-4** and **section 4.2**). The amount of intact HemN was even higher after reconstitution than after anaerobic purification. This was indicated by the intense brown color of the protein solution and proved by the higher iron content per molecule HemN with 4.1 iron/HemN compared to mean 2.0 after anaerobic purification.

As the aerobic purification and subsequent reconstitution of the [4Fe-4S]-cluster of HemN is more convenient and reproducible than the anaerobic purification it is more applicable and will become the standard procedure in future experiments.

5.2 Analysis of the SAM2 and Substrate Binding Sites

The first structural analysis of HemN unexpectedly located a second SAM molecule adjacent to the catalytic SAM involved in coordinating the [4Fe-4S]-cluster. As HemN needs to catalyze two equivalent reactions on two side chains of copro'gen, each of which occurs at the expense of a molecule of SAM, SAM2 could be of physiological relevance. This has been investigated previously primarily by analyzing the effect of substituting individual residues involved in SAM2-binding or inferred to be relevant to substrate binding (Grage, 2005). The analyses of HemN variants in this work were *inter alia* thought to extend the analyses of the SAM2 and substrate binding sites. Three residues were substituted to investigate their role in detail: Gln311, Arg22 and Arg359. Gln311 was supposed to be involved in direct SAM2 coordination by contributing hydrogen bonds to the adenosine moiety of SAM2 (**Figure 5-1**). The non conservative exchange of this residue to alanine has already been analyzed (Layer *et al.*, 2005a). It was shown that the mutant protein did not show any CPO activity anymore despite of the ability to still cleave a single SAM molecule per HemN. Consequently a loss of SAM2 was postulated. In this work it was tested whether or not a conservative exchange to asparagine had the same effects. As shown in **Figure 4-8** and **Table 4-1** wildtype HemN and the Q311N variant had comparable iron contents and were able to cleave SAM in similar rates. The ability of Q311N to convert copro'gen to proto'gen, however, was reduced to 42 % of the wildtype activity. As there is no structural data available for this variant, the substitution can only be modeled. The three most favored rotamers for Gln311 are presented in **Figure 5-1**.

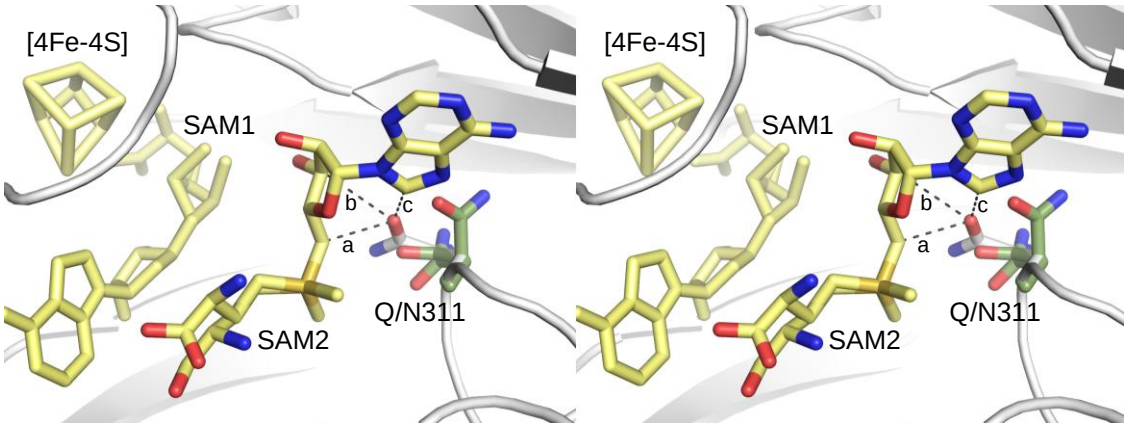

Figure 5-1: Three rotamers of Gln311 of the Q311N variant (stereo view). The HemN structure is shown in gray, cofactors in yellow. Gln311 is shown in gray sticks for wildtype HemN; in green the three most favored rotamers for the substituted asparagine in the Q311N variant are presented. Dashed lines show the hydrophilic interactions of Gln311 in the wildtype structure. The labeled distances are 2.9 (a), 3.5 (b), and 3.1 Å (c).

In contrast to alanine the similar side chain of asparagine in Q311N obviously can compensate for the missing glutamine resulting only in a reduced but not diminished activity of HemN. Two rotamers of Asp311 could still contribute similar hydrophilic interactions as glutamine albeit weaker as the distances to SAM2 would be elongated. The third rotamer would be in a longer distance from the ribose but closer to the adenine moiety which it could stabilize (see **Figure 5-1**). Presumably the effects of this conservative amino acid substitution on the HemN activity are caused rather by a weakened SAM2 binding than by a complete loss of SAM2. To clarify the physiological relevance of SAM2, however, additional mutational analyses are needed.

Amino acid exchanges on two arginines supposed to be involved in substrate binding were also performed throughout this work. These arginines are highly conserved and their positively charged side chains are thought to counterbalance the negative charges of the respective propionate side chains of copro'gen. Arg22 is likely to lie opposite of SAM2 at the active site cleft, but as a part of the flexible N-terminal ‘trip-wire’ it is not defined in the crystal structure of wildtype HemN. Additionally the ‘trip-wire’ is postulated to rearrange upon substrate binding. The position of Arg22 might therefore be different in the postulated closed conformation. Consequently, an amino acid exchange could not be modeled. Arg22 was exchanged by alanine and lysine in this work. For both variants no or only residual conversion of copro'gen to proto'gen was detected. Obviously Arg22 is crucial for HemN activity, as even a conservative mutation to lysine has a severe effect.

Hence an involvement in substrate binding is likely although the possibility of effects independent of Arg22 cannot be excluded.

The variant R359K had already been analyzed prior to this work and this conservative mutation revealed no effect on the iron content or the activity of HemN (Layer *et al.*, 2005a). Substitution of Arg359 by alanine was analyzed in this work and showed only minor effects on the functionality of HemN. The iron content and the activity were only slightly reduced. Hence the function of this arginine is still unclear. Its charge and position in the active site cleft indicate a possible involvement in substrate binding (see **Figure 5-2**), but obviously its loss can be well compensated. However, the position of the flexible substrate in **Figure 5-2** is just modeled and protein rearrangements upon substrate binding cannot be excluded. In addition, Arg359 is positioned in the C-terminal domain which like the trip-wire is supposed to move after substrate-binding (Layer *et al.*, 2003). Hence the position of this arginine might be different when the substrate is bound and a structure of the postulated closed conformation of HemN may reveal the function of this residue.

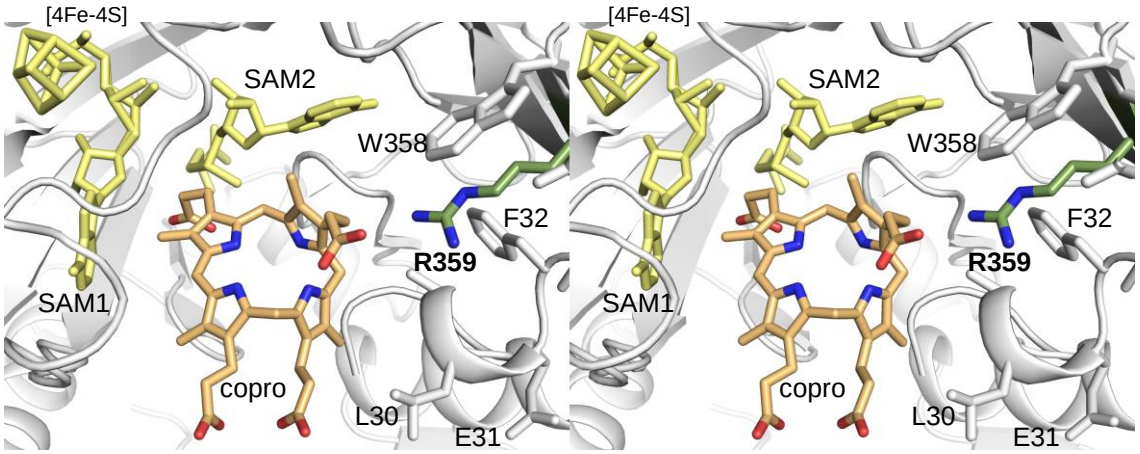

Figure 5-2: Arg359 in the wildtype HemN structure with modeled coproporphyrinogen III. Arg359 and cofactors are shown as green and yellow sticks, respectively. Copro'gen (in orange) was modeled according to **Figure 4-15**. The position and orientation of Arg359 indicate a role of this residue in substrate coordination. Copro: copro'gen.

The presented results support the role of the discussed HemN variants in substrate and SAM2 binding. However, structural information on all variants, especially in combination with substrate, product or intermediate product, is needed to unambiguously clarify their function during HemN catalysis.

5.3 Harderoporphyrinogen as a Possible Reaction Intermediate of HemN

The oxygen-dependent copro'gen oxidase (HemF) has been demonstrated to convert the propionate side chain on pyrrole ring A to the corresponding vinyl group before repeating the reaction on the propionate moiety of ring B – creating the intermediate hardero'gen (Jackson *et al.*, 1980). Correspondingly, HemF converts its natural substrate hardero'gen to proto'gen with a ten-fold higher rate compared to the isomer isohardero'gen (Cavaleiro *et al.*, 1974; Games *et al.*, 1976).

In the case of HemN, the order of the propionate decarboxylations on rings A and B and hence the nature of the intermediate product is currently still unclear. In this thesis the analyses of the oxidized reaction products of wildtype HemN by HPLC revealed two intermediate peaks in addition to the copro' and proto' peaks, with retention times of 12.1 and 13.7 min. A corresponding peak of 609 Da for a monovinylic intermediate (e.g. hardero' oder isohardero') in the HemN reaction was confirmed by mass spectrometric analysis (**Figure 4-11**) indicating that the two propionate side chains of copro'gen are successively decarboxylated to the corresponding vinyl groups. The peaks of the HPLC analyses are equivalent to intermediate peaks of the HemF variant R401K. This variant is known to accumulate hardero'gen (presumably due to the role of Arg401 in substrate binding (Schmitt *et al.*, 2005; Stephenson *et al.*, 2007)) and was therefore used to synthesize hardero'gen that after its oxidation served as a hardero' standard in HPLC analyses. To verify the intermediate peak of the HemF variant R401K as hardero', chemically synthesized hardero' tetramethylester was hydrolyzed and used as hardero' standard by Dr. Gunhild Layer (TU Braunschweig). Although the HPLC analysis appeared to indicate that this standard is chemically not homogeneous resulting in an ambiguous pattern of peaks, a main peak was detected at equivalent retention time to the main intermediate peaks of the HemN and HemF variant R401K activity. Overall, these results confirm the retention behavior of hardero' and indicate that hardero'gen is a reaction intermediate of HemN. However, it cannot be excluded, that the observed peak corresponds to isohardero. Although an isohardero' standard was not available, a methyl ester derivative of this tetrapyrrole has been reported to elute later than a correspondingly

modified hardero' in HPLC-analyses using ethylacetate/cyclohexane (1:3 v/v) and chloroform (stabilized with 0.2 % alcohol)-cyclohexane mixtures (Nordmann *et al.*, 1983; Cavaleiro *et al.*, 1974). Isohardero' should thus have had a higher retention time than that observed for hardero' in the HPLC-setup used for the current analysis.

Recent results from our collaboration partner Dr. Gunhild Layer (TU Braunschweig) revealed that hardero'gen can be utilized and converted to proto'gen by wildtype HemN. The chemically synthesized hardero' was successfully hydrolyzed and reduced with Na-amalgam and provided as a substrate in a HemN activity assay (Dr. Gunhild Layer, TU Braunschweig, personal communication). In the HemN reaction after 30 min the peak corresponding to hardero' was clearly reduced compared to the control reaction without HemN. At present it can, however, not be excluded, that isohardero'gen is a HemN intermediate product as well that can be converted to the product proto'gen.

The peak height associated with the HemN reaction intermediate is at a maximum after 30 min, kept constant until 60 min, and largely disappears after ~90 min (**Figure 4-10**). HemN is thus able to use the intermediate to produce proto'gen, indicating that it is a true intermediate and not a by-product. HemN has previously been observed to be a particularly slow enzyme with a turnover of 5-8 molecules of copro'gen per HemN and hour (Layer *et al.*, 2005a). Other Radical SAM enzymes have similarly been reported to be slow including ThiH with 2.76 conversions/h (Kriek *et al.*, 2007) and anSME from *Clostridium perfringens* (reaction monitored for 6 h) (Benjdia *et al*., 2007). In the cases of MiaB, biotin synthase, and LipA each molecule could even only perform one substrate conversion (Hernández *et al.*, 2007; Tse Sum Bui *et al.*, 1998; Gibson *et al.*, 1999; Cicchillo and Booker, 2005) leading to the notion of a sacrificial role of these proteins in their respective reactions (Booker *et al.*, 2007). At least for biotin synthase other authors described several conversions per molecule under different conditions proposing another, PLP dependent, reaction pathway possibly product-inhibited by biotin (Ollagnier-de-Choudens *et al.*, 2002; Picciocchi *et al.*, 2001; Choi-Rhee and Cronan, 2005). Only recently Challand *et al.* (2009) showed that BioB, LipA, and ThiH are efficiently inhibited by 5'-deoxyadenosine and methionine *in vitro*. They also observed that in the presence of the 5'-deoxyadenosin hydrolyzing nucleosidase MTAN this inhibition was

removed and the activity of the tested enzymes was increased. Hence the possibility that the absence of several turnovers is due to suboptimal *in vitro* conditions must be regarded for all Radical SAM enzymes using SAM as co-substrate including HemN.

5.4 SAM2-Binding not Affected by Replacement of Isoleucine-329 by Alanine

The role of SAM2 in the catalysis of HemN has been under discussion ever since its unexpected identification in the crystal structure of this enzyme (Layer *et al.*, 2003). The presence of two SAM molecules in the active site matches the requirement of oxidizing two propionate side chains of the substrate and the later observation that two SAM molecules are converted per catalytic turn-over (Layer *et al.*, 2005a). SAM2 is furthermore located in the active site cleft immediately adjacent to SAM1 and is specifically recognized by numerous individual interactions including some highly conserved residues. Three distinct reaction mechanisms have been postulated for HemN each involving SAM2 (Layer *et al.*, 2003; Layer, 2004). The involvement of SAM2 in the reaction mechanism was investigated by site-directed mutagenesis studies including the residues involved in SAM2 binding (Layer *et al.*, 2005a). All variants were observed to have lost their CPO activity and most did no longer cleave SAM. Two variants, Q311A and I329A, proved particularly interesting as both were shown to cleave only a single SAM per molecule of HemN potentially implying a loss of SAM2-binding and indirectly confirming the importance of SAM2. As this observation could indicate a reaction intermediate being caught in the active site during catalysis (Grage, 2005), these variants appeared particularly interesting for crystallization experiments. As part of this thesis, the crystal structure of HemN variant I329A was solved and refined. Despite repeated attempts to induce the partial reaction of the substrate copro'gen, no tetrapyrrole was observed in the active site. In contrast to the conclusions of previous experiments, I329A still binds SAM2 (see **Figure 4-23**). In wildtype HemN, Ile329 helps to stabilize SAM2 binding by hydrophobic interactions involving its side chain and by two hydrogen bonds through its back bone O and N (Layer *et al.*, 2003; Grage, 2005). Comparing the variant to the wildtype structure indicates an essentially unaltered backbone (r.m.s.d. for all atoms is 0.56 Å, for C_α-atoms 0.28 Å). Correspondingly, the backbone hydrogen bonds to

SAM2 are maintained in the variant structure (indicated by the dashed lines in **Figure 5-3**). Residues Tyr56, Phe310, and Gln311 compensate the loss of the hydrophobic side chain of Ile329 stabilizing SAM2 (**Figure 5-3**):

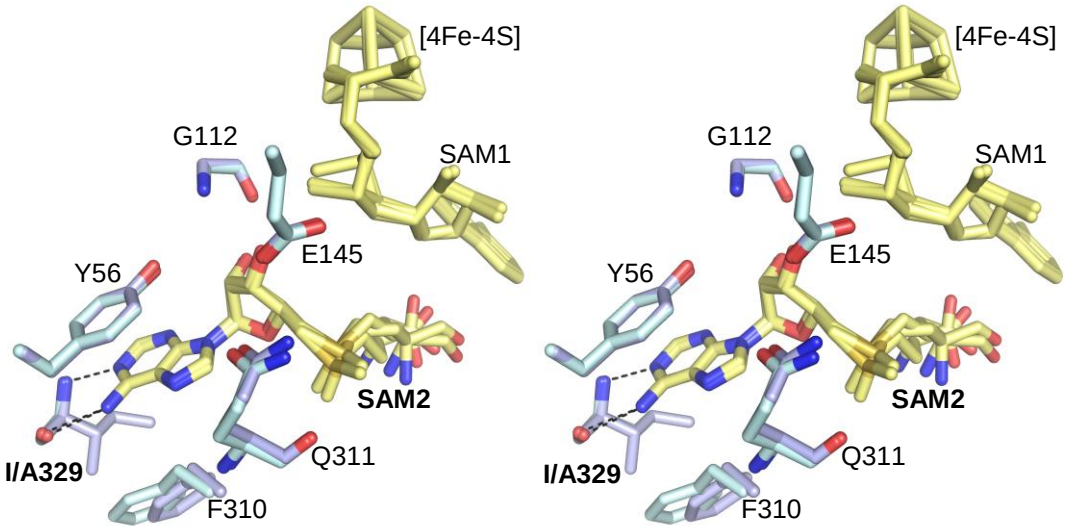

Figure 5-3: Coordination of SAM2 in wildtype HemN and variant I329A (stereo view). Cofactors are colored yellow (SAM2 with four conformations for the flexible methionine moiety is additionally colored by atom), amino acids coordinating SAM2 in cyan (I329A) and blue (wt). Hydrogen bonds between SAM2 and the Ile/Ala329 backbone are indicated by dashed lines.

On a structural level, the loss of CPO activity by I329A thus remains unclear. The location of Ile329 in the active site could, however, indicate that substrate binding may be affected (Grage, 2005 and **Figure 5-5**). Substrate binding is unlikely to be completely lost, as SAM-cleavage was strongly increased in the presence of the substrate compared to assays without substrate (Layer *et al.*, 2005a). Instead, a later step of the chemical reaction could be impaired resulting in a significantly slower or ceased overall reaction.

At present the physiological relevance of SAM2 is thus only supported indirectly while the presence of SAM2 in crystals where SAM was omitted from the crystallization condition further points on its physiological relevance. Unequivocally resolving this issue would still require the successful co-crystallization and structure determination of HemN with bound substrate.

5.5 Co-crystallization of Wildtype HemN with its Substrate

Observed Electron Density Cannot be Explained Unambiguously with Tetrapyrrole Model

A major aim of this thesis was to describe substrate-binding of HemN in detail by X-ray crystallography. A wide range of techniques was used to provide and incorporate the substrate into the active site of HemN including *inter alia* the production and purification of four different enzymes to synthesize the substrate *in vitro*. Each resulting HemN crystal structure was solved and refined, and the active site cleft was checked for difference electron density indicative of substrate copro'gen, product proto'gen or a reaction intermediate. In a crystal structure resulting from the co-crystallization of wildtype HemN with chemically reduced substrate, difference features were indeed observed that were reminiscent of a tetrapyrrole – albeit at very low occupancy (**Figure 4-14**). Copro'gen was modeled into this density at two distinct positions and refined by real-space refinement. However, modeling was not straight forward both due to the poor occupancy of the substrate and the inherent flexibility of copro'gen. The validity of these models is therefore difficult to assess.

Currently only two crystal structures are available for complexes of reduced tetrapyrroles with enzymes (Phillips *et al.*, 2003; Schubert *et al.*, 2008). In 2001 modeling uro'gen into the first crystal structure of uro'gen decarboxylase from *Nicotiana tabacum* proved difficult due to the paucity of crystallographic data on reduced tetrapyrroles (Martins *et al.*, 2001). In 2008 only a single crystallization condition of uro'gen synthase with its product uro'gen non-reproducibly yielded the required complex (Schubert *et al.*, 2008) illustrating the difficulty of preparing such complexes. The lack of a complex between HemF and its substrate or product, despite a plethora of studies on this enzyme, further underlines the challenge of preparing such complexes. **Figure 5-4** shows the two conformations of reduced tetrapyrroles found in protein crystals.

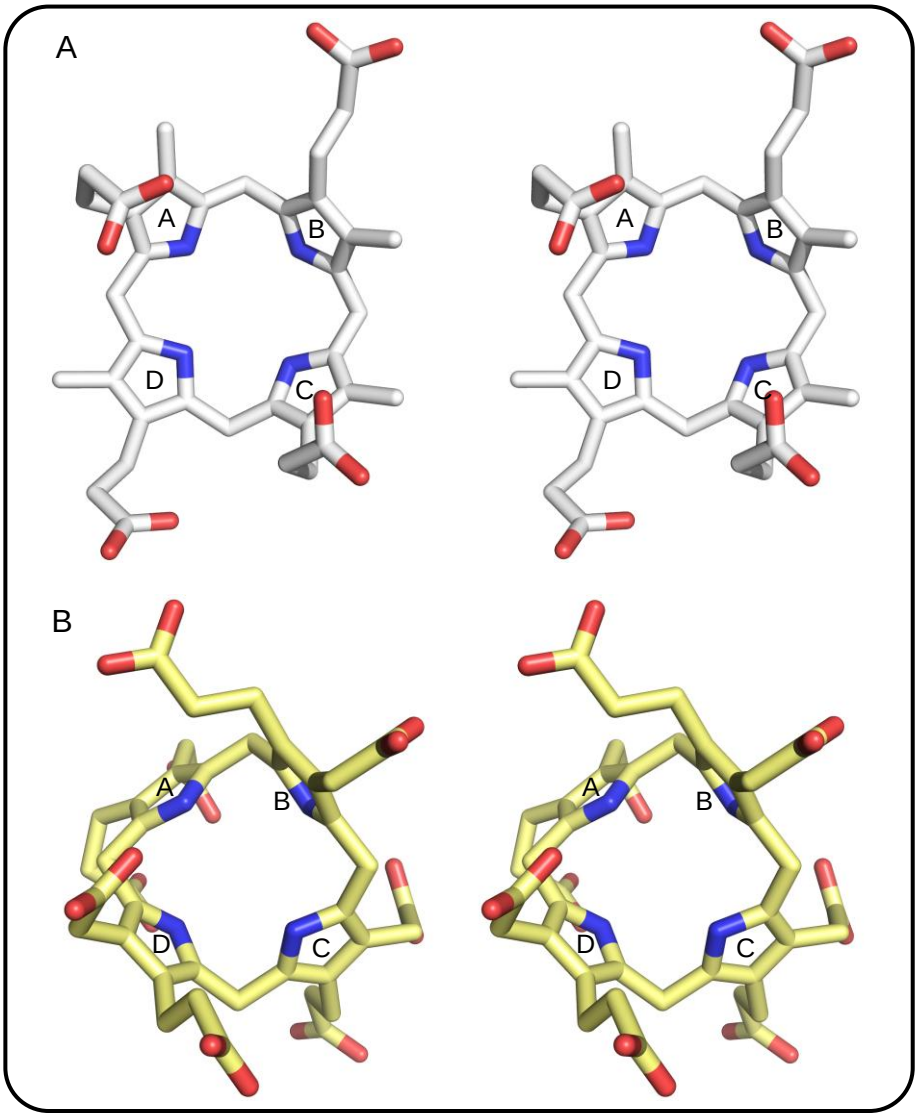

Figure 5-4: Porphyrinogens as observed in complex crystal structures (stereo view). The reduced tetrapyrroles are shown in stick representation. Pyrrole rings are labeled A-D in each molecule. **A**: copro'gen, the product of uro'gen decarboxylase taken from PDB entry 1r3y. **B**: Uro'gen, the substrate of uro'gen synthase (from PDB entry 3d8n).

The crystal structure of uro'gen decarboxylase in complex with its reaction product copro'gen reveals the latter adopting a basket-shaped asymmetric conformation (Phillips *et al.*, 2003; PDB entry: 1r3y) (compare **Figure 5-4**, **A**). In the second structure involving a reduced tetrapyrrole (uro'gen synthase in complex with uro'gen), the latter adopts a 'two-up, two-down' conformation, in which the nitrogen atoms on rings A and C point 'upward', while those on rings B and D point 'downward' (Schubert *et al.*, 2008; PDB entry: 3d8n; **Figure 5-4**, **B**). The two complex structures also differ with respect to the coordination mode of the tetrapyrrole. Whereas in the case of uro'gen decarboxylase the

side chains of the involved residues coordinate the tetrapyrrole, coordination is achieved by hydrogen bonds to the main chain amino groups of the protein in the case of uro'gen synthase.

In view of the two distinct tetrapyrrole conformations, a prediction of the copro'gen conformation in complex with HemN is impossible. Copro'gen was previously modeled in a planar conformation, due to the lack of any data on its actual conformation (Layer *et al.*, 2003 and **Figure 5-5**). In this thesis two real-space refined models were postulated. Both would imply significant deviations from a planar conformation. The first model positions the four pyrrole rings of copro'gen into the observed density (**Figure 4-15**). The individual pyrrole rings in this model matched the observed electron density features surprisingly well indicating the potential validity of the model. The copro'gen side chains were, however, not visible in this electron density. A problem encountered in this complex structure involves the position of the propionate side chain of pyrrole ring A, which would require the methionine moiety of SAM2 to move away. As the SAM2 methionine is invariably less well resolved in all crystal structures, it appears highly flexible and thus justifies the modeled conformational change. The shorter distance of the propionate side chain of pyrrole ring A, which is likely to be converted first (discussed in **section 5.3**), to SAM2 than to SAM1 indicates that the hydrogen is abstracted by the radical originating from SAM2 (**Figure 4-15**). Hence this model supports the functional importance of SAM2 although it does not explain how in this scenario electron transfer to SAM2 and its cleavage would proceed. Omitting SAM from crystallization experiments with wildtype HemN and proto'gen did not result in a lower occupancy of either SAM molecule (**section 4.5.4**) further supporting the physiological relevance of SAM2 on the one hand. On the other hand these results disagree with the second model as this would only be possible in the absence of SAM2. In this model SAM2 is completely substituted by copro'gen (**Figure 4-16**). Here the electron density accounts for the pyrrole rings and three of the propionate groups of copro'gen. As in this model the propionate side chain of pyrrole ring A is closer to SAM1 than in the first model, hydrogen abstraction by a 5'-deoxyadenosyl radical arising from SAM1 cleavage would be possible. Both real-space refined models are compared to that previously proposed (Layer *et al.*, 2003) in **Figure 5-5**.

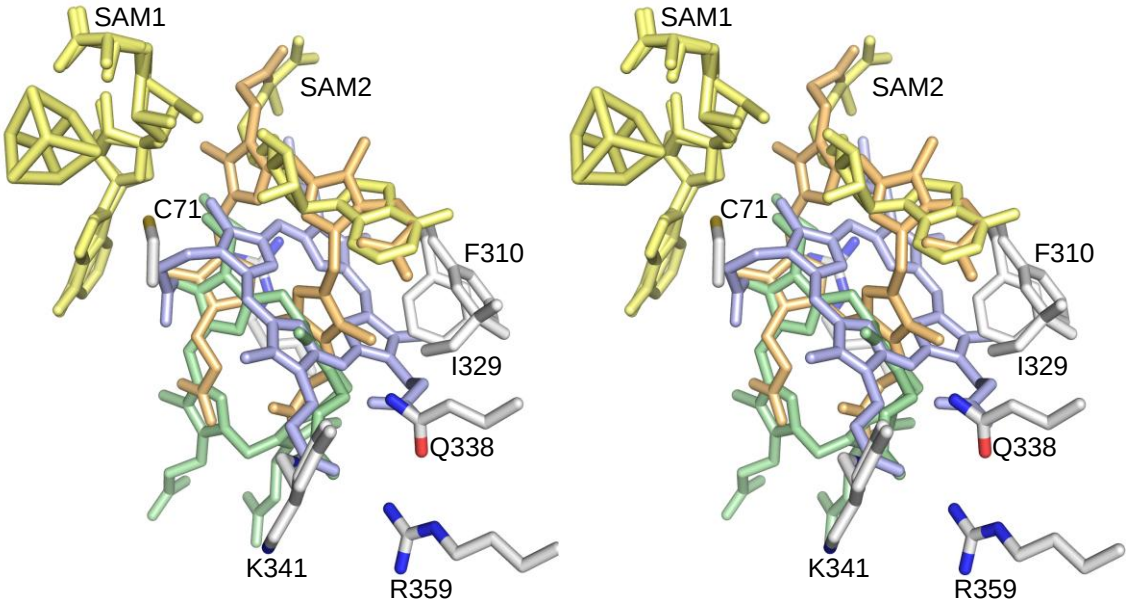

Figure 5-5: Three possible positions for coproporphyrinogen III (stereo view). Cofactors are shown in yellow, amino acids potentially involved in substrate binding in gray. The model from Layer *et al*., (2003) is shown in blue, the current models in green and orange. Arg22 is located behind copro'gen in this model.

Despite a significant shift in the position of copro'gen, substrate recognition by coordination of negatively charged propionate side chains or by hydrophobic interactions with individual pyrrole rings is vaguely possible in both models. Clearly, both models are based on two variable partners. HemN may be expected to undergo some substrate-induced conformational changes, while the flexibility of copro'gen prevents its conformation being predicted without reliable additional data. Unfortunately, after refinement of each model, neither the resulting electron density nor the R-factors supported any model. A poor occupancy of the tetrapyrrole may be responsible for the weak definition in the electron density. Refinement of the tetrapyrrole model at the present resolution might also be impeded by the lack of an appropriate model. Finally it is also possible that the observed electron density results from water or PEG molecules. None of these possibilities can be excluded at this point and further efforts have to be made to get a structure where the substrate is clearly defined by the observed electron density.

5.6 Modified Crystal Packing of HemN by Crystal Engineering

The original crystal structure of HemN was based on crystals of space group $P6_3$ (Layer *et al.*, 2003). In addition to refining these known conditions, new crystallization conditions were identified. Surprisingly, despite unrelated crystallization conditions, all crystals retained the $P6_3$-packing, despite morphologies ranging from rod-like cylinders to flat disks (**Figure 4-13**). Diffraction data for several crystals of wildtype HemN as well as of variant I329A were collected. In each case the space group and the cell dimensions were identical.

The open nature of the HemN active site and the shape complementarity of the catalytic and C-terminal domains of HemN suggested conformational changes upon substrate binding entailing the C-terminal domain moving and closing the active site (Layer *et al.*, 2003). This hypothesis implied that it should be possible to trap HemN in its substrate-bound, closed conformation. However all attempts to induce and crystallize this closed state were without success. The addition of an artificial electron donor, the use of the catalytically restricted HemN variant I329A, and differentially reduced copro'gen could not induce a substrate-bound complex of HemN. Analyzing the arrangement of the HemN molecules in the obtained crystals indicated that the C-terminal domain only partly participates in crystal contacts. Closure of the active site should thus be possible without causing the crystals of HemN to collapse.

As the substrate-induced reorientation of the C-terminal domain is a hypothesis only, the details of the closed conformation are not clear. A simple model of the closed conformation was developed by rotating the C-terminal domain as a rigid unit around the loop connecting it to the catalytic domain (**Figure 4-25**, **B**). Both the catalytic domain and the position of the trip-wire were not modified. As a result, minor clashes between the C-terminal domain and the N-terminal trip-wire occur while some inter-residue distances are not optimal. The lack of secondary structure and its poor definition in the electron density imply the N-terminal trip-wire to be highly flexible. It is, therefore, likely that it will adopt another conformation upon substrate binding and C-terminal domain rearrangement.

Correlating the domain movement and the crystal packing arrangement of HemN indicate that the path of the C-terminal domain is obstructed by two α-helices of the adjoining catalytic domain (**Figure 4-25**). As a result, the crystal packing of HemN is not compatible with a closed conformation preventing substrate-binding through soaking experiments in pre-existing crystals. As the same crystal packing arrangement resulted from very different crystallization conditions, the contacts for this packing arrangement appear particularly stable.

Mutational surface engineering is a tool routinely used in protein crystallography to facilitate protein crystallization by creating novel crystal contacts or to improve the X-ray diffraction potential of existing crystals (Derewenda, 2004b; Cooper *et al.*, 2007). The technique has also been used for integral membrane proteins (Liu *et al.*, 2007). Mostly lysine and glutamate residues are replaced as they are generally located on the protein surface and have high conformational entropies (8.4 kJ/mol and 6.5-7.3 kJ/mol for lysine and glutamate, respectively) (Derewenda, 2004a). As part of this project, crystal contact engineering was used to prevent the observed crystal packing potentially locking HemN in an open conformation. Analyzing the crystal packing arrangement allowed four amino acids to be identified being critical for these contacts. Proposed substitutions gave rise to the three HemN variants Q78A-H80A, D87R, and T247R.

All variants retain some CPO activity, although the proto'gen yield was only ~20 % compared to that of wildtype activity. Crystals were, however, only obtained for T247R. For none of the three variants the original packing was observed, indicating that the substitutions had the desired effect of suppressing the original crystal packing.

Crystals of HemN variant T247R belong to the cubic space group F23. As designed, the introduction of a bulky side chain sterically prevents the molecular arrangement observed in the $P6_3$-crystals (see **Figure 5-6**). The crystal architecture, though clearly distinct from the wildtype protein, however, retains HemN trimers as a central building block. The rigidity of the HemN trimer repeatedly allows this axis to align with a crystallographic three-fold axis, a phenomenon observed for both space groups $P6_3$ and F23 (**Figure 4-28**).

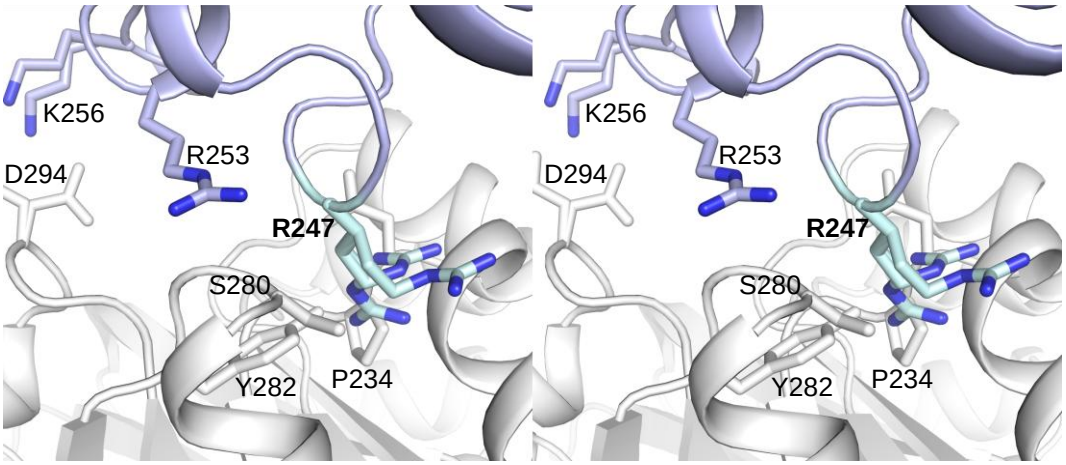

Figure 5-6: HemN variant T247R prevents the crystal packing arrangement required for space group $P6_3$ (stereo view). Three possible conformations of Arg247 (cyan) of one HemN molecule (blue) are shown. Their physical size prevents a close contact of the HemN molecule to the neighboring symmetry related molecule (gray) at this position.

HemN variants engineered to prevent trimer formation did not yield crystals, indicating that smaller, monomeric building blocks without internal symmetry are more difficult to crystallize. The recurrence of the trimeric building block may indicate that HemN is trimeric in solution as well. However, size exclusion chromatography and glycerol gradient centrifugation experiments identified HemN to be a monomer in solution (Layer *et al.*, 2002).

In this particular case, the higher surface entropy of arginine relative to that of threonine is not crucial as both residues frequently occur in protein contacts (Dasgupta *et al.*, 1997; Derewenda and Vekilov, 2006). In fact, arginine is the only amino acid prominent in both intra-oligomer as well as in crystal contacts. Replacing lysine by arginine has therefore been proposed as a tool to create or improve crystal contacts (Dasgupta *et al.*, 1997). Arg247 could thus, in principle, result in novel HemN crystal contacts. In the resulting crystal structure, it is, however, not clear to what extent this materialized due to the lack of high resolution data. Three possible conformations of Arg247 and the neighboring symmetry related molecule imply that Arg247 is indeed involved in novel crystal contacts (**Figure 5-7**).

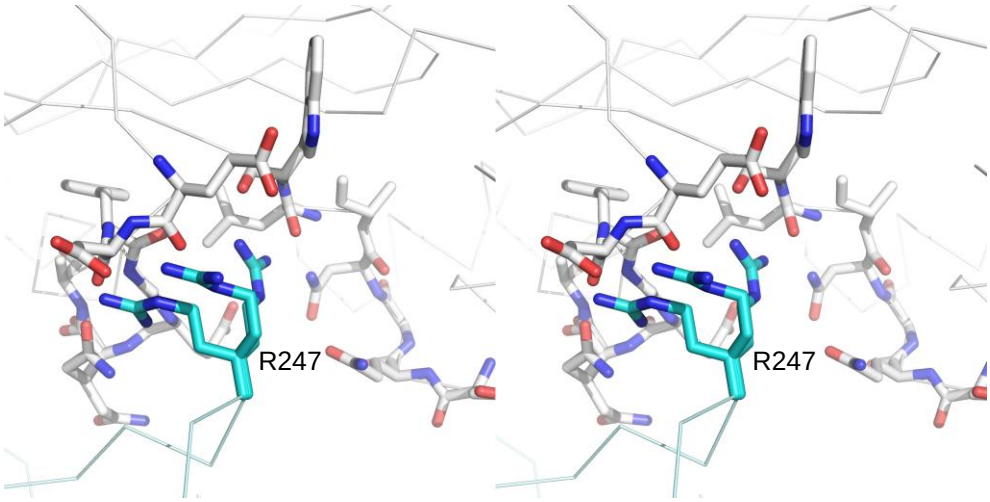

Figure 5-7: Crystal contact of HemN variant T247R (stereo view). The HemN molecule presenting Arg247 is shown in turquoise, the adjacent molecule in gray(both as ribbon representation). Amino acids possibly involved in crystal contacts are shown as sticks.

In the crystal structure of HemN variant T247R, HemN is again in an open conformation, immediately raising the question of whether a movement of the C-terminal domain would be possible in this crystal packing arrangement. **Figure 5-8** depicts the arrangement of HemN-molecules in the F23-crystal packing, emphasizing the C-terminal domains (blue).

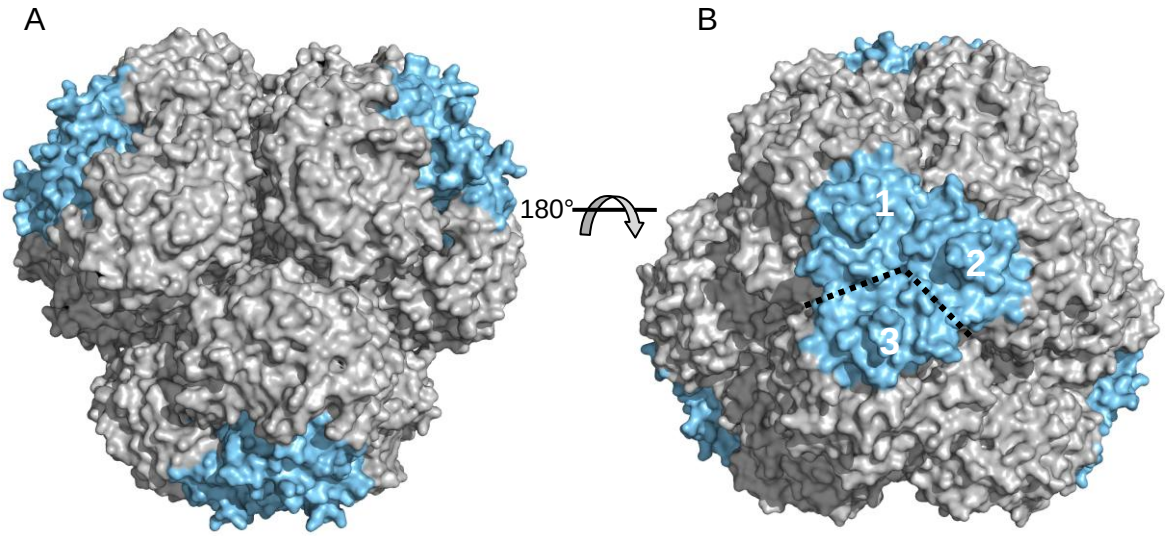

Figure 5-8: HemN crystal packing in F23 with C-terminal domains highlighted. All molecules are rendered in gray with the C-terminal domains of each molecule rendered in blue. **A**: View like in **Figure 4-28 A**. **B**: View after 180° rotation. A cluster of three C-terminal domains is noticeable. Dotted lines mark the contour of one C-terminal domain. The three central C-terminal domains are labeled 1-3.

Although intramolecular salt bridges or hydrogen bonds cannot be identified with confidence, the arrangement of the C-terminal domains in **Figure 5-8 B** clearly indicates interactions between the three domains in the center of the picture. Hence it appears unlikely, that the domains would be able to move in response to substrate binding in spite of this trimeric arrangement. Soaking experiments with these crystals would therefore be not particularly promising. Re-engineering the crystal packing arrangement of HemN did thus not result in an arrangement favoring a closed conformation, nor is it clear, whether it would allow the postulated tipping of the C-terminal domain.

5.7 Substitution of Threonine-247 Slows HemN Catalysis

Although the substitution of Thr247 by arginine was chosen to modify the crystal packing of HemN, this modification serendipitously also affected HemN catalytic activity. Following protein purification and successful FeS-cluster reconstitution, the catalytic activity of the T247R variant was always lower than that of wildtype HemN. More interestingly, the fluorescence spectra of T247R activity assays are similar to that of the HemF variant R401K known to accumulate hardero'gen during catalysis (Schmitt *et al.*, 2005; **Figure 4-27**, **B** and **Figure 4-9**). The accumulation of hardero'gen results in a distinct peak (or more often a shoulder) between those of copro' (618 nm) and proto' (633 nm) due to the increasing electron affinity of the respective side chains (Falk, 1964). In HemF variant R401K this shift results in the broadening of the substrate fluorescence peak from 618 to 633 nm after 5 min. The observation of the same phenomenon for the HemN variant T247R – though only after 90 min – may indicate that it accumulates a reaction intermediate, too. Whether this intermediate is hardero'gen or isohardero'gen would need to be investigated experimentally possibly by HPLC analysis.

Why the substitution of Thr247 by arginine should have this effect is not immediately obvious from the crystal structure as this residue is not located in the immediate vicinity of any cofactor coordination or the proposed substrate binding pocket (**Figure 5-9 A**). On the other hand, Thr247 has been proposed to be involved in binding of the external electron donor (presumably flavodoxin (Layer *et al.*, 2002)), required to initiate the catalytic reaction. Although Thr247 is not strictly conserved in HemN of other species, it

is adjacent to a stretch of hydrophobic residues that could accommodate an electron donor (Layer *et al.*, 2003). Replacing Thr247 by arginine could thus affect the efficient binding of flavodoxin and accordingly the rate of electron transfer to the [4Fe-4S]-cluster of HemN.

Thr247 is further located alongside the substrate binding pocket. It could therefore also be required during the substrate-induced reorientation of the C-terminal domain. In a first model of the closed conformation, Thr247 is in close contact to Ala427, Thr426, and Arg430 of the C-terminal domain (**Figure 5-9 B**). Placing an arginine at position 247 could thus also perturb the closed conformation.

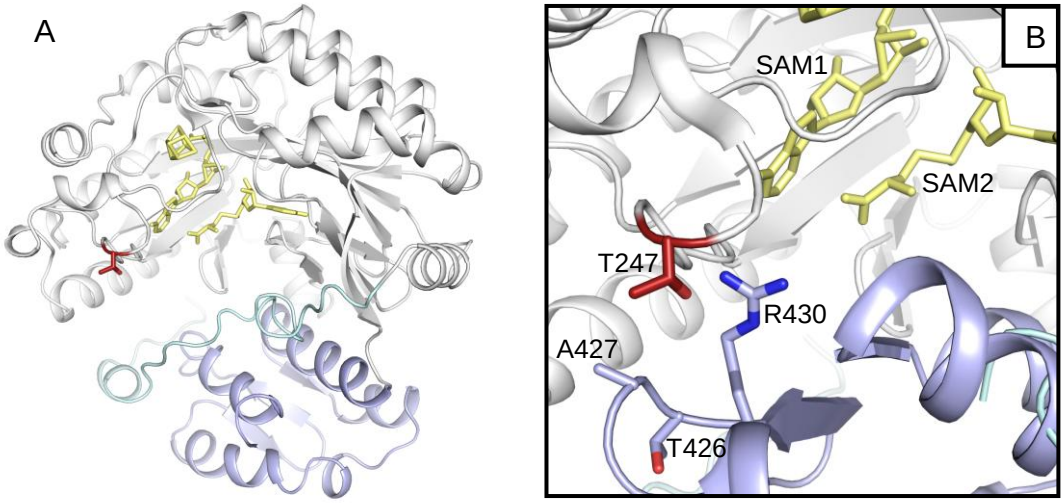

Figure 5-9: Position of Thr247 in wildtype HemN in both open and modeled closed conformation. The catalytic domain is shown in gray, the C-terminal domain in blue, the 'trip-wire' in cyan. Cofactors and Thr247 are shown as yellow or red sticks, respectively. **A**: HemN (overview) in the open conformation. **B**: detailed view of Thr247 and adjacent amino acids in the postulated closed conformation.

The current analysis can only be superficial at best, as substrate-binding and active site closure may result in conformational changes that are difficult to predict. Despite the observation that the activity of HemN variant T247R is suppressed, the exact identification of its cause is currently not possible. Nevertheless, T247R remains an interesting HemN variant that could provide a suitable starting point to investigate the reaction mechanism of HemN. Especially the accumulation of a presumed intermediate product calls for further investigations.

6 Outlook

Information about the exact reaction mechanism, the mode of substrate binding as well as about the nature of possible intermediates is limited for *E. coli* HemN. Using diverse biochemical methods and X-ray crystallography this work expanded the previous knowledge. In addition the established anaerobic working station in combination with the improved HemN purification protocol and the tetrapyrrole reduction system set the very basis for further experiments.

This thesis provides first evidence, that hardero'gen is the intermediate product of the HemN reaction. Utilizing the chemically synthesized hardero' in further experiments may emphasize these results. In addition H_2/Pd-reduced hardero'gen may serve to get a complex structure of wildtype HemN or one of the variants constructed in this work. Finally it may help to clarify the described effects of the amino acid exchanges of the variants I329A and T247R on the HemN activity. Some of these experiments are currently performed by Dr. Gunhild Layer (TU Braunschweig).

The identification of the physiological electron donor and acceptor is still required. Flavodoxin/ flavodoxin oxidoreductase was postulated as the electron donor system (Layer *et al.*, 2002). Recombinantly produced and purified flavodoxin/ flavodoxin oxidoreductase could thus be used I) in biochemical analyses of HemN with the yet to be determined electron acceptor to give clearly defined conditions (i.e. without the demand for an *E. coli* cell free extract) and II) for co-crystallization experiments. Combining HemN and flavodoxin in crystallization experiments may induce HemN to adopt the postulated closed conformation in the presence of its substrate.

Rational crystal engineering performed in this work resulted in a new crystal packing arrangement of HemN. Still an enzyme-substrate complex structure is one major aim of HemN studies as the new crystal packing arrangement is unlikely to allow for the presumed closed conformation after substrate binding. Further surface mutagenesis may result in yet another crystal packing arrangement that may promote crystallization of HemN in the substrate bound, closed conformation. Residues suitable for amino acid

exchanges include Arg253, Lys256, and Asp294 that are all involved in crystal contacts. These residues promote ‘intertrimer’ contacts. Arg253 and Lys256 are not conserved in HemN and are not described to be essential for HemN activity. Exchanges of these residues are therefore unlikely to inhibit substrate binding. Additionally, due to their position in the HemN molecule, it is unlikely that variations of these residues may negatively influence the postulated movement of the C-terminal domain. In contrast Asp294 is conserved in 70 % of HemN structures compared by Layer *et al.* (2003) and is postulated to be involved in binding of the electron acceptor of HemN. Changing the electron acceptor binding site in combination with flavodoxin or an artificial electron donor may help to stabilize substrate binding, start the reaction, and trap HemN in the closed conformation during crystallization.

The crystal structure of the I329A variant of HemN proved that the loss of activity is not caused by the absence of SAM2 as previously assumed. As the presence or absence of SAM2 is still unclear and a crystal structure of a bound tetrapyrrole together with SAM2 is still not available, further mutational analyses of HemN are required to determine the nature of SAM2. If SAM2 is physiologically irrelevant, this again needs to be confirmed by a crystal structure of a HemN variant where no SAM2 binding can be observed. The ability of such a variant to still bind and convert copro'gen in activity assays would confirm SAM2 to be a crystallographic artifact. Exchanging Gln311 by arginine, for example, may lack SAM2 binding due to the loss of three hydrogen bonds to SAM2 while the positive charge of arginine could counterbalance the negative charge of a propionate side chain (pyrrole ring A) of copro'gen (**Figure 6-1**).

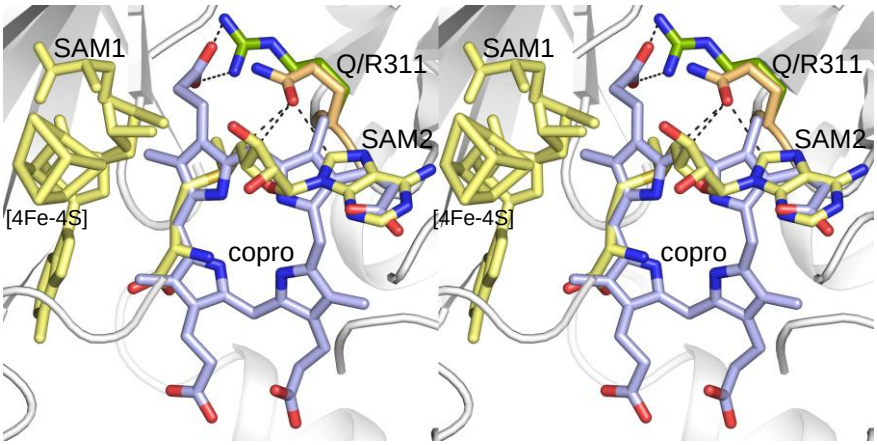

Figure 6-1: Modeled substitution of Gln311 by arginine (stereo view). Copro'gen is modeled according to **Figure 4-16**. Here it clashes with SAM2 which is presented in the conformation usually observed in HemN crystals. The presented arginine rotamer could stabilize substrate binding while SAM2 binding is weakened due to the loss of hydrogen bonds. Hydrogen bonds between Gln311 and SAM2 and possible ionic interactions between Arg311 and copro'gen are indicated by dashed lines. Copro: copro'gen.

7 References

Anton, B.P., Saleh, L., Benner, J.S., Raleigh, E.A., Kasif, S. and Roberts, R.J. (2008). RimO, a MiaB-like enzyme, methylthiolates the universally conserved Asp88 residue of ribosomal protein S12 in *Escherichia coli*. *Proc. Natl. Acad. Sci. U.S.A.* 105, 1826–1831.

Arsenault, G.P., Bullock, E. and MacDonald, S.F. (1960). Pyrromethanes and Porphyrins Therefrom. *J. Am. Chem. Soc.* 82, 4384–4389.

Astner, I., Schulze, J.O., van den Heuvel, J., Jahn, D., Schubert, W.D. and Heinz, D.W. (2005). Crystal structure of 5-aminolevulinate synthase, the first enzyme of heme biosynthesis, and its link to XLSA in humans. *EMBO J.* 24, 3166–3177.

Ausubel, F.M., Brent, R., Kingston, R.E., Moor, D.D., Seidman, J.G., Smith, J.A. and Struhl, K. (2007). Current protocols in molecular biology. John Wiley & Sons Inc.

Barras, F., Loiseau, L. and Py, B. (2005). How *Escherichia coli* and *Saccharomyces cerevisiae* Build Fe/S Proteins. *Adv. Appl. Microbiol.* 50, 41–101.

Batlle, A.M.C., Benson, A. and Rimington, C. (1965). Purification and Properties of Coproporphyrinogenase. *Biochem. J.* 97, 731-740.

Beinert, H. (2000). A tribute to sulfur. *Eur. J. Biochem.* 267, 5657–5664.

Benjdia, A., Leprince, J., Guillot, A., Vaudry, H., Rabot, S. and Berteau, O. (2007). Anaerobic sulfatase-maturating enzymes: radical SAM enzymes able to catalyze *in vitro* sulfatase post-translational modification. *J. Am. Chem. Soc.* 129, 3462–3463.

Bergonia, H.A., Phillips, J.D. and Kushner, J.P. (2009). Reduction of porphyrins to porphyrinogens with palladium on carbon. *Anal. Biochem.* 384, 74–78.

Berkovitch, F., Nicolet, Y., Wan, J.T., Jarrett, J.T. and Drennan, C.L. (2004). Crystal structure of biotin synthase, an *S*-adenosylmethionine-dependent radical enzyme. *Science* 303, 76–79.

Bertoloni, G., Salvato, B., Dall'Acqua, M., Vazzoler, M. and Jori, G. (1984). Hematoporphyrin-sensitized photoinactivation of *Streptococcus faecalis*. *Photochem. Photobiol.* 39, 811–816.

Booker, S.J., Cicchillo, R.M. and Grove, T.L. (2007). Self-sacrifice in radical *S*-adenosylmethionine proteins. *Curr. Opin. Chem. Biol.* 11, 543–552.

Breckau, D., Mahlitz, E., Sauerwald, A., Layer, G. and Jahn, D. (2003). Oxygen-dependent coproporphyrinogen III oxidase (HemF) from *Escherichia coli* is stimulated by manganese. *J. Biol. Chem.* 278, 46625–46631.

Broderick, J.B. (2000). Pyruvate Formate-Lyase-Activating Enzyme Strictly Anaerobic Isolation Yields Active Enzyme Containing a [3Fe-4S]$^{+}$ Cluster. *Biochem. Biophys. Res. Commun.* 269, 451–456.

Broderick, J.B., Duderstadt, R.E., Fernandez, D.C., Wojtuszewski, K., Henshaw, T.F. and Johnson, M.K. (1997). Pyruvate Formate-Lyase Activating Enzyme Is an Iron-Sulfur Protein. *J. Am. Chem. Soc.* 119, 7396–7397.

Burton, G., Fagerness, P.E., Hosozawa, S., Jordan, P.M. and Scott, A.I. (1979). ^{13}C N.M.R Evidence for a New Intermediate, Pre-uroporphyrinogen, in the Enzymic Transformation of Porphobilinogen into Uroporphyrinogens I and III. *J. Chem. Soc. Chem. Commun.*, 202–204.

Carr, R.P., Jackson, A.H., Kenner, G.W. and Sach, G.S. (1971). Pyrroles and related compounds. Part XVI. Synthesis of protoporphyrin-IX by the a- and b-oxobilane routes. *J. Chem. Soc. Chem. Commun.*, 487–502.

Cavaleiro, J.A., Kenner, G.W. and Smith, K.M. (1973). Biosynthetic intermediates between coproporphyrinogen-III and protoporphyrin-IX. *J. Chem. Soc. Chem. Commun.*, 183–184.

Cavaleiro, J.A., Kenner, G.W. and Smith, K.M. (1974). Pyrroles and related compounds. Part XXXII. Biosynthesis of protoporphyrin-IX from coproporphyrinogen-III. *J. Chem. Soc. Perkin Trans. I*, 1188–1194.

Challand, M.R., Ziegert, T., Douglas, P., Wood, R.J., Kriek, M., Shaw, N.M. and Roach, P.L. (2009). Product inhibition in the radical S-adenosylmethionine family. *FEBS Lett.* 583, 1358–1362.

Chatterjee, A., Li, Y., Zhang, Y., Grove, T.L., Lee, M., Krebs, C., Booker, S.J., Begley, T.P. and Ealick, S.E. (2008). Reconstitution of ThiC in thiamine pyrimidine biosynthesis expands the radical SAM superfamily. *Nat. Chem. Biol.* 4, 758–765.

Cheek, J. and Broderick, J.B. (2001). Adenosylmethionine-dependent iron-sulfur enzymes: versatile clusters in a radical new role. *J. Biol. Inorg. Chem.* 6, 209–226.

Chen, D., Frey, P.A., Lepore, B.W., Ringe, D. and Ruzicka, F.J. (2006). Identification of structural and catalytic classes of highly conserved amino acid residues in lysine 2,3-aminomutase. *Biochemistry* 45, 12647–12653.

Chen, Q., Huggins, M.T., Lightner, D.A., Norona, W. and McDonagh, A.F. (1999). Synthesis of a 10-Oxo-Bilirubin: Effects of the Oxo Group on Conformation, Transhepatic Transport, and Glucuronidation. *J. Am. Chem. Soc.* 121, 9253–9264.

Choi-Rhee, E. and Cronan, J.E. (2005). Biotin Synthase Is Catalytic *In Vivo*, but Catalysis Engenders Destruction of the Protein. *Chem. Biol.* 12, 461–468.

Cicchillo, R.M. and Booker, S.J. (2005). Mechanistic Investigations of Lipoic Acid Biosynthesis in *Escherichia coli*: Both Sulfur Atoms in Lipoic Acid are Contributed by the Same Lipoyl Synthase Polypeptide. *J. Biol. Chem.* 127, 2860–2861.

Coligan, J.E. (2003). Short protocols in protein science. A compendium of methods from Current protocols in protein science. John Wiley & Sons Inc.

Collaborative Computational Project Number 4 (1994). The CCP4 Suite: Programs for Protein Crystallography (50). *Acta Crystallogr. D Biol. Crystallogr.* 50, 760–763.

Coomber, S.A., Jones, R.M., Jordan, P.M. and Hunter, C.N. (1992). A putative anaerobic coproporphyrinogen III oxidase in *Rhodobacter sphaeroides*. I. Molecular cloning, transposon mutagenesis and sequence analysis of the gene. *Mol. Microbiol.* 6, 3159–3169.

Cooper, D.R., Boczek, T., Grelewska, K., Pinkowska, M., Sikorska, M., Zawadzki, M. and Derewenda, Z. (2007). Protein crystallization by surface entropy reduction: optimization of the SER strategy. *Acta Crystallogr. D Biol. Crystallogr.* 63, 636–645.

Dailey, H.A. (2002). Terminal steps of haem biosynthesis. *Biochem. Soc. Trans.* 30, 590–595.

Dasgupta, S., Iyer, G.H., Bryant, S.H., Lawrence, C.E. and Bell, J.A. (1997). Extent and nature of contacts between protein molecules in crystal lattices and between subunits of protein oligomers. *Acta Crystallogr. D Biol. Crystallogr.* 28, 494–514.

DeLano, W.L. (2002). The PyMOL Molecular Graphics System. DeLano Scientific.

Derewenda, Z.S. (2004a). Rational protein crystallization by mutational surface engineering. *Structure* 12, 529–535.

Derewenda, Z.S. (2004b). The use of recombinant methods and molecular engineering in protein crystallization. *Methods* 34, 354–363.

Derewenda, Z.S. and Vekilov, P.G. (2006). Entropy and surface engineering in protein crystallization. *Acta Crystallogr. D Biol. Crystallogr.* 62, 116–124.

Dolmans, D.E.J.G.J., Fukumura, D. and Jain, R.K. (2003). Photodynamic therapy for cancer. *Nat. Rev. Cancer* 3, 380–387.

Ehteshamuddin, A.F. (1968). Anaerobic formation of protoporphyrin IX from coproporphyrinogen III by bacterial preparations. *Biochem. J.* 107, 446–447.

Elder, G.H., Evans, J.O., Jackson, J.R. and Jackson, A.H. (1978). Factors determining the sequence of oxidative decarboxylation of the 2- and 4-propionate substituents of coproporphyrinogen III by coproporphyrinogen oxidase in rat liver. *Biochem. J,* 169,215–223.

Emsley, P. and Cowtan, K. (2004). Coot: model-building tools for molecular graphics. *Acta Crystallogr. D Biol. Crystallogr.* 60, 2126–2132.

Esberg, B., Leung, H.C., Tsui, H.C., Björk, G.R. and Winkler, M.E. (1999). Identification of the *miaB* gene, involved in methylthiolation of isopentenylated A37 derivatives in the tRNA of *Salmonella typhimurium* and *Escherichia coli*. *J. Bacteriol.* 181, 7256–7265.

Falk, J.E. (1964). Porphyrins and Metalloporphyrins. Their General, Physical and Coordination Chemistry, and Laboratory Methods. 1st. 2 Vol. Elsevier Publishing Company.

Flint, D.H. (1996). *Escherichia coli* contains a protein that is homologous in function and N-terminal sequence to the protein encoded by the *nifS* gene of *Azotobacter vinelandii* and that can participate in the synthesis of the Fe-S cluster of dihydroxy-acid dehydratase. *J. Biol. Chem.* 271, 16068–16074.

Flint, D.H., Smyk-Randall, E., Tuminello, J.F., Draczynska-Lusiak, B. and Brown, O.R. (1993a). The inactivation of dihydroxy-acid dehydratase in *Escherichia coli* treated with hyperbaric oxygen occurs because of the destruction of its Fe-S cluster, but the enzyme remains in the cell in a form that can be reactivated. *J. Biol. Chem.* 268, 25547–25552.

Flint, D.H., Tuminello, J.F. and Emptage, M.H. (1993b). The inactivation of Fe-S cluster containing hydro-lyases by superoxide. *J. Biol. Chem.* 268, 22369–22376.

Frankenberg, N., Moser, J. and Jahn, D. (2003). Bacterial heme biosynthesis and its biotechnological application. *Appl. Microbiol. Biotechnol.* 63, 115–127.

Frankenberg, N., Erskine, P.T., Cooper, J.B., Shoolingin-Jordan, P.M., Jahn, D. and Heinz, D.W. (1999). High resolution crystal structure of a Mg^{2+}-dependent porphobilinogen synthase. *J. Mol. Biol.* 289, 591–602.

Frazzon, J. and Dean, D.R. (2003). Formation of iron-sulfur clusters in bacteria: an emerging field in bioinorganic chemistry. *Curr. Opin. Chem. Biol.* 7, 166–173.

Frère, F., Schubert, W.D., Stauffer, F., Frankenberg, N., Neier, R., Jahn, D. and Heinz, D.W. (2002). Structure of Porphobilinogen Synthase from *Pseudomonas aeruginosa* in Complex with 5-Fluorolevulinic Acid Suggests a Double Schiff Base Mechanism. *J. Mol. Biol.* 320, 237–247.

Frey, P.A. and Magnusson, O.T. (2003). *S*-Adenosylmethionine: a wolf in sheep's clothing, or a rich man's adenosylcobalamin. *Chem. Rev.* 103, 2129–2148.

Games, D.E., Jackson, A.H., Jackson, J.R., Belcher, R.V. and Smith, S.G. (1976). Bio-ynthesis of protoporphyrin-IX from coproporphyrinogen-III. *J. Chem. Soc. Chem.Commun.*, 187–188.

Gardner, P.R. and Fridovich, I. (1991). Superoxide sensitivity of the *Escherichia coli* aconitase. *J. Biol. Chem.* 266, 19328–19333.

Gibson, K.J., Pelletier, D.A. and Turner, I.M. (1999). Transfer of Sulfur to Biotin from Biotin Synthase (BioB protein). *Biochem. Biophys. Res. Commun.* 254, 632–635.

Goto-Ito, S., Ishii, Ryohei, Ito, T., Shibata, R., Fusatomi, E., Sekine, S.-i., Bessho, Y. and Yokoyama, S. (2007). Structure of an archaeal TYW1, the enzyme catalyzing the second step of wye-base biosynthesis. *Acta Crystallogr. D Biol. Crystallogr.* 63, 1059–1068.

Grage, K. (2005). Oxygen-independent Coproporphyrinogen III Oxidase: Characterization of *Escherichia coli* HemN and Investigation of Proposed Functional Analogs. PhD thesis. Technische Universität Carolo-Wilhelmina zu Braunschweig, Fachbereich für Biowissenschaften und Psychologie.

Grandchamp, B. and Nordmann, Y. (1982). Coproporphyrinogen III oxidase assay. *Enzyme* 28, 196–205.

Granick, S. (1954). Enzymatic Conversion of δ-Amino Levulinic Acid to Porphobilinogen. *Science* 120, 1105–1106.

Green, J., Bennett, B., Jordan, P., Ralph, E.T., Thomson, A.J. and Guest, J.R. (1996). Reconstitution of the [4Fe-4S] cluster in FNR and demonstration of the aerobic-anaerobic transcription switch *in vitro*. *Biochem. J.* 316, 887–892.

Grove, T.L., Lee, K.-H., St. Clair, J., Krebs, C. and Booker, S.J. (2008). *In Vitro* Characterization of AtsB, a Radical SAM Formylglycine-Generating Enzyme That Contains Three [4Fe-4S] Clusters. *Biochemistry* 47, 7523–7538.

Guianvarc'h, D., Florentin, D., Tse Sum Bui, B., Nunzi, F. and Marquet, A. (1997). Biotin synthase, a new member of the family of enzymes which uses *S*-adenosylmethionine as a source of deoxyadenosyl radical. *Biochem. Biophys. Res. Commun.* 236, 402–406.

Hänzelmann, P. and Schindelin, H. (2004). Crystal structure of the *S*-adenosylmethionine-dependent enzyme MoaA and its implications for molybdenum cofactor deficiency in humans. *Proc. Natl. Acad. Sci. U.S.A.* 101, 12870–12875.

Hänzelmann, P., Hernandez, H.L., Menzel, C., Garcia-Serres, R., Huynh, B.H., Johnson, M.K., Mendel, R.R. and Schindelin, H. (2004). Characterization of MOCS1A, an Oxygen-sensitive Iron-Sulfur Protein Involved in Human Molybdenum Cofactor Biosynthesis. *J. Biol. Chem.* 279, 34721–34732.

Hernández, H.L., Pierrel, F., Elleingand, E., García-Serres, R., Huynh, B.H., Johnson, M.K., Fontecave, M. and Atta, M. (2007). MiaB, a bifunctional radical-*S*-adenosylmethionine enzyme involved in the thiolation and methylation of tRNA, contains two essential [4Fe-4S] clusters. *Biochemistry* 46, 5140–5147.

Hou, X., Liu, R., Ross, S., Smart, E.J., Zhu, H. and Gong, W. (2007). Crystallographic studies of human MitoNEET. *J. Biol. Chem.* 282, 33242–33246.

Huber, C. and Wächtershäuser, G. (1997). Activated acetic acid by carbon fixation on (Fe,Ni)S under primordial conditions. *Science* 276, 245–247.

Ilag, L.L., Jahn, D., Eggertsson, G. and Söll, D. (1991). The *Escherichia coli hemL* gene encodes glutamate 1-semialdehyde aminotransferase. *J. Bacteriol.* 173, 3408–3413.

Imlay, J.A. (2006). Iron-sulphur clusters and the problem with oxygen. *Mol. Microbiol.* 59, 1073–1082.

Jackson, A.H., Jones, D.M., Philip, G., Lash, T.D., Batlle, A.M.C. and Smith, S.G. (1980). Synthetic and biosynthetic studies of porphyrins, Part IV. Further studies of the conversion of corporporhyrinogen-III to protoporphyrin-IX: mass spectrometric investigations of the incubation of specifically deuteriated coproporhyringen-III with chicken red cell haemolysates. *Int. J. Biochem.* 12, 681–688.

Jahn, D., Verkamp, E. and Söll, D. (1992). Glutamyl-transfer RNA: a precursor of heme and chlorophyll biosynthesis. *Trends Biochem. Sci.* 17, 215–218.

Johnson, D.C., Dean, D.R., Smith, A.D. and Johnson, M.K. (2005). Structure, function, and formation of biological iron-sulfur clusters. *Annu. Rev .Biochem.* 74, 247–281.

Jordan, P.M., Burton, G., Nordlöv, H., Schneider, M.M., Pryde, L. and Scott, A.I. (1979). Preuroporphyrinogen, a Substrate for Uroporphyrinogen III Cosynthetase. *J .Chem. Soc. Chem. Commun.*, 204-205.

Kabsch, W. (1976). A solution for the best rotation to relate two sets of vectors. *Acta Crystallogr. A* 32, 922–923.

Kabsch, W. (1988). Evaluation of single-crystal X-ray diffraction data from a position-sensitive detector. *J. Appl. Cryst.* 21, 916–924.

Kennedy, M.C., Werst, M., Telser, J., Emptage, M.H., Beinert, H. and Hoffman, B.M. (1987). Mode of substrate carboxyl binding to the $[4Fe\text{-}4S]^{+}$ cluster of reduced aconitase as studied by ^{17}O and ^{13}C electron-nuclear double resonance spectroscopy. *Proc. Natl. Acad. Sci. U.S.A.* 84, 8854–8858.

Kikuchi, G., Kumar, A., Talmage, P. and Shemin, D. (1958). The enzymatic synthesis of delta-aminolevulinic acid. *J. Biol. Chem.* 233, 1214–1219.

Kiley, P.J. and Beinert, H. (2003). The role of Fe-S proteins in sensing and regulation in bacteria. *Curr. Opin. Microbiol.* 6, 181–185.

Knappe, J., Neugebauer, F.A., Blaschkowski, H.P. and Gänzler, M. (1984). Post-translational activation introduces a free radical into pyruvate formate-lyase. *Proc. Natl. Acad. Sci. U.S.A.* 81, 1332–1335.

Koch, M., Breithaupt, C., Kiefersauer, R., Freigang, J., Huber, R. and Messerschmidt, A. (2004). Crystal structure of protoporphyrinogen IX oxidase: a key enzyme in haem and chlorophyll biosynthesis. *EMBO J.* 23, 1720–1728.

Kohno, H., Furukawa, T., Tokunaga, R., Taketani, S. and Yoshinaga, T. (1996). Mouse coproporphyrinogen oxidase is a copper-containing enzyme: expression in *Escherichia coli* and site-directed mutagenesis. *Biochim. Biophys. Acta* 1292, 156–162.

Kriek, M., Martins, F., Challand, M.R., Croft, A. and Roach, P.L. (2007). Thiamine biosynthesis in *Escherichia coli*: identification of the intermediate and by-product derived from tyrosine. *Angew. Chem. Int. Ed. Engl.* 46, 9223–9226.

Krissinel, E. and Henrick, K. (2004). Secondary-structure matching (SSM), a new tool for fast protein structure alignment in three dimensions. *Acta Crystallogr. D Biol. Crystallogr.* 60, 2256–2268.

Küster, W. (1912). Beiträge zur Kenntnis des Bilirubins und Hämins. *Physiol. Chem.* 82, 463–483.

Lapointe, J. and Söll, D. (1972). Glutamyl transfer ribonucleic acid synthetase of *Escherichia coli*. I. Purification and properties. *J. Biol. Chem.* 247, 4966–4974.

Lash, T.D., Mani, U.N., Drinan, M.A., Zhen, C., Hall, T. and Jones, M.A. (1999). Normal and Abnormal Heme Biosynthesis. 1. Synthesis and Metabolism of Di- and Monocarboxylic Porphyrinogens Related to Coproporphyrinogen-III and Harderoporphyrinogen; A Model for the Active Site of Coproporphyrinogen Oxidase. *J. Org. Chem.* 64, 464–477.

Laskowski, R.A., MacArthur, M.W. and Thornton, J.M. (1998). Validation of protein models derived from experiment. *Curr. Opin. Struct. Biol.* 8, 631–639.

Layer, G. (2004). Structure and Function of the Oxygen-Independent Coproporphyrinogen III Oxidase HemN from *Escherichia coli*. PhD thesis. Technische Universität Carolo-Wilhelmina zu Braunschweig, Gemeinsame Naturwissenschaftliche Fakultät.

Layer, G., Gaddam, S.A., Ayala-Castro, C.N., Ollagnier-de Choudens, S., Lascoux, D., Fontecave, M. and Outten, F.W. (2007). SufE Transfers Sulfur from SufS to SufB for Iron-Sulfur Cluster Assembly. *J. Biol. Chem.* 282, 13342–13350.

Layer, G., Grage, K., Teschner, T., Schünemann, V., Breckau, D., Masoumi, A., Jahn, M., Heathcote, P., Trautwein, A.X. and Jahn, D. (2005a). Radical *S*-adenosylmethionine enzyme coproporphyrinogen III oxidase HemN: functional features of the [4Fe-4S] cluster and the two bound *S*-adenosyl-L-methionines. *J. Biol. Chem.* 280, 29038–29046.

Layer, G., Heinz, D.W., Jahn, D. and Schubert, W.D. (2004). Structure and function of radical SAM enzymes. *Curr. Opin. Chem. Biol.* 8, 468–476.

Layer, G., Kervio, E., Morlock, G., Heinz, D.W., Jahn, D., Retey, J. and Schubert, W.D. (2005b). Structural and functional comparison of HemN to other radical SAM enzymes. *Biol. Chem.* 386, 971–980.

Layer, G., Moser, J., Heinz, D.W., Jahn, D. and Schubert, W.D. (2003). Crystal structure of coproporphyrinogen III oxidase reveals cofactor geometry of Radical SAM enzymes. *EMBO J.* 22, 6214–6224.

Layer, G., Pierik, A.J., Trost, M., Rigby, S.E., Leech, H.K., Grage, K., Breckau, D., Astner, I., Jänsch, L., Heathcote, P., Warren, M.J., Heinz, D.W. and Jahn, D. (2006). The substrate radical of *Escherichia coli* oxygen-independent coproporphyrinogen III oxidase HemN. *J. Biol. Chem.* 281, 15727–15734.

Layer, G., Verfürth, K., Mahlitz, E. and Jahn, D. (2002). Oxygen-independent coproporphyrinogen-III oxidase HemN from *Escherichia coli*. *J. Biol. Chem.* 277, 34136–34142.

Lazazzera, B.A., Beinert, H., Khoroshilova, N., Kennedy, M.C. and Kiley, P.J. (1996). DNA binding and dimerization of the Fe-S-containing FNR protein from *Escherichia coli* are regulated by oxygen. *J. Biol. Chem.* 271, 2762–2768.

Lecerof, D., Fodje, M., Hansson, A., Hansson, M. and Al-Karadaghi, S. (2000). Structural and mechanistic basis of porphyrin metallation by ferrochelatase. *J. Mol. Biol.* 297, 221–232.

Lee, D.-S., Flachsová, E., Bodnárová, M., Demeler, B., Martásek, P. and Raman, C.S. (2005). Structural basis of hereditary coproporphyria. *Proc. Natl. Acad. Sci. U.S.A.* 102, 14232–14237.

Leimkuhler, S. and Rajagopalan, K.V. (2001). A Sulfurtransferase Is Required in the Transfer of Cysteine Sulfur in the *in Vitro* Synthesis of Molybdopterin from Precursor Z in *Escherichia coli*. *J. Biol. Chem.* 276, 22024–22031.

Lepore, B.W., Ruzicka, F.J., Frey, P.A. and Ringe, D. (2005). The x-ray crystal structure of lysine-2,3-aminomutase from *Clostridium subterminale*. *Proc. Natl. Acad. Sci. U.S.A.* 102, 13819–13824.

Leslie, A.G. (1992). MOSFLM. Joint CCP4 and ESF-EACBM Newsletter on Protein Crystallography, Daresbury Laboratory, Warrington, UK.

Lieder, K.W., Booker, S., Ruzicka, F.J., Beinert, H., Reed, G.H. and Frey, P.A. (1998). *S*-Adenosylmethionine-dependent reduction of lysine 2,3-aminomutase and observation of the catalytically functional iron-sulfur centers by electron paramagnetic resonance. *Biochemistry* 37, 2578–2585.

Lill, R. and Mühlenhoff, U. (2005). Iron-sulfur-protein biogenesis in eukaryotes. *Trends Biochem. Sci.* 30, 133–141.

Liu, B., Luna, V.M., Chen, Y., Stout, C.D. and Fee, J.A. (2007). An unexpected outcome of surface engineering an integral membrane protein: improved crystallization of cytochrome ba(3) from *Thermus thermophilus*. *Acta Crystallogr. F Struct. Biol. Cryst. Commun.* 63, 1029–1034.

Lovenberg, W., Buchanan, B.B. and Rabinowitz, J.C. (1963). Studies on the Chemical Nature of Clostridial Ferredoxin. *J. Biol. Chem.*, 3899–3913.

Ludwig, J. and Lehr, M. (2004). Convenient Synthesis of Pyrrole- and Indolecarboxylic Acid tert-Butylesters. *Syn. Comm.* 34, 3691–3695.

Luer, C., Schauer, S., Mobius, K., Schulze, J., Schubert, W.D., Heinz, D.W., Jahn, D. and Moser, J. (2005). Complex Formation between Glutamyl-tRNA Reductase and Glutamate-1-semialdehyde 2,1-Aminomutase in *Escherichia coli* during the Initial Reactions of Porphyrin Biosynthesis. *J. Biol. Chem.* 280, 18568–18572.

Malkin, R. and Rabinowitz, J.C. (1966). The reconstitution of clostridial ferredoxin. *Biochem. Biophys. Res. Commun.* 23, 822–827.

Martinez-Gomez, N.C. and Downs, D.M. (2008). ThiC is an [Fe-S] cluster protein that requires AdoMet to generate the 4-amino-5-hydroxymethyl-2-methylpyrimidine moiety in thiamin synthesis. *Biochemistry* 47, 9054–9056.

Martins, B.M., Grimm, B., Mock, H.-P., Huber, R. and Messerschmidt, A. (2001). Crystal Structure and Substrate Binding Modeling of the Uroporphyrinogen-III Decarboxylase from *Nicotiana tabacum*. IMPLICATIONS FOR THE CATALYTIC MECHANISM. *J. Biol. Chem.* 276, 44108–44116.

Masoumi, A., Heinemann, I.U., Rohde, M., Koch, M., Jahn, M. and Jahn, D. (2008). Complex formation between protoporphyrinogen IX oxidase and ferrochelatase during haem biosynthesis in *Thermosynechococcus elongatus*. *Microbiology (Reading, Engl.)* 154, 3707–3714.

Mathews, M.A., Schubert, H.L., Whitby, F.G., Alexander, K.J., Schadick, K., Bergonia, H.A., Phillips, J.D. and Hill, C.P. (2001). Crystal structure of human uroporphyrinogen III synthase. *EMBO J.* 20, 5832–5839.

Matthews, B. W. (1968). Solvent content of protein crystals. *J. Mol. Biol.* 33: 491-497.

McCoy, A.J., Grosse-Kunstleve, R.W., Storoni, L.C. and Read, R.J. (2005). Likelihood-enhanced fast translation functions. *Acta Crystallogr. D Biol. Crystallogr.* 61, 458–464.

Moser, J., Lorenz, S., Hubschwerlen, C., Rompf, A. and Jahn, D. (1999). *Methanopyrus kandleri* glutamyl-tRNA reductase. *J. Biol. Chem.* 274, 30679–30685.

Moser, J., Schubert, W.D., Beier, V., Bringemeier, I., Jahn, D. and Heinz, D.W. (2001). V-shaped structure of glutamyl-tRNA reductase, the first enzyme of tRNA-dependent tetrapyrrole biosynthesis. *EMBO J.* 20, 6583–6590.

Moser, J., Schubert, W.-D., Heinz, D.W. and Jahn, D. (2002). Structure and function of glutamyl-tRNA reductase involved in 5-aminolaevulinic acid formation. *Biochem. Soc. Trans.* 30, 579–584.

Moss, M.L. and Frey, P.A. (1990). Activation of lysine 2,3-aminomutase by *S*-adenosylmethionine. *J. Biol. Chem.* 265, 18112–18115.

Murshudov, G.N., Vagin, A.A. and Dodson, E.J. (1997). Refinement of macromolecular structures by the maximum-likelihood method. *Acta Crystallogr. D Biol. Crystallogr.* 53, 240–255.

Nicolet, Y. and Drennan, C.L. (2004). AdoMet radical proteins--from structure to evolution--alignment of divergent protein sequences reveals strong secondary structure element conservation. *Nucleic Acids Res.* 32, 4015–4025.

Nicolet, Y., Rubach, J.K., Posewitz, M.C., Amara, P., Mathevon, C., Atta, M., Fontecave, M. and Fontecilla-Camps, J.C. (2008). X-ray structure of the [FeFe]-hydrogenase maturase HydE from *Thermotoga maritima*. *J. Biol. Chem.* 283, 18861–18872.

Nitzan, Y., Wexler, H.M. and Finegold, S.M. (1994). Inactivation of anaerobic bacteria by various photosensitized porphyrins or by hemin. *Photochem. Photobiol.* 29, 125–131.

Nordmann, Y., Grandchamp, B., Verneuil, H. de, Phung, L., Cartigny, B. and Fontaine, G. (1983). Harderoporphyria: a variant hereditary coproporphyria. *J. Clin. Invest.* 72, 1139–1149.

O'Brien, J.R., Raynaud, C., Croux, C., Girbal, L., Soucaille, P. and Lanzilotta, W.N. (2004). Insight into the Mechanism of the B_{12}-Independent Glycerol Dehydratase from *Clostridium butyricum*: Preliminary Biochemical and Structural Characterization. *Biochemistry* 43, 4635–4645.

Ollagnier, S., Mulliez, E., Schmidt, P.P., Eliasson, R., Gaillard, J., Deronzier, C., Bergman, T., Gräslund, A., Reichard, P. and Fontecave, M. (1997). Activation of the anaerobic ribonucleotide reductase from *Escherichia coli*. The essential role of the iron-sulfur center for *S*-adenosylmethionine reduction. *J. Biol. Chem.* 272, 24216–24223.

Ollagnier-de Choudens, S., Sanakis, Y., Hewitson, K.S., Roach, P., Baldwin, J.E., Munck, E. and Fontecave, M. (2000). Iron-Sulfur Center of Biotin Synthase and Lipoate Synthase. *Biochemistry* 39, 4165–4173.

Ollagnier-de-Choudens, S., Mulliez, E. and Fontecave, M. (2002). The PLP-dependent biotin synthase from *Escherichia coli*: mechanistic studies. *FEBS Lett.* 532, 465–468.

Otwinowski Z. and Minor W. (1997). Macromolecular Crystallography Part A: [20] Processing of X-ray diffraction data collected in oscillation mode. *Meth. Enzymol.* 276, 307-326.

Outten, F.W. and Storz, O.D.G. (2004). A *suf* operon requirement for Fe-S cluster assembly during iron starvation in *Escherichia coli*. *Mol. Microbiol.* 52, 861–872.

Padovani, D., Thomas, F., Trautwein, A.X., Mulliez, E. and Fontecave, M. (2001). Activation of Class III Ribonucleotide Reductase from *E. coli*. The Electron Transfer from the Iron-Sulfur Center to *S*-Adenosylmethionine. *Biochemistry* 40, 6713–6719.

Panek, H. and O'Brian, M.R. (2002). A whole genome view of prokaryotic haem biosynthesis. *Microbiology (Reading, Engl.)* 148, 2273–2282.

Phillips, J.D., Whitby, F.G., Kushner, J.P. and Hill, C.P. (1997). Characterization and crystallization of human uroporphyrinogen decarboxylase. *Protein Sci.* 6, 1343–1346.

Phillips, J.D., Whitby, F.G., Kushner, J.P. and Hill, C.P. (2003). Structural basis for tetrapyrrole coordination by uroporphyrinogen decarboxylase. *EMBO J.* 22, 6225–6233.

Phillips, J.D., Whitby, F.G., Warby, C.A., Labbe, P., Yang, C., Pflugrath, J.W., Ferrara, J.D., Robinson, H., Kushner, J.P. and Hill, C.P. (2004). Crystal structure of the oxygen-dependant coproporphyrinogen oxidase (Hem13p) of *Saccharomyces cerevisiae*. *J. Biol. Chem.* 279, 38960–38968.

Picciocchi, A., Douce, R. and Alban, C. (2001). Biochemical characterization of the *Arabidopsis* biotin synthase reaction. The importance of mitochondria in biotin synthesis. *Plant Physiol.* 127, 1224–1233.

Pierrel, F., Douki, T., Fontecave, M. and Atta, M. (2004). MiaB protein is a bifunctional radical-*S*-adenosylmethionine enzyme involved in thiolation and methylation of tRNA. *J. Biol. Chem.* 279, 47555–47563.

Pilet, E., Nicolet, Y., Mathevon, C., Douki, T., Fontecilla-Camps, J.C. and Fontecave, M. (2009). The role of the maturase HydG in [FeFe]-hydrogenase active site synthesis and assembly. *FEBS Lett.* 583, 506–511.

Posewitz, M.C., King, P.W., Smolinski, S.L., Zhang, L., Seibert, M. and Ghirardi, M.L. (2004). Discovery of two novel radical *S*-adenosylmethionine proteins required for the assembly of an active [Fe] hydrogenase. *J. Biol. Chem.* 279, 25711–25720.

Poulson, R. (1976). The enzymic conversion of protoporphyrinogen IX to protoporphyrin IX in mammalian mitochondria. *J. Biol. Chem.* 251, 3730–3733.

Raulfs, E.C., O'Carroll, I.P., Dos Santos, P.C., Unciuleac, M.-C. and Dean, D.R. (2008). *In vivo* iron-sulfur cluster formation. *Proc. Natl. Acad. Sci. U.S.A.* 105, 8591–8596.

Raux, E., Leech, H.K., Beck, R., Schubert, H.L., Santander, P.J., Roessner, C.A., Scott, A.I., Martens, J.H., Jahn, D., Thermes, C., Rambach, A. and Warren, M.J. (2003). Identification and functional analysis of enzymes required for precorrin-2 dehydrogenation and metal ion insertion in the biosynthesis of sirohaem and cobalamin in *Bacillus megaterium*. *Biochem. J.* 370, 505–516.

Raynaud, C., Sarçabal, P., Meynial-Salles, I., Croux, C. and Soucaille, P. (2003). Molecular characterization of the 1,3-propanediol (1,3-PD) operon of *Clostridium butyricum*. *Proc. Natl. Acad. Sci. U.S.A.* 100, 5010–5015.

Reedy, C.J., Elvekrog, M.M. and Gibney, B.R. (2008). Development of a heme protein structure-electrochemical function database. *Nucleic Acids Res.* 36, 307-313.

Rubach, J.K., Brazzolotto, X., Gaillard, J. and Fontecave, M. (2005). Biochemical characterization of the HydE and HydG iron-only hydrogenase maturation enzymes from *Thermatoga maritima*. *FEBS Lett.* 579, 5055–5060.

Sambrook, J. and Russell, D.W. (2000). Molecular Cloning - a laboratory manual. Cold Spring Harbor Laboratory Press.

Sano, S. and Granick, S. (1961). Mitochondrial coproporphyrinogen oxidase and protoporphyrin formation. *J. Biol. Chem.* 236, 1173–1180.

Schmitt, C., Gouya, L., Malonova, E., Lamoril, J., Camadro, J.-M., Flamme, M., Rose, C., Lyoumi, S., Da Silva, V., Boileau, C., Grandchamp, B., Beaumont, C., Deybach, J.-C. and Puy, H. (2005). Mutations in human CPO gene predict clinical expression of either hepatic hereditary coproporphyria or erythropoietic harderoporphyria. *Hum. Mol. Genet.* 14, 3089–3098.

Schubert, H.L., Phillips, J.D., Heroux, A. and Hill, C.P. (2008). Structure and Mechanistic Implications of a Uroporphyrinogen III Synthase-Product Complex. *Biochemistry* 47, 8648–8655.

Schubert, W.D., Moser, J., Schauer, S., Heinz, D.W. and Jahn, D. (2002). Structure and function of glutamyl-tRNA reductase, the first enzyme of tetrapyrrole biosynthesis in plants and prokaryotes. *Photosyn. Res.* 74, 205–215.

Schulze, J.O., Masoumi, A., Nickel, D., Jahn, M., Jahn, D., Schubert, W.D. and Heinz, D.W. (2006). Crystal structure of a non-discriminating glutamyl-tRNA synthetase. *J. Mol. Biol.* 361, 888–897.

Seehra, J.S., Jordan, P.M. and Akhtar, M. (1983). Anaerobic and aerobic coproporphyrinogen III oxidases of *Rhodopseudomonas spheroides*. Mechanism and stereochemistry of vinyl group formation. *Biochem. J.* 209, 709–718.

Sellers, V.M., Johnson, M.K. and Dailey, H.A. (1996). Function of the [2Fe-2S] cluster in mammalian ferrochelatase: a possible role as a nitric oxide sensor. *Biochemistry* 35, 2699–2704.

Shemin, D. and Rittenberg, D. (1945). The Utilization of Glycine for the Synthesis of a Porphyrin. *J. Biol. Chem.* 159, 567–568.

Shemin, D. and Russell, C.S. (1953). δ-Aminolevulinic acid, its role in the biosynthesis of porphyrins and purines. *J. Am. Chem. Soc.* 75, 4873–4874.

Smith, J.L., Zaluzec, E.J., Wery, J.P., Niu, L., Switzer, R.L., Zalkin, H. and Satow, Y. (1994). Structure of the allosteric regulatory enzyme of purine biosynthesis. *Science* 264, 1427–1433.

Sofia, H.J., Chen, G., Hetzler, B.G., Reyes-Spindola, J.F. and Miller, N.E. (2001). Radical SAM, a novel protein superfamily linking unresolved steps in familiar biosynthetic pathways with radical mechanisms: functional characterization using new analysis and information visualization methods. *Nucleic Acids Res.* 29, 1097–1106.

Stephenson, J.R., Stacey, J.A., Morgenthaler, J.B., Friesen, J.A., Lash, T.D. and Jones, M.A. (2007). Role of aspartate 400, arginine 262, and arginine 401 in the catalytic mechanism of human coproporphyrinogen oxidase. *Protein Sci.* 16, 401–410.

Storoni, L.C., McCoy, A.J. and Read, R.J. (2004). Likelihood-enhanced fast rotation functions. *Acta Crystallogr. D Biol. Crystallogr.* 60, 432–438.

Studier, F.W. (2005). Protein production by auto-induction in high density shaking cultures. *Protein Expr. Purif.* 41, 207–234.

Suzuki, Y., Noma, A., Suzuki, T., Senda, M., Senda, T., Ishitani, R. and Nureki, O. (2007). Crystal structure of the radical SAM enzyme catalyzing tricyclic modified base formation in tRNA. *J. Mol. Biol.* 372, 1204–1214.

Tait, G.H. (1969). Coproporphyrinogenase activity in extracts from *Rhodopseudomonas spheroides*. *Biochem. Biophys. Res. Commun.* 37, 116–122.

Tait, G.H. (1972). Coproporphyrinogenase activities in extracts of *Rhodopseudomonas spheroides* and *Chromatium* strain D. *Biochem. J.* 128, 1159–1169.

Tamarit, J., Mulliez, E., Meier, C., Trautwein, A. and Fontecave, M. (1999). The anaerobic ribonucleotide reductase from *Escherichia coli*. The small protein is an activating enzyme containing a $[4fe\text{-}4s]^{(2+)}$ center. *J. Biol. Chem.* 274, 31291–31296.

Troup, B., Hungerer, C. and Jahn, D. (1995). Cloning and characterization of the *Escherichia coli hemN* gene encoding the oxygen-independent coproporphyrinogen III oxidase. *J. Bacteriol.* 177, 3326–3331.

Tse Sum Bui, B., Florentin, D., Fournier, F., Ploux, O., Méjean, A. and Marquet, A. (1998). Biotin synthase mechanism: on the origin of sulphur. *FEBS Lett.* 440, 226–230.

Verfürth, K. (1999). Das *Escherichia coli hemN* Gen kodiert für einen Bestandteil der sauerstoff-unabhängigen Coproporphyrinogen III Oxidase. Diploma thesis. Universität Freiburg, Mikrobiologie.

Vey, J.L., Yang, J., Li, M., Broderick, W.E., Broderick, J.B. and Drennan, C.L. (2008). Structural basis for glycyl radical formation by pyruvate formate-lyase activating enzyme. *Proc. Natl. Acad. Sci. U.S.A.* 105, 16137–16141.

Walther, J., Bröcker, M.J., Wätzlich, D., Nimtz, M., Rohde, M., Jahn, D. and Moser, J. (2009). Protochlorophyllide: a new photosensitizer for the photodynamic inactivation of Gram-positive and Gram-negative bacteria. *FEMS Microbiol. Lett.* 290, 156–163.

Wang, S.C. and Frey, P.A. (2007). *S*-adenosylmethionine as an oxidant: the radical SAM superfamily. *Trends Biochem. Sci.* 32, 101–110.

Wang, Y., Gatti, P., Sadílek, M., Scott, C.R., Turecek, F. and Gelb, M.H. (2008). Direct assay of enzymes in heme biosynthesis for the detection of porphyrias by tandem mass spectrometry. Uroporphyrinogen decarboxylase and coproporphyrinogen III oxidase. *Anal. Chem.* 80, 2599–2605.

Wittenberg, B.A., Wittenberg, J.B. and Caldwell, P.R. (1975). Role of myoglobin in the oxygen supply to red skeletal muscle. *J. Biol. Chem.* 250, 9038–9043.

Xu, K. and Elliott, T. (1994). Cloning, DNA sequence, and complementation analysis of the *Salmonella typhimurium hemN* gene encoding a putative oxygen-independent coproporphyrinogen III oxidase. *J. Bacteriol.* 176, 3196–3203.

Yang, J., Bitoun, J.P. and Ding, H. (2006). Interplay of IscA and IscU in biogenesis of iron-sulfur clusters. *J. Biol. Chem.* 281, 27956–27963.

Yokoyama, K., Numakura, M., Kudo, F., Ohmori, D. and Eguchi, T. (2007). Characterization and mechanistic study of a radical SAM dehydrogenase in the biosynthesis of butirosin. *J. Am. Chem. Soc.* 129, 15147–15155.

Figures

Tables

Danksagung

Bei Prof. Dr. Dirk Heinz möchte ich mich für die Möglichkeit zur Promotion im spannenden Bereich der Strukturbiologie, der damit verbundenen Herausforderung und für sein Engagement für optimale Arbeitsbedingungen bedanken.

Dr. Gunhild Layer möchte ich für die Übernahme des Zweitgutachtens sowie für Ihre stete Diskussionsbereitschaft und die vielen Tipps und Tricks zum Umgang mit HemN danken.

Herrn Prof. Dr. Ralf Mendel danke ich für die Übernahme des Vorsitzes der Prüfungskommission.

Prof. Dr. Dieter Jahn danke ich für sein Interesse und aktives Mitwirken an diesem Projekt und die Teilnahme an den Thesis Commitees. Dr. Martina Jahn danke ich für die Leihgabe der Anaerobisierungsanlage. Dem gesamten Institut für Mikrobiologie der TU Braunschweig (insbesondere den “Anaeroben” unter ihnen) danke ich für die freundliche Aufnahme in den Laboren und die tolle Unterstützung in und um den 17° C-Raum.

Prof. Dr. Markus Kalesse und besonders Claudia Noll danke ich für die aufwändige Harderoporphyrin-Synthese.

Dr. Wolf-Dieter Schubert gilt ein besonderer Dank für seine unendliche Geduld im Grafikraum, bei den Seminaren und meinen ständigen Fragen über HemN sowie für seine Unterstützung bei den Thesis Commitees.

Den Arbeitsgruppen von Prof. Dr. Ralf Ficner und Prof. Dr. Dietmar Manstein möchte ich für die Möglichkeit zur Nutzung ihrer Röntgengeräte und ihre Unterstützung dabei danken. Auch allen Beamline Scientists vom DESY in Hamburg und dem ESRF in Grenoble möchte ich für ihre Hilfe bei den zahlreichen Röntgenversuchen danken.

Für das tolle Arbeitsklima und die kollegiale Unterstützung bedanke ich mich bei allen Kollegen der Strukturbiologie. Nicht nur für die unvergesslichen Kaffeepausen sondern auch für die vielen nicht selbstverständlichen Gesten, die ich hier nicht alle einzeln

erwähnen kann, geht mein besonderer Dank dabei an: Carina, Christin, Christine, Daniela, Davide, Felix, Gregor, Hartmut, Hubi, Joop, Jörg, Maike B., Nadine, Nils, Rita, Sabine, Steffi, Thomas, Ulrich, Ute G., Ute W., Uwe, Victor , nicht zu vergessen an JR für den unermüdlichen IT-Support und natürlich an Maike, Lilia, Christian und Boris. Vielen, vielen Dank!

Dankeschön auch an Bettina, Maren, Theda, Kristina, alle Freunde sowie an die Fussballmädels, die mein Leben ausserhalb der Wissenschaft aufrecht erhalten haben.

Ein dickes, dickes Dankeschön geht an meine Familie. Mama, Papa, Nikolai, Franziska, Oma Erna und Oma Anna, Isabelle, Tante Cornelia und alle Sturms, Sigrid und Meint: vielen Dank für die Unterstützung und die Aufmunterungen zu jeder Zeit. Es ist gut zu wissen, einen so starken Rückhalt zu haben.

Und Ulfert, für Dich schreibe ich nun die letzten Sätze meiner Arbeit. Da ich nicht weiß, wo ich anfangen und wo ich aufhören soll, sag ich es einfach wie es ist: toda raba für ALLES!